Higher-order supersymmetric contributions to electroweak precision observables

Haestier, James

Higher-Order Supersymmetric Contributions to Electroweak Precision Observables

A thesis presented for the degree of

Doctor of Philosophy

by

James Haestier

Institute for Particle Physics Phenomenology

University of Durham

September 2005

Abstract

The dominant electroweak two-loop corrections to the precision observables M_W and $\sin^2\theta_{\text{eff}}$ are calculated in the MSSM. They are obtained by evaluating the two-loop Yukawa contributions of $\mathcal{O}(\alpha\alpha_s)$ and $\mathcal{O}(\alpha_t^2)$, $\mathcal{O}(\alpha_t\alpha_b)$, $\mathcal{O}(\alpha_b^2)$ to the quantity $\Delta\rho$. A review of the one-loop *Standard Model* calculation is given in the large Top-Yukawa coupling limit.

The $\mathcal{O}(\alpha_t^2)$, $\mathcal{O}(\alpha_t\alpha_b)$, $\mathcal{O}(\alpha_b^2)$ result, involving the contributions from Standard Model fermions, sfermions, Higgs bosons and higgsinos, is derived in the gaugeless limit for arbitrary values of the lightest $\mathcal{CP}$-even Higgs boson mass. A thorough discussion of the parameter relations enforced by supersymmetry is given. Two different renormalisation schemes are applied. Compared to the previously known result for the quark-loop contribution we find a shift of up to +8 MeV in M_W and -4×10^{-5} in $\sin^2\theta_{\text{eff}}$. Detailed numerical estimates of the remaining uncertainties of M_W and $\sin^2\theta_{\text{eff}}$ from unknown higher-order contributions are obtained for different values of the supersymmetric mass scale.

The calculations are preceded by a review of EWPO and supersymmetry. The electroweak precision variable $\Delta\rho$ is defined. We renormalise using both dimensional regularisation and dimensional reduction.

Acknowledgements

First and foremost I need to thank my supervisor, Georg Weiglein. Without his help and guidance there would have been no possibility of me ever successfully completing this thesis. I owe a similar debt to Dominik Stöckinger for his help with the completion of the work presented here. Thanks also to Sven Heinemeyer for help with our paper, much of which is presented here.

I would also like to thank Jon Level for providing the LaTeX template used for writing the thesis. Thanks also to Michael Dinsdale who has provided helpful physics and computing advice on countless occasions with seemingly endless patience.

Thanks to Wolfram Research Inc. for their unruly software.

Special thanks to all at the IPPP, including: Tom Birthwright, Angelique Talbot, Paul Brooks, Mark Morley-Fletcher and all the students, postdocs and staff for making my time here so enjoyable.

This work was funded by a PPARC studentship and their support is gratefully acknowledged.

Declaration

I declare that no material presented in this thesis has previously been submitted for a degree at this or any other university.

The research described in this thesis has been carried out in collaboration with Dr. Georg Weiglein, Dr. Dominik Stöckinger and Dr. Sven Heinemeyer has been published as follows:

- Electroweak Precision Observables: Two-loop Yukawa Corrections of Supersymmetric particles
  J Haestier, S Heinemeyer, D Stöckinger, G Weiglein,
  (hep-th/0508139)

Contents

List of Figures

List of Tables

Chapter 1

Introduction

If you want to make an apple pie from scratch, you must first create the universe.

Carl Sagan (1934 - 1996)

The *Standard Model (SM)* [1] of particle physics, developed over the last fifty years, has been hugely successful in describing observed natural phenomena at the current energy scale. It agrees with all confirmed experimental data from accelerators but is theoretically very unsatisfactory. It fails to explain a large number of phenomena observed in nature such as the quantum numbers electric charge Q, weak isospin I, hypercharge Y and colour. It contains at least 19 free parameters in the form of masses, mixing angles, vector boson couplings and CP-violating phases. It also requires the existence of a scalar (Higgs) boson whose coupling to the other SM particles is proportional their masses but no elementary scalar bosons have yet been observed.

Despite its success it is clear that the SM is incomplete and cannot be the full description of nature, not least because gravity is completely omitted. In addition

the Standard Model suffers from quadratic divergences [2]. Consider, for example, the contribution of the heavy fermion loops to the two-point function of the SM Higgs as shown in Fig.1.1. The SM Higgs mass, M_H, must be ≤ 1 TeV to preserve unitary of the WW scattering amplitudes [3]. Here we see that if the H-F-$\bar{\text{F}}$ cou-

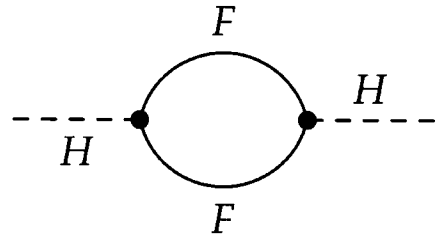

Figure 1.1: Fermion-Antifermion contribution to the self energy of the Higgs Boson in the Standard Model

pling is λ and N(F) is a multiplicity factor (eg. N(b) = 3 for bottom quarks from the colour summation) then the correction is given by [2]

$$\begin{aligned}\Pi^F_{HH}(0) &= -N(F)\int \frac{d^4k}{(2\pi)^4} tr[(i\lambda)\frac{i}{\not k - m_f}(i\lambda)\frac{i}{\not k - m_f}] \\ &= -4N(F)\lambda^2 \int \frac{d^4k}{(2\pi)^4}[\frac{1}{k^2-m_f^2} + \frac{2m_f^2}{(k^2-m_f^2)^2}] \qquad (1.1)\end{aligned}$$

The first term in the last line above is quadratically divergent. We could regulate the divergence by imposing a cut-off, Λ. To do this we must assume that the SM is valid up to the scale Λ. If the SM is valid up to the plank scale, M_{pl}, then the cut-off is $\mathcal{O}(M_{pl})$. If the divergence is replaced by M^2_{Pl} it one would expect that $M_H \simeq M_{pl}$, otherwise huge fine-tuning is necessary.

The question that now arises is what new physics might we expect to discover in future experiments. Clearly one could formulate all kinds of new theories so it would be helpful if we could use the current experimental data to restrict or

guide our ideas. With this in mind we shall review some theoretical contributions to precisely measured observables. In this thesis we limit the discussion to Electroweak Precision Observables (EWPO) and in particular the contributions to the rho parameter, ρ.

1.1 The search for new Physics

Restrictions on new physics can be imposed using both direct and indirect constraints. The unsuccessful direct search for the Higgs Boson at LEP places a lower bound on the SM Higgs mass of $M_H \gtrsim 114$ GeV [4]. Indirect constraints are imposed by the measurement to very high precision of known processes and comparing the result with the theoretical prediction. This analysis of precision physics was successfully used to predict the mass of the Top quark to within 10% of the direct measurement at the Tevatron [5] of

$$m_t = 172.7 \pm 2.9\text{GeV} \tag{1.2}$$

which agrees well with the value derived from precision electroweak data [4] of

$$m_t = 172.3^{+12}_{-9}\text{GeV} \tag{1.3}$$

Current experimental high-precision measurements agree well with SM. This puts an upper bound on effects from extensions of the SM. Thus corrections from any proposed extension must be relatively small in order to maintain good agreement with experimental data.

High precision experimental results require equally precise theoretical predictions in order for comparisons to be made. It is insufficient to just use tree level results

for SM processes when performing this type of analysis as both 1- and 2- loop corrections will produce measurable effects. Whilst this makes the theoretical calculations more involved, it also gives the possibility of observing the effects of new phenomena. Since both 1- and 2-loop SM contributions have been calculated and provide small corrections to the tree-level result, it is plausible that contributions from new models in further loop corrections will give rise to equally small but noticeable effect, and may even provide a better description of data than the SM. We will therefore proceed by taking our favoured theory of new physics and calculate higher order corrections to precision observables in that theory to constrain (or even exclude) the parameter space of that model.

1.2 Thesis Outline

This thesis is in two parts: Chapters 2 - 4 contain a brief introduction to the physics used in later calculations and serves to define our notation. Chapters 5 - 7 give details of three calculations performed by the author.

In the next chapter we review the ρ parameter and discuss the leading order result for $\Delta\rho$. We justify the need to renormalise the calculations presented later and outline our calculational method and choice of regulator.

In the following chapter will introduce supersymmetry and define our notation for later chapters. Chapter 4 introduces renormalisation using counterterms gives describes their implementation in our calculations.

In chapter 5 we present the leading QCD corrections to scalar quark contributions. Leading two-loop electroweak corrections are presented in chapter 6 in the heavy supersymmetric limit. Both these results have been published previously but are

reproduced here independently both to introduce the calculational method in a more simple framework and to verify the previous results.

Leading Squark Yukawa corrections are presented in chapter 7. This chapter contains some new results, as well as giving explanation for many of the observations made in the original publications of the work presented in chapter 6.

In the final chapter we conclude.

Chapter 2

Electroweak precision observables and calculation of loop corrections

A vacuum is a hell of a lot better than some of the stuff that nature replaces it with.

Tennessee Williams, "Cat on a Hot Tin Roof (1955)"

Electroweak precision observables (EWPO), like the masses of the W and Z boson $M_{W,Z}$ or the effective leptonic weak mixing angle $\sin^2\theta_{\text{eff}}$, are highly sensitive probes of the quantum structure of the electroweak interactions. The standard model (SM) and any extension or alternative predicts certain relations between these observables that can be tested against the corresponding experimental values. The experimental resolution is better than the per-mille level, and thus the measurements can be sensitive to even two-loop effects. Hence the EWPO are very powerful for discriminating between different models of electroweak interactions and for deriving indirect constraints on unknown parameters such as the masses of the SM Higgs boson or supersymmetric particles.

An important part of the theoretical predictions of all EWPO both in the SM and in extensions of it is contained in $\Delta\rho$ (see section 2.4). The follow section gives a brief explanation as to why.

2.1 Muon decay and Δr

The muon lifetime,τ_μ, is a very precisely know experimental value. It can also be calculated theoretically from first principles [6]

$$\frac{1}{\tau_\mu} = \frac{G_\mu^2 m_\mu^5}{192\pi^3} F(\frac{m_e^2}{m_\mu^2})(1 + \frac{3m_\mu^2}{5M_W^2})(1 + \Delta q) \tag{2.1}$$

with $F(x) = 1 - 8x - 12x^2 log(x) + 8x^3 - x^4$ and where m_e, m_μ are the electron and muon masses respectively and Δq represents QED corrections from the Fermi model. Equation 2.1 can be used to define the Fermi constant G_μ. By comparing the theoretical prediction for the muon lifetime within a given model with Eq. 2.1 a relation between G_μ and the parameters of the model can be derived. This relation receives radiative corrections from vertex, box and self-energies diagrams (see, for example, fig 2.2), which, at first order, can be parameterised by the quantity Δr:

$$G_\mu = \frac{\pi\alpha}{\sqrt{2}s_w^2 M_W^2}(1 + \Delta r), \tag{2.2}$$

where $s_w^2 = 1 - M_W^2/M_Z^2$ and α is the electromagnetic coupling constant. For $\Delta r = 0$ this relation corresponds to the lowest-order SM prediction. In accordance with the definition of G_μ in Eq. 2.1, the contribution corresponding to the QED correction in the Fermi model has to be extracted from Δr

At one-loop order of the SM, Δr is a finite combination of one-loop diagrams and

counterterms(see chapter 4). It can be decomposed in the following way:

$$\begin{aligned} \Delta r_{1-\text{loop}} = \quad & \Delta\alpha \quad - \quad \frac{c_w^2}{s_w^2}\Delta\rho \quad + \quad \Delta r_{\text{remainder}}(M_H) \\ & \sim \log\frac{M_Z}{m_f} \quad \sim m_t^2 \qquad \sim \log(M_H) \\ & \sim 6\% \qquad \sim 3.3\% \qquad \sim 1\% \end{aligned} \tag{2.3}$$

where $\Delta\alpha$ is the correction from the running of α, $\Delta\rho$ is the leading top mass (m_t) contribution to EWPO entering quadratically and $\Delta r_{\text{remainder}}(M_H)$ are the remaining one-loop contributions. This later term contains the leading M_H dependence ($\sim log(M_H)$). Since the correction from $\Delta\alpha$ is $\sim \log\frac{M_Z}{m_f}$ it is shielded from the effect of heavier fermions and thus makes it a poor choice to examine new physics (where one typically expects masses to be larger than those of SM particles). $\Delta\rho$, however, can provide corrections $\mathcal{O}(\frac{m_t^2}{M_W^2})$ (or possibly even larger for new physics models), proportional to the mass splitting of isodoublets, allowing one to calculate measurable corrections to EWPO.

2.2 The ρ parameter

The ρ parameter [7] is defined as the ratio of the neutral current to the charged current in processes such as those in Fig.2.1

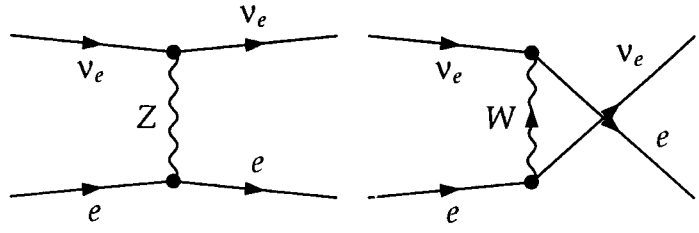

Figure 2.1: Electron - Neutrino scattering via neutral and charged currents

At tree level ρ is given by

$$\begin{aligned} \rho &= \frac{M_W^2}{c_w^2 M_Z^2} \\ &= 1 \end{aligned} \tag{2.4}$$

where $M_{Z,W}$ are the masses of the Z and W boson respectively and c_w is $\cos(\theta_W)$, θ_W the weak mixing angle. In equation 2.4, $\rho = 1$ at tree level is a manifestation of the custodial symmetry in the SM [8]. At higher orders, ρ receives corrections from vertex loops, box loops and propagator loops (see figure 2.2). In this thesis we will only be concerned with leading corrections to the internal propagators (ie. the third diagram in fig. 2.2).

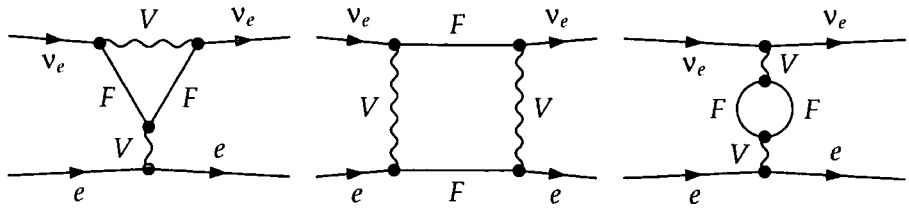

Figure 2.2: Examples of Vertex, Box and Propagator loop corrections to ρ . V is either a Z or W boson; F is an electron or neutrino

Loop diagrams such as those shown in fig.2.2 give rise to integrals such as those seen earlier in chapter 1 (equation 1.1). Before proceeding we briefly discuss the problems of evaluating such expressions.

2.3 Loop calculations: Regularisation + Computation

The integral expressions for loop diagrams are formally infinite in the limit $k \to \infty$ (ultra-violet divergent) [9]. That is, the 'bare' parameters that appear in the Lagrangian (eg. mass, charge) are infinite and cannot be physical parameters. In order to overcome this problem one must regulate these divergences away to leave only renormalised (finite), physical values.

This could be be done by imposing a cut-off on the integral, introducing some (arbitrary) upper bound and taking the limit as the cut-off $\to \infty$ in the final result. In practice, however, it turns out to be more convenient to use dimensional regularisation [10] [11], that is to shift the integral from 4 to $D = 4-2\epsilon$ dimensions, working in the limit of $\epsilon \to 0$. The divergences then show up as poles in ϵ. Dimensional regularisation has the advantage of respecting gauge invariance, as well as regularising infra-red ($k \to 0$) divergences.

Dimensional regularisation is not without problems, however. The γ_5 matrix is not well defined in dimension $D \neq 4$ [12], since it is intrinsically a 4-dimension object. The problems arise when trying to evaluate the trace of four or more γ matrices. Fortunately in the calculations presented in this thesis we will only be concerned with two-loop self-energies where there will be maximum of three independent momentum parameters, and consequently a maximum of three γ matrices. Thus we never meet these problems here.

In later chapters we will be performing calculations in supersymmetry (SUSY), where extending dimensions to $D > 4$ is not straight forward. SUSY is a symmetry between fermions and bosons. Changing the dimension from 4 to D changes the number of degrees of freedom of vector bosons, as they are D-dimensional objects.

The number of degrees of freedom of the fermions remains unchanged. This leads to a contradiction in SUSY and therefore in supersymmetric calculations we work in the analogue of dimensional regularisation: dimensional reduction [13]. The most notable difference between the two schemes is that $g^{\mu}{}_{\mu} = 4$ in dimensional reduction (ie.not D as in dimension regularisation) to avoid potential conflicts.

All Feynman diagrams in this thesis, unless explicitly stated, have been calculated using the following procedure: The amplitudes for each diagram are produced with the Mathematica package *FeynArts* [14], making use of the MSSM model file [15] where appropriate. Unless stated otherwise, we work in the Feynman gauge.
Dirac algebra and traces have been evaluated using the program *Twocalc* [16]. The reduction to scalar integrals has been performed also using the routines built into *Twocalc*, which performs the integrals using dimensional regularisation (for SM diagrams) or dimensional reduction (for Supersymmetric diagrams).
As a result we obtained the analytical expression for $\Delta\rho$ in terms of the one-loop integral functions A_0 and B_0 [17] and on the two-loop integral function T_{134} [16,18]. For the further evaluation the analytical expressions for A_0, B_0 and T_{134} have been inserted. The scalar integrals are given in Appendix A. Both infra-red and ultra-violet divergences show up as poles in ϵ, in the limit as $\epsilon \to 0$. Summing all diagrams for a physical process and series-expanding[1] in ϵ gives a finite result in the limit $\epsilon \to 0$. Finally, numerical analysis is performed.

2.4 $\Delta\rho$ at one loop

To calculate the rho parameter at a given order one has to calculate the full neutral current (Z-exchange) and charged current (W-exchange) processes at this order (ie.

[1]Because of problems discovered with some of the numerical routines in Mathematica, the series expansion and algebraic manipulation is performed in Maple.

all possible diagrams in fig. 2.2) and take their ratio. Performing this calculation gives (amongst others) a term from the renormalisation of the weak-mixing angle of the form

$$(\frac{\Sigma^T_{ZZ}(M_Z{}^2)}{M_Z{}^2} - \frac{\Sigma^T_{WW}(M_W{}^2)}{M_W{}^2}). \tag{2.5}$$

This term contains the leading top/bottom contribution in the SM. In the low energy limit this contribution can be obtained in the approximation of evaluating the Z/W self-energies at zero momentum. This quantity is what one usually calls $\Delta\rho$:

$$\Rightarrow \rho \rightarrow \rho + \Delta\rho \tag{2.6}$$

$$= \rho + (\frac{\Sigma^T_{ZZ}(0)}{M_Z{}^2} - \frac{\Sigma^T_{WW}(0)}{M_W{}^2}) \tag{2.7}$$

where $\Sigma^T_{ZZ}(0), \Sigma^T_{WW}(0)$ denote the transverse parts of the unrenormalized Z and W boson self-energies, respectively, at zero momentum transfer. Here the transverse (and longitudinal) self-energy parts are defined by decomposing the self-energy $\Sigma_{VV}(q^2)$ into Lorentz tensors and scalar parts as follows:

$$\Sigma_{VV,\mu\nu}(q^2) = -(g_{\mu\nu} + \frac{q_\mu q_\nu}{q^2})\Sigma^T_{VV}(q^2) - \frac{q_\mu q_\nu}{q^2}\Sigma^L_{VV}(q^2) \tag{2.8}$$

The term on the right of Eq.2.7 is a finite correction to ρ.

Historically the ρ parameter was a precision observable measured in experiments. In more recent experiments observables measured to high precision include M_W and $\sin^2\theta_{\text{eff}}$. The quantity $\Delta\rho$ is a useful parameter to calculate as it parametrises the leading universal corrections from vector boson self energies induced by the mass splitting between fields in an isospin doublet [7]. Any contribution to $\Delta\rho$

induces the following shifts to M_W and $\sin^2\theta_{\text{eff}}$:

$$\delta M_W \approx \frac{M_W}{2}\frac{c_w^2}{c_w^2 - s_w^2}\Delta\rho \tag{2.9}$$

$$\delta \sin^2\theta_{\text{eff}} \approx -\frac{c_w^2 s_w^2}{c_w^2 - s_w^2}\Delta\rho \tag{2.10}$$

Experimentally ρ is very close to one. It turns out that any model with only Higgs doublets (and singlets) will automatically give $\rho = 1$ at tree level (with small corrections at higher orders). Thus $\Delta\rho$ is a very useful quantity exactly to calculate for constraining new physics through higher order corrections.

For reference we now present the dominant one loop correction to $\Delta\rho$ in the SM. As previously stated the dominant contribution in the SM arises from the top/bottom sector due to the large mass splitting in the quark doublet. To obtain this contribution one must calculate the Feynman diagrams show in Fig 2.3

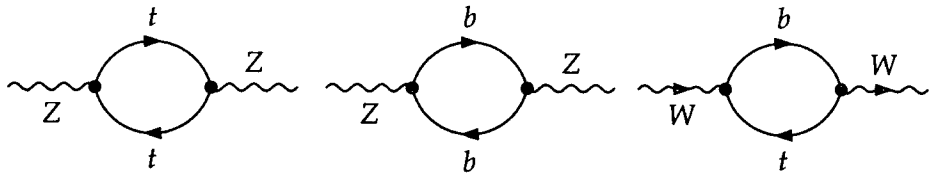

Figure 2.3: Leading corrections to Z and W self-energies within the SM entering $\Delta\rho$

The divergent parts of the one-loop SM result for the Z and W self-energies in fig 2.3 are:

$$Z : \frac{3e^2\,(m_b^2 + m_t^2)M_Z^2}{32\pi^2\epsilon\,(M_W^2 - M_Z^2)} \cdot \frac{M_Z^2}{M_W^2} \tag{2.11}$$

$$W : \frac{3e^2\,(m_b^2 + m_t^2)M_Z^2}{32\pi^2\epsilon\,(M_W^2 - M_Z^2)} \tag{2.12}$$

where $m_{b,t}$ are the mass of the bottom, top quark respectively.

One may now calculate the correction to $\Delta\rho$ using equation 2.7. From equations (2.11) and (2.12) it is manifest that at one-loop the top/bottom contribution to $\Delta\rho$ is *finite without renormalisation.* This is not just by chance. Since $\rho = 1$ at tree level, there are no parameters to renormalise at the one-loop level. For higher orders in general, however, corrections to $\Delta\rho$ will not be finite and we will need to renormalise the calculation. This is one of the more appealing aspects of the $\Delta\rho$ calculation as all renormalisation scheme dependence is suppressed to the two-loop level. The method of renormalisation is described in chapter 4 and exact renormalisation schemes will be defined as required.

The finite one-loop SM result for the diagrams in fig. 2.3 is:

$$\delta\rho = \frac{-3e^2(m_b^4 - m_t^4 + 2m_b^2 m_t^2(\log[\frac{m_t^2}{m_b^2}]))}{64\pi^2(M_W^2 - M_Z^2)(m_b^2 - m_t^2)} \tag{2.13}$$

$$\simeq 0.00986 \tag{2.14}$$

where e is the electron charge and $m_t = 178$ GeV, $m_b = 4$ GeV. Thus the leading SM result gives a small but measurable contribution of about 1%, which corresponds to (using Eq. 2.3) a 3.3% correction to Δr.

The result can be rewritten in the compact form

$$\Delta\rho_0^{\rm SM} = \frac{3\,G_\mu}{8\sqrt{2}\,\pi^2}\,F_0(m_t^2, m_b^2), \tag{2.15}$$

where

$$F_0(x,y) = x + y - \frac{2\,x\,y}{x-y}\log\frac{x}{y}. \tag{2.16}$$

F_0 has the properties $F_0(m_1^2, m_2^2) = F_0(m_2^2, m_1^2)$, $F_0(m^2, m^2) = 0$, $F_0(m^2, 0) = m^2$.

One therefore obtains $F_0(m_t^2, m_b^2) \approx m_t^2$, giving rise to the well-known quadratic dependence of the one-loop corrections to the EWPO on the top-quark mass. In this form it is manifest that the largest contribution to $\Delta\rho$ at one-loop comes from the t/b-isodoublet due the large mass-splitting.

Chapter 3

Supersymmetry

'Supersymmetry must exist in order to solve the problem of what to give graduate students to calculate...'

Conversation with Nick Evans, Spring 2003

Supersymmetry[1] [20] (SUSY) is regarded by many theorists as the most attractive extension of the SM. Proponents of SUSY highlight the following as evidence of the model's appeal: It is the only non-trivial extension of the Poincaré group; consistent with the unification of the gauge couplings beyond the TeV scale; provides a natural solution to the dark matter problem; can incorporate a description of gravity; solves the Hierarchy problem.

Here we do not attempt to justify SUSY from a theoretical point of view but take a more pragmatic approach. We take the model and ask what, if any, region of the parameter space allows us to make predictions consistent with the current experimental evidence. By restricting the parameter space we hope to narrow the search for supersymmetric particles at the next generation of colliders. Conversely,

[1]Much of the information in this chapter appears in ref. [19] but is reproduced here to define notation

we may also hope to find regions of the parameter space that provide contributions to EWPO giving better agreement with current data than the SM.
Supersymmetry, as the name suggests, is a symmetry in nature between bosons and fermions. The fermionic operator Q generates the transformations:

$$Q|Boson> = |Fermion> \tag{3.1}$$

$$Q|Fermion> = |Boson> \tag{3.2}$$

SUSY predicts that every particle within the SM has a supersymmetric partner. The superpartner will have identical quantum numbers with the corresponding SM particle with the exception of spin. The spin is a half integer difference, hence SUSY maps bosons to fermions and vice-versa.

There is an obvious problem with SUSY: no superpartners have yet been observed in nature so immediately we see that the symmetry must be broken. This is not the disaster that it might at first seem. The success of the SM illustrates the usefulness of broken symmetries. In general SUSY breaking leads to 105 free parameters. For simplicity however, many of these can be restricted by assuming a breaking mechanism, although full understanding of the breaking mechanism will require the discovery and measurement of several key SUSY parameters.

3.1 The MSSM particle spectrum

The Minimal Supersymmetric Standard Model (MSSM) is the simplest supersymmetric extension of the SM. It contains only those particles necessary to build a consistent theory. The quarks and leptons have superpartners squarks and sleptons, respectively. The photon, Z and W bosons have superpartners: the photino,

zino and wino, all with spin $\frac{1}{2}$. These are not physical states however, as they mix with the SUSY partners from the Higgs sector, the higgsinos, to form physical mixing states: neutralinos and charginos. The full particle spectrum of the MSSM can be seen in table 3.1.

	Spin $\frac{1}{2}$	Spin 0
(S)Quarks	$[u, d, c, s, t, b]_{L,R}$	$[\tilde{u}, \tilde{d}, \tilde{c}, \tilde{s}, \tilde{t}, \tilde{b}]_{L,R}$
(S)Leptons	$[e, \mu, \tau]_{L,R}$, $[\nu_{e,\mu,\tau}]_L$	$[\tilde{e}, \tilde{\mu}, \tilde{\tau}]_{L,R}$, $[\tilde{\nu}_{e,\mu,\tau}]_L$

	Spin 1	Spin 0	Spin $\frac{1}{2}$
Neutral Bosons (Bosinos)	γ, Z	h^0, H^0, A^0	$\tilde{\chi}^0_{1,2,3,4}$
Charged Bosons (Bosinos)	$W^{\pm}$	$H^{\pm}$	$\tilde{\chi}^{\pm}$
Gluon (gluino)	g	-	$\tilde{g}$

Table 3.1: The Particle Spectrum of the MSSM

3.1.1 The Higgs Sector of the MSSM

The most noticeable difference between the MSSM and the SM can be seen in the Higgs sector. In SUSY at least two Higgs doublet superfields are required. A supersymmetric model with only a single Higgs doublet superfield suffers from quadratic divergences, has non-vanishing gauge anomalies and cannot give masses to the both the up- and down-type fermions [2]. The MSSM thus contains two Higgs doublet superfields, $\mathcal{H}_1$ and $\mathcal{H}_2$, where the first doublet, $\mathcal{H}_1$, gives mass to the d-type fermions (with weak isospin I $= -\frac{1}{2}$) and the second, $\mathcal{H}_2$, gives mass to the u-type fermions (I $= +\frac{1}{2}$).

The introduction of a two Higgs doublet to the MSSM gives rise to five[2] physical Higgs bosons. In contrast to the SM, where the Higgs boson mass is a free parameter, the quartic couplings of the Higgs potential in the MSSM are fixed by the

[2]The Goldstone Bosons, G^0 and $G^{\pm}$ in the MSSM are 'eaten' by the Z and $W^{\pm}$ in the same way as in the SM.

gauge couplings as a consequence of SUSY. So in the MSSM one parameter, μ, replaces two parameters in the Higgs sector of SM. Unfortunately SUSY breaking in general leads to the introduction of many more free parameters.

The Higgs masses can all be predicted from two free parameters at tree level (along with other SM parameters), conventionally chosen to be M_A, the mass of the $\mathcal{CP}$-odd Higgs boson and $\tan(\beta) = v_2/v_1$, the ratio of the vacuum expectation values of the Higgs doublets.

The two Higgs doublets form the Higgs potential [21]

$$\begin{aligned} V_{MSSM}^{Higgs} &= (m_1^2 + |\mu|^2)|\mathcal{H}_1|^2 + (m_2^2 + |\mu|^2)|\mathcal{H}_2|^2 - m_{12}^2(\epsilon_{ab}\mathcal{H}_1^a\mathcal{H}_2^b + h.c.) \\ &+\frac{1}{8}(g_1^2 + g_2^2)[|\mathcal{H}_1|^2 + |\mathcal{H}_2|^2]^2 + \frac{1}{2}g_2^2|\mathcal{H}_1^\dagger\mathcal{H}_2|^2 \end{aligned} \tag{3.3}$$

where m_1, m_2, m_{12} are soft SUSY breaking parameters and μ is the Higgsino mass parameter. g_1 and g_2 are the *U(1)* and *SU(2)* gauge couplings and $\epsilon_{12} = -1$. The Higgs doublet fields $\mathcal{H}_1$ and $\mathcal{H}_2$ are given a vacuum expectation value (vev) in the following way:

$$\mathcal{H}_1 = \begin{pmatrix} \mathcal{H}_1^0 \\ \mathcal{H}_1^- \end{pmatrix} = \begin{pmatrix} v_1 + \frac{1}{\sqrt{2}}(\phi_1^0 - i\chi_1^0) \\ -\phi_1^- \end{pmatrix} \tag{3.4}$$

$$\mathcal{H}_2 = \begin{pmatrix} \mathcal{H}_2^+ \\ \mathcal{H}_2^0 \end{pmatrix} = \begin{pmatrix} \phi_2^+ \\ v_2 + \frac{1}{\sqrt{2}}(\phi_2^0 - i\chi_2^0) \end{pmatrix} \tag{3.5}$$

The potential, Eq (3.3) can be re-parameterised in terms of M_{A^0} and $\tan(\beta)$ and SM parameters (M_Z). This can be achieved by substituting equations 3.4 and 3.5 into 3.3 and making use of the minimum conditions, i.e. the first order terms in the neutral fields must vanish.

Diagonalisation of the bilinear part of the Higgs potential, i.e. the Higgs mass

matrices, is performed via the orthogonal transformations:

$$\begin{pmatrix} H^0 \\ h^0 \end{pmatrix} = \begin{pmatrix} \cos\,\alpha & \sin\,\alpha \\ -\sin\,\alpha & \cos\,\alpha \end{pmatrix} \begin{pmatrix} \phi_1^0 \\ \phi_2^0 \end{pmatrix} \tag{3.6}$$

$$\begin{pmatrix} G^0 \\ A^0 \end{pmatrix} = \begin{pmatrix} \cos\,\beta & \sin\,\beta \\ -\sin\,\beta & \cos\,\beta \end{pmatrix} \begin{pmatrix} \chi_1^0 \\ \chi_2^0 \end{pmatrix} \tag{3.7}$$

$$\begin{pmatrix} G^\pm \\ H^\pm \end{pmatrix} = \begin{pmatrix} \cos\,\beta & \sin\,\beta \\ -\sin\,\beta & \cos\,\beta \end{pmatrix} \begin{pmatrix} \phi_1^\pm \\ \phi_2^\pm \end{pmatrix} \tag{3.8}$$

where the mixing angle α is defined through

$$\tan 2\alpha = \tan 2\beta \, \frac{M_{A^0}^2 + M_Z^2}{M_{A^0}^2 - M_Z^2}, \quad -\frac{\pi}{2} < \alpha < 0 \tag{3.9}$$

and the masses of the gauge bosons are given in analogy with the SM:

$$M_W^2 = \frac{1}{2} g_2^2 (v_1^2 + v_2^2); \qquad M_Z^2 = \frac{1}{2}(g_1^2 + g_2^2)(v_1^2 + v_2^2); \qquad M_\gamma = 0 \tag{3.10}$$

At tree level the mass matrix of the $\mathcal{CP}$-even Higgs bosons in the $\phi_1 - \phi_2$ basis is given by

$$\begin{aligned} M_{Higgs,even}^{2,tree} &= \begin{pmatrix} m_{\phi_1}^2 & m_{\phi_1\phi_2}^2 \\ m_{\phi_1\phi_2}^2 & m_{\phi_2}^2 \end{pmatrix} \\ &= \begin{pmatrix} M_{A^0}^2 S_\beta^2 + M_Z^2 C_\beta^2 & -(M_{A^0}^2 + M_Z^2) S_\beta \, C_\beta \\ -(M_{A^0}^2 + M_Z^2) S_\beta \, C_\beta & M_{A^0}^2 C_\beta^2 + M_Z^2 S_\beta^2 \end{pmatrix} \end{aligned} \tag{3.11}$$

where $C_\beta, S_\beta = \cos(\beta), \sin(\beta)$. The mass matrix for the $\mathcal{CP}$-odd Higgs boson

is [22][3]:

$$M^{2,tree}_{Higgs,odd} = \begin{pmatrix} m^2_{\chi_1} & m^2_{\chi_1\chi_2} \\ m^2_{\chi_1\chi_2} & m^2_{\chi_2} \end{pmatrix} = \begin{pmatrix} M^2_{A^0}S^2_\beta & M^2_{A^0}\, S_\beta\, C_\beta \\ M^2_{A^0}\, S_\beta\, C_\beta & M^2_{A^0}C^2_\beta \end{pmatrix} \tag{3.12}$$

Similarly the mass matrix for the charged Higgs bosons is:

$$M^{2,tree}_{Higgs,charged} = \begin{pmatrix} m^2_{\phi_1^\pm} & m^2_{\phi_1^\pm\phi_2^\pm} \\ m^2_{\phi_1^\pm\phi_2^\pm} & m^2_{\phi_2^\pm} \end{pmatrix} = \begin{pmatrix} (M^2_{A^0}+M^2_W)S^2_\beta & (M^2_{A^0}+M^2_W)S_\beta\, C_\beta \\ (M^2_{A^0}+M^2_W)S_\beta\, C_\beta & (M^2_{A^0}+M^2_W)C^2_\beta \end{pmatrix} \tag{3.13}$$

The $\mathcal{CP}$-even Higgs mass matrix, Eq.(3.11), can be diagonalised using Eq.(3.6)to give the tree level Higgs boson masses

$$M^{2,tree}_{Higgs,even} \xrightarrow{\alpha} \begin{pmatrix} m^2_{H,tree} & 0 \\ 0 & m^2_{h,tree} \end{pmatrix} \tag{3.14}$$

The results for the tree level neutral Higgs bosons masses are

$$m^2_{H,h} = \frac{1}{2}\left[M^2_{A^0} + M^2_Z \pm \sqrt{(M^2_{A^0}+M^2_Z)^2 - 4M^2_Z M^2_{A^0} cos^2 2\beta}\right], \tag{3.15}$$

which yields an upper bound of $m_{h,tree} < M_Z$ for the lightest $\mathcal{CP}$-even Higgs boson mass. Such a value for the mass has already been experimentally excluded [23],

[3]For the benefit of the reader who is cross-referencing with ref. [22], in this thesis we work only in the real (CP-conserving) MSSM so η, the possible phase between the two Higgs doublets in ref. [22], is set to zero and hence $\bar{M}_{H^\pm}(= M_H + M_W$ in [22])$= M_{A^0}$

but because of large higher order corrections the MSSM prediction for the lightest Higgs mass is not excluded. In fact the combined effect of 1st and 2nd order corrections increases the theoretical bound to $m_h \lesssim 135$ GeV. [24]
The $\mathcal{CP}$-odd and charged Higgs boson masses can be deduced similarly by diagonalising the mass-matrices 3.12 and 3.13 using equations (3.7) and (3.8) respectively. For reference the Higgs boson masses are given by:

$$M_H^2 = \frac{1}{2}\left[M_A^2 + M_Z^2 + \sqrt{(M_A^2 + M_Z^2)^2 - 4M_A^2 M_Z^2 \cos^2 2\beta}\right] \tag{3.16}$$

$$M_{H^\pm}^2 = M_A^2 + M_W^2 \tag{3.17}$$

$$M_G^2 = M_Z^2 \tag{3.18}$$

$$M_{G^\pm}^2 = M_W^2, \tag{3.19}$$

3.1.2 The Squark Sector of the MSSM

The Squark mass term of the MSSM Lagrangian is

$$\mathcal{L}_{m_{\tilde{f}}} = -\frac{1}{2}(\tilde{f}_L^\dagger, \tilde{f}_R^\dagger)\mathbf{Z}\begin{pmatrix}\tilde{f}_L \\ \tilde{f}_R\end{pmatrix} \tag{3.20}$$

where $\mathbf{Z} = M^2_{\{\tilde{u},\tilde{d}\}}$, the mass matrices for the {u,d} type squarks. In this thesis we will be only concerned with the dominant corrections from the squark sector. At the one-loop level the dominant contribution is from the stop/sbottom sector due to the large mass-splitting between the top and bottom quarks. At two-loops, diagrams containing, for example, a squark-squark-Higgs vertex are enhanced by a factor (M_{quark}/M_W). Since the top mass is so much greater than the other quark masses contributions from the other squarks is usually negligible. The off-diagonal terms in the sbottom sector, however, are multiplied by a factor $\tan\beta$ and so for

large values of $\tan\beta$ the sbottom sector produces measurable effects. The sbottom sector is also required for SU(2) gauge invariance. We therefore restrict further discussion of the squark sector to only the stop and sbottom squarks.

The mass matrices for the stop and sbottom squarks are

$$\mathcal{M}_{\tilde{t}}^2 = \begin{pmatrix} \bar{M}_{\tilde{t}_L}^2 + \cos 2\beta(\frac{1}{2} - \frac{2}{3}s_W^2)M_Z^2 & m_t X_t \\ m_t X_t & \bar{M}_{\tilde{t}_R}^2 + \frac{2}{3}s_W^2 \cos 2\beta M_Z^2 \end{pmatrix} \tag{3.21}$$

$$\mathcal{M}_{\tilde{b}}^2 = \begin{pmatrix} \bar{M}_{\tilde{b}_L}^2 + \cos 2\beta(-\frac{1}{2} + \frac{1}{3}s_W^2)M_Z^2 & m_b X_b \\ m_b X_b & \bar{M}_{\tilde{b}_R}^2 - \frac{1}{3}s_W^2 \cos 2\beta M_Z^2 \end{pmatrix} \tag{3.22}$$

Here $\bar{M}_{\tilde{q}_{\{L;R\}}}^2 = M_{\tilde{q}_{\{L;R\}}}^2 + m_q^2$, where $M_{\tilde{q}_{\{L;R\}}}^2$ are the left- and right-handed squark masses. Also

$$X_t = A_t - \mu\ cot\beta \tag{3.23}$$

$$X_b = A_b - \mu\ tan\beta \tag{3.24}$$

where A_q are the soft-SUSY breaking trilinear couplings. Furthermore, SU(2) gauge invariance at tree level requires

$$M_{\tilde{t}_L} = M_{\tilde{b}_L} \tag{3.25}$$

In order to diagonalise the mass matrices and determine the physical mass eigenstates the following rotation is performed:

$$\begin{pmatrix} \tilde{f}_1 \\ \tilde{f}_2 \end{pmatrix} = \begin{pmatrix} \cos\theta_{\tilde{f}} & \sin\theta_{\tilde{f}} \\ -\sin\theta_{\tilde{f}} & \cos\theta_{\tilde{f}} \end{pmatrix} \begin{pmatrix} \tilde{f}_L \\ \tilde{f}_R \end{pmatrix} \tag{3.26}$$

A_f can then be written as follows

$$A_f = \frac{\sin\theta_{\tilde{f}}\cos\theta_{\tilde{f}}(m^2_{\tilde{f}_1} - m^2_{\tilde{f}_2})}{m_f} + \mu\{\cot\beta; \tan\beta\} \tag{3.27}$$

where $\{\cot\beta; \tan\beta\}$ correspond to the t,b-type squarks.

3.1.3 Charginos and Neutralinos

The chargino and neutralino part of the MSSM Lagrangian is given in ref. [25]. Here it will suffice to define their masses through the diagonalisation of the following matrices. First for charginos, the mass matrix, $\mathbf{X}$ is given by

$$\mathbf{X} = \begin{pmatrix} M_2 & \sqrt{2}M_W \sin\beta \\ \sqrt{2}M_W \cos\beta & \mu \end{pmatrix} \tag{3.28}$$

and for neutralinos, the mass matrix $\mathbf{Y}$ is given by

$$\mathbf{Y} = \begin{pmatrix} M_1 & 0 & -M_Z s_W \cos\beta & M_Z s_W \sin\beta \\ 0 & M_2 & M_Z c_W \cos\beta & -M_Z c_W \sin\beta \\ -M_Z s_W \cos\beta & M_Z c_W \cos\beta & 0 & -\mu \\ M_Z s_W \sin\beta & -M_Z c_W \sin\beta & -\mu & 0 \end{pmatrix} \tag{3.29}$$

Chapter 4

Renormalisation

*I don't do this for my health, you understand. I do it for the pain. I *LOVE* the pain!*

Professor Hugh D. Young, quoted out of context.

As explained in earlier chapters, when performing loop calculations infinities do not generally cancel and divergences have to be regularised (see section 2.3). Renormalisation is required in order to achieve a finite (physically meaningful) result. Renormalisation of many hundreds of diagrams is both technically challenging and computationally demanding and so must be done in a systematic way. Here we renormalise using counterterms and illustrate our method in the following schematic example. We use dimensional regularisation [11] for SM calculations and dimensional reduction [13] for calculations involving SUSY.

4.1 Renormalisation of higher order terms

Consider the Lagrangian

$$\mathcal{L} = A(P^2 - {M_A}^2)A \tag{4.1}$$

where A is some field with mass M_A. All parameters in the Lagrangian need to be renormalised [9] in order to be finite (physically meaningful). The field A is renormalised by

$$A \rightarrow A(1 + \frac{1}{2}\delta Z_A) \tag{4.2}$$

and the mass M_A by

$${M_A}^2 \rightarrow {M_A}^2 + \delta {M_A}^2 \tag{4.3}$$

So the Lagrangian becomes

$$\mathcal{L} \rightarrow \mathcal{L}' = \mathcal{L} + A(P^2 - {M_A}^2)A\delta Z_A - A\delta {M_A}^2 A \tag{4.4}$$

in first order of the counterterms δZ_A, $\delta {M_A}^2$.

In the on-shell scheme the mass and field renormalisation constants are given by

$$\delta {M_A}^2 = \Sigma_A(p^2 = {M_A}^2) \tag{4.5}$$

$$\delta Z_A = \frac{d\Sigma_A(p^2)}{dp}|_{p^2={M_A}^2} \tag{4.6}$$

where $\Sigma_A(p^2)$ represents the self-energy of the A field.

Since the calculations presented in this thesis are for physical (measurable) pa-

rameters, the field renormalisation parameters, δZ_A, must all cancel in the final result. For simplicity (and to save computer time) these renormalisation constants are often set to zero at an early stage.

The additional mass term $A\delta {M_A}^2 A$ in the renormalised Lagrangian, Eq. 4.4, yields a new *counterterm* propagator which has to be added to the ordinary Feynman rules and leads to a counterterm graph (see fig 4.1). For a given particle, the addition of the counterterm to the one-loop self-energy renormalises the mass. Renormalisation of a more general Lagrangian, eg. the MSSM Lagrangian, will also require vertex renormalisation and hence vertex counterterms (and vertex counterterms graphs). The renormalisation scheme and exact definition of δm^2 is

$\Sigma(p^2)$ + δm^2

Figure 4.1: Example of mass renormalisation: Self-energy + Counterterm yielding a finite mass

given as required in later chapters.

Renormalisation of two-loop self-energy diagrams, such as the example shown in figure 4.2, is performed using a similar but increasingly laborious method.

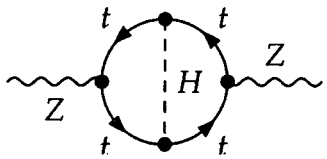

Figure 4.2: Two-loop Z Self-energy

The two-loop Z and W self-energies, such as that shown here and which will be encountered often in later chapters, can be renormalised by five counterterm diagrams as shown in figure 4.3.

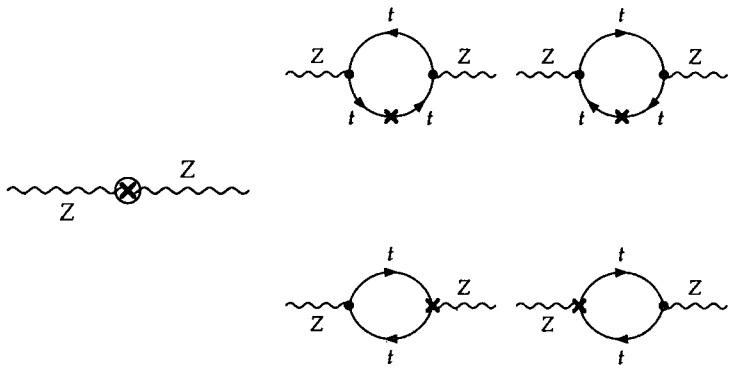

Figure 4.3: Z counterterms contributions to the two-loop self-energy

Recall that the one-loop result is finite without renormalisation. As a consequence at the renormalisation at the two-loop level only requires one-loop counterterms. The two-loop counterterm, shown on the left of figure 4.3 is not required.

4.2 Implementation of Counterterms

As explained in section 2.3, the amplitude for all diagrams are produced using *FeynArts*. Whilst the Feynman rules for SM counterterms have already been programmed in the *FeynArts* model files, the Feynman rules for SUSY counterterms have not been introduced. They have therefore been calculated explicitly and appended to the MSSM model file. We now briefly describe our approach.

4.2.1 Squark sector counterterms

Consider first the squark sector of the MSSM. We begin by renormalising the Vector boson-Squark-Squark vertices. In principle all parameters appearing in the vertex should be renormalised. Calculations presented in this thesis, however, can be of many hundreds or thousands of Feynman diagrams and expressions can be large and cumbersome. To reduce calculational complexity we systematically group the diagrams in to classes that give a contribution of a given order and consider only those class of diagrams that give a contribution of dominant order. It follows that only those parameters that give a contribution of the same order when renormalised need to be included in the renormalisation procedure. To demonstrate this we take, as an example, the Z-Stop-Stop vertex coupling, $C[\tilde{t}_{s1}, \tilde{t}_{s2}, Z]$ in the MSSM:

$$C[\tilde{t}_{s1}, \tilde{t}_{s2}, Z] = \frac{(-3 + 4S_W^2)U^{t*}_{s1,1}U^t_{s2,1} + 4S_W^2 U^{t*}_{s1,2}U^t_{s2,2}}{C_W S_W} \tag{4.7}$$

where $\tilde{t}_{[1,2]}$ represents the $\tilde{t}_1, \tilde{t}_2$ squark and $U^t_{x,y}$ is the Stop mixing matrix:

$$U^t_{x,y} = \begin{pmatrix} \cos\theta_{\tilde{t}} & \sin\theta_{\tilde{t}} \\ -\sin\theta_{\tilde{t}} & \cos\theta_{\tilde{t}} \end{pmatrix} \tag{4.8}$$

for $\theta_{\tilde{t}}$ the Stop mixing angle.

In the calculation of $\mathcal{O}(\alpha\alpha_s)$ and $\mathcal{O}(\alpha_t^2)$ yukawa contributions to $\Delta\rho$ presented in this thesis only the renormalisation of the squark masses and mixing angles produce corrections of the same order. Since these are the dominant effects the renormalisation of the electric charge, e, and Weak mixing angle, S_W, can be omitted. In the example above only the Stop mixing matrix requires renormalising.

Thus the renormalised vertex is given by

$$C[\tilde{t}_{s1}, \tilde{t}_{s2}, Z] = \frac{1}{C_W S_W} \left((-3 + 4S_W^2)(\delta U^{t^*}_{s1,1} U^t_{s2,1} + U^{t^*}_{s1,1} \delta U^t_{s2,1}) \right.$$
$$\left. + 4S_W^2 (\delta U^{t^*}_{s1,2} U^t_{s2,2} + U^{t^*}_{s1,2} \delta U_{s2,2})\right) \tag{4.9}$$

where $\delta U^t_{x,y}$ represents the renormalisation of the Stop mixing angle given by [1]

$$\theta_{\tilde{t}} \rightarrow \theta_{\tilde{t}} + \delta\theta_{\tilde{t}} \tag{4.10}$$

which leads directly to

$$\cos\theta_{\tilde{t}} \rightarrow \cos\theta_{\tilde{t}} - \sin\theta_{\tilde{t}}\delta\theta_{\tilde{t}}, \qquad \sin\theta_{\tilde{t}} \rightarrow \sin\theta_{\tilde{t}} + \cos\theta_{\tilde{t}}\delta\theta_{\tilde{t}} \tag{4.11}$$

and thus

$$\delta U^t_{x,y} = \begin{pmatrix} -\sin\theta_{\tilde{t}} & \cos\theta_{\tilde{t}} \\ -\cos\theta_{\tilde{t}} & -\sin\theta_{\tilde{t}} \end{pmatrix} \delta\theta_{\tilde{t}} \tag{4.12}$$

Equation 4.9 should also contain field renormalisation parameters but these have been omitted here for simplicity.

The squark mass-matrix renormalisation is performed in analogy with equation 4.3. In *FeynArts 3* however, Feynman rules are expressed in terms of the physical masses $M_{\tilde{f}_{1,2}}$, not the parameters $M_{\tilde{f}_{L,R}}$ which appear in the Lagrangian. The mass-matrix has therefore to be diagonalised, in accordance with Eq.(3.26), before renormalising. As a result the squark mixing renormalisation parameter $\delta\theta_{\tilde{f}}$ appears in the mass-counterterms along with the mass renormalisation constants.

[1] The renormalisation of the Sbottom mixing angle is defined in an analogous way

In this diagonal basis the squark mass-matrices become:

$$M_{\tilde{f}_{1,2}} \rightarrow M_{\tilde{f}_{1,2}} + \delta M_{\tilde{f}_{1,2}} \tag{4.13}$$

with

$$M_{\tilde{f}_{1,2}} = \begin{pmatrix} M_{\tilde{f}_1} & 0 \\ 0 & M_{\tilde{f}_2} \end{pmatrix} \tag{4.14}$$

and

$$\delta M_{\tilde{f}_{1,2}} = \begin{pmatrix} \delta M_{\tilde{f}_1} & (M^2_{\tilde{f}_1} - M^2_{\tilde{f}_2})\delta\theta_{\tilde{q}} \\ (M^2_{\tilde{f}_1} - M^2_{\tilde{f}_2})\delta\theta_{\tilde{q}} & \delta M_{\tilde{f}_2} \end{pmatrix} \tag{4.15}$$

where field renormalisation constants have again been ignored.

4.2.2 Higgs sector counterterms

Recall from section 3.1.1 that the Higgs sector of the MSSM depends on two SM parameters, M_Z and M_W, and two free MSSM parameters: M_{A^0}, $\tan\beta$. To renormalise the Higgs sector in principle all these parameters should be renormalised. Fortunately, once again the calculation can be simplified: The quantity $\Delta\rho$ is only well define in the *gauge-less limit*[2]. In this limit the vector boson masses, M_Z and M_W, are set to zero (whilst keeping the ratio M_Z/M_W fixed). Therefore the W and Z boson masses do not require renormalisation and we are left with only M_{A^0} and $\tan\beta$. In fact the renormalisation of $\tan\beta$ does not produce contributions of $\mathcal{O}(\alpha\alpha_s)$ or $\mathcal{O}(\alpha_t^2), \mathcal{O}(\alpha_t\alpha_b), \mathcal{O}(\alpha_b^2)$ and can therefore be omitted from further discussion.

[2]A full discussion of the gauge-less limit is given, as required, in later chapters

There is, however, one further complication. In section 3.1.1 it was noted that in order to reparameterise the Higgs sector in terms of M_{A^0} and $\tan\beta$ one had to make use of the minimum conditions (ie. linear terms in the neutral Higgs fields must vanish). At higher orders these linear terms are in fact the tadpole terms and must be included in the mass-matrices and thus appear in the Higgs counterterms. The full derivation of the resulting Higgs mass-matrices can be found in ref. [22]. Here we state the results, first for the neutral $\mathcal{CP}$-even Higgs boson:

$$
\begin{aligned}
M^2_{H^0,h^0} = \quad & \delta M^2_{A^0} \begin{pmatrix} (c_\beta s_\alpha - c_\alpha s_\beta)^2 & s_\beta c_\beta (s_\alpha^2 - c_\alpha^2) + s_\alpha c_\alpha (c_\beta^2 - s_\beta^2) \\ s_\beta c_\beta (s_\alpha^2 - c_\alpha^2) + s_\alpha c_\alpha (c_\beta^2 - s_\beta^2) & (c_\beta c_\alpha + s_\alpha s_\beta)^2 \end{pmatrix} \\
& + \bar{t}_1 \begin{pmatrix} -c_\beta s_\beta^2 s_\alpha^2 + 2 s_\alpha c_\alpha s_\beta^3 + c_\beta c_\alpha^2 (1 + s_\beta^2) & s_\beta^3 (c_\alpha^2 - s_\alpha^2) - s_\alpha c_\alpha c_\beta (1 + 2 s_\beta^2) \\ s_\beta^3 (c_\alpha^2 - s_\alpha^2) - s_\alpha c_\alpha c_\beta (1 + 2 s_\beta^2) & -2 c_\alpha s_\alpha s_\beta^3 + c_\beta (-c_\alpha^2 s_\beta^2 + s_\alpha^2 (1 + s_\beta^2)) \end{pmatrix} \\
& + \bar{t}_2 \begin{pmatrix} 2 c_\alpha s_\alpha c_\beta^3 - c_\alpha^2 c_\beta^2 s_\beta + s_\beta s_\alpha^2 (1 + c_\beta^2) & c_\beta^3 (c_\alpha^2 - s_\alpha^2) + s_\alpha c_\alpha s_\beta (1 + 2 c_\beta^2) \\ c_\beta^3 (c_\alpha^2 - s_\alpha^2) + s_\alpha c_\alpha s_\beta (1 + 2 c_\beta^2) & -2 c_\alpha s_\alpha c_\beta^3 + s_\beta (c_\alpha^2 (1 + c_\beta^2) - s_\alpha^2 c_\beta^2) \end{pmatrix}
\end{aligned}
\tag{4.16}
$$

where $c_\alpha = \cos\alpha$, $s_\alpha = \sin\alpha$, $c_\beta = \cos\beta$ and $s_\beta = \sin\beta$. Also $\delta M^2_{A^0}$ is the renormalisation constant for $M^2_{A^0}$ and $\bar{t}_x = t_x \frac{e}{2 s_w M_W}$ are the tadpole terms.
The neutral $\mathcal{CP}$-odd Higgs boson mass-matrix now follows:

$$
M^2_{G^0,A^0} = \begin{pmatrix} c_\beta \bar{t}_1 + s_\beta \bar{t}_2 & s_\beta \bar{t}_1 - c_\beta \bar{t}_2 \\ s_\beta \bar{t}_1 - c_\beta \bar{t}_2 & M^2_{A^0} \end{pmatrix}. \tag{4.17}
$$

And the charged Higgs boson mass-matrix is given by:

$$
M^2_{G^\pm,H^\pm} = \begin{pmatrix} c_\beta \bar{t}_1 + s_\beta \bar{t}_2 & +s_\beta \bar{t}_1 - c_\beta \bar{t}_2 \\ +s_\beta \bar{t}_1 - c_\beta \bar{t}_2 & M^2_{A^0} \end{pmatrix}. \tag{4.18}
$$

4.3 Summary

All the mathematical tools and conventions required for the calculations presented in this thesis have been illustrated in this and the previous chapters. In the following three chapters we present three independently performed calculations. Each of the calculations forms a well defined and separately renormalisable subset of the dominant two-loop contributions to $\Delta\rho$. For all calculations presented the required counterterm propagators and vertices have been derived using the methods illustrated in this chapter and appended to the MSSM model file in *FeynArts*. The renormalisation scheme and renormalisation parameters are defined in later chapters.

Chapter 5

Leading QCD Corrections to Squark Contributions to $\delta\rho$

It is a good morning exercise for a research scientist to discard a pet hypothesis every day before breakfast. It keeps him young.

Konrad Lorenz (1903 - 1989)

In the MSSM [26], the theoretical evaluation of the EWPO is not as advanced as in the SM. In order to fully exploit the experimental precision for testing the MSSM and deriving constraints on the supersymmetric parameters, it is desirable to reduce the theoretical uncertainty of the MSSM predictions to the same level as the SM uncertainties. So far, the one-loop SM contributions to Δr and $\sin^2\theta_{\rm eff}$ have been evaluated completely [27,28]. In the case of non-minimal flavour violation the leading one-loop contributions are known [29]. At the two-loop level, the leading $\mathcal{O}(\alpha\alpha_s)$ corrections to $\Delta\rho$ [30] and the gluonic two-loop corrections to Δr [19,31] are known, see Ref. [19] for a review.

The dominant gluonic $\mathcal{O}(\alpha\alpha_s)$ correction [30] is now reproduced here to provide an independent verification of the previous result and to check our calculational method[1] and numerical routines.

5.1 One-loop result

To begin, the one-loop result is presented for reference. Within the MSSM the dominant correction to $\Delta\rho$ from SUSY particles at the one-loop level arises from the scalar top and bottom contribution, shown in fig. 5.1. Even at the one-loop level the number of MSSM diagrams to be calculated is significantly greater than in the SM as a consequence of the larger particle spectrum and possible combinations of sparticles within loops.

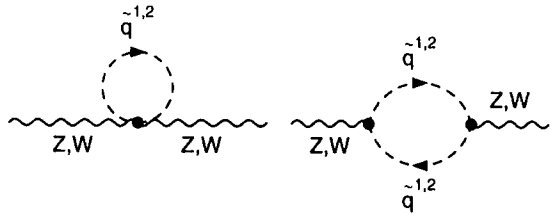

Figure 5.1: One-loop Z,W Vector Boson self Energies in the MSSM. Here V represents a Z or W boson, $\tilde{q}$ represents a stop or sbottom squark.

5.1.1 Analytical result

As in the SM, the result is finite without renormalisation as a consequence of the same custodial symmetry. We have explicitly checked that the result is analytically

[1] In ref. [30] the amplitudes were generated using *FeynArts 2.0* [14] (FA2), which performs calculations in the $\tilde{q}_{L,R}$ basis in the squark sector (ie. using Lagrangian parameters). Here we use FA3, where the Feynman rules are written in terms of the mass eigenstates. The calculation presented here also provides a consistency check between the two versions.

identical to that in ref. [32] and is given by equation (5.1). The behaviour of this result is now examined for some common SUSY scenarios.

$$\begin{aligned}\Delta\rho^{\mathrm{SUSY}}_{One-Loop} = \frac{3\,G_\mu}{8\sqrt{2}\,\pi^2}\Big[&- \sin^2\theta_{\tilde{t}}\cos^2\theta_{\tilde{t}}F_0(m^2_{\tilde{t}_1},m^2_{\tilde{t}_2}) - \sin^2\theta_{\tilde{b}}\cos^2\theta_{\tilde{b}}F_0(m^2_{\tilde{b}_1},m^2_{\tilde{b}_2}) \\ &+ \cos^2\theta_{\tilde{t}}\cos^2\theta_{\tilde{b}}F_0(m^2_{\tilde{t}_1},m^2_{\tilde{b}_1}) + \cos^2\theta_{\tilde{t}}\sin^2\theta_{\tilde{b}}F_0(m^2_{\tilde{t}_1},m^2_{\tilde{b}_2}) \\ &+ \sin^2\theta_{\tilde{t}}\cos^2\theta_{\tilde{b}}F_0(m^2_{\tilde{t}_2},m^2_{\tilde{b}_1}) + \sin^2\theta_{\tilde{t}}\sin^2\theta_{\tilde{b}}F_0(m^2_{\tilde{t}_2},m^2_{\tilde{b}_2})\Big]\end{aligned} \tag{5.1}$$

Here $m_{\tilde{t}_i}, m_{\tilde{b}_i}(i = 1,2)$ denote the stop and sbottom masses; $\theta_{\tilde{t}}, \theta_{\tilde{b}}$ are the mixing angles in the stop and in the sbottom sector. G_μ is the Fermi constant. F_0 was defined in chapter 2.

Yet to be enforced is the SU(2) gauge relation, Eq.3.25, which reduces the number of free SUSY parameters from 6 (4 masses and 2 mixing angles) to 5 by setting $\tilde{t}_L = \tilde{b}_L = M_{Q_L}$.

We analyse the result for different mass and mixing scenarios. In principle those scenarios which show the greatest contrast in results (ie. those scenarios that give the extreme values for $\Delta\rho$) are of most interest since they show the limits of the $\Delta\rho$ corrections from the MSSM. As we shall now see, however, it is not always trivial to infer these values of the SUSY parameters.

To begin we look at the Squark mass matrices given in chapter 2. There are three free parameters in the stop sector, which may be chosen as $M_{\tilde{t}_1}$,$M_{\tilde{t}_2}$ and X_t. Using equations 3.23 and 3.27 we can rewrite X_t as

$$X_t = \frac{\sin\theta_{\tilde{t}}\cos\theta_{\tilde{t}}(m^2_{\tilde{t}_1} - m^2_{\tilde{t}_2})}{m_t} \tag{5.2}$$

By forming a rotation matrix from the normalised eigenvectors of the stop-mass matrix (3.21) and equating with the rotation matrix (3.26) X_t can conveniently

be rewritten in terms of $M^2_{\tilde{t}_L}$, $M^2_{\tilde{t}_R}$ and $\sin\theta_{\tilde{t}}$

$$X_t = \frac{\sin\theta_{\tilde{t}}\ \cos\theta_{\tilde{t}}\ (6M^2_{\tilde{t}_R} - 6M^2_{\tilde{t}_L} + (-3 + 8S^2_W)M^2_Z\cos(2\beta))}{6m_t(1 - 2\sin^2\theta_{\tilde{t}})} \tag{5.3}$$

The behaviour of X_t against $\sin\theta_{\tilde{t}}$ is shown in fig. 5.2 for the case when $M^2_{\tilde{t}_R} = M^2_{\tilde{t}_L}$ (a commonly used simplification when performing numerical analysis). Notice that X_t diverges as $\sin\theta_{\tilde{t}}$ approaches $\frac{1}{\sqrt{2}}$. This is the region referred to as 'maximal mixing' in ref [30]. Here we will consider the same scenario to allow direct comparison of our result, thus verifying our numerical routines before analysing the (more complex) two-loop contribution.

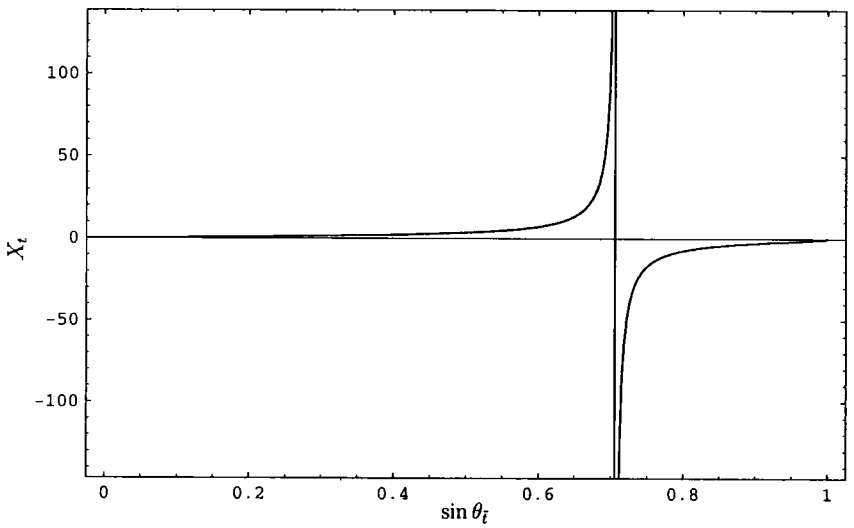

Figure 5.2: X_t (GeV) against $\sin\theta_{\tilde{t}}$ for $M_{\tilde{t}_L} = M_{\tilde{t}_R}$, $m_t = 175$ GeV and $\tan\beta = 1.6$

Evaluating the $\Delta\rho$ result at $\sin\theta_{\tilde{t}} = \frac{1}{\sqrt{2}}$ is not straight forward. From equation 5.3 we see the the divergence of X_t only disappears if the numerator is equal to zero, ie. the off diagonal terms in the squark mass-matrix are zero and thus the mixing angle is $\frac{\pi}{4}$ ($\sin\theta_{\tilde{t}} \rightarrow \frac{1}{\sqrt{2}}$)[2]. Therefore, where appropriate, X_t is used as an input

[2]In fact the mass-matrix will only produce a rotation matrix with $\sin\theta_{\tilde{t}} = \frac{1}{\sqrt{2}}$ if it is diagonal and the diagonal elements are equal.

parameter rather than $\sin\theta_{\tilde{t}}$. The (arbitrary) value of $X_t = 200$ GeV, chosen in ref [30], gives an approximation in the region where $\sin\theta_{\tilde{t}} \to \frac{1}{\sqrt{2}}$.

5.1.2 Numerical analysis at one-loop

In Figures 5.3 and 5.5 we display the one-loop correction to ρ from the $\tilde{t}, \tilde{b}$ isodoublet. For comparison with ref. [30] we plot the result against M_Q (defined below) and $\sin\theta_{\tilde{t}}$ in the same scenarios. The scalar squark masses are assumed to be equal for simplicity: $M_{\tilde{t}_L} = M_{\tilde{t}_R} = M_{\tilde{b}_L} = M_{\tilde{b}_R} = M_Q$. In this limit equation 5.3 implies $\sin\theta_{\tilde{t}} \neq \frac{1}{\sqrt{2}}$ unless $M_Z = 0$. Here, however, we have set M_Z to its experimental value of 91.187 GeV. As we will show, deviations from this M_Q choice can be large. For illustration in ref. [30] $\tan\beta$ is set equal to 1.6 but since X^t (not A_t and μ) is used as the input parameter, analysis depends only marginally on $\tan\beta$. For large values $\tan\beta \sim m_t/m_b$, the mixing in the sbottom sector should be taken into account. It was observed in ref. [30] that due to the comparatively small b-quark mass the effect from large $\tan\beta$ and large off-diagonal (X_b) terms in the sbottom sector on the one-loop result is barely noticeable. We have checked that varying the value of $\tan\beta$ produces almost indistinguishable results. Here and throughout this chapter we use $m_t = 175$ GeV and $m_b = 4$ GeV.

Figure 5.3 shows the one-loop correction against M_Q for $X_t = 0$ and 200 GeV. As the value of $X_t = 200$ GeV is only an arbitrary approximation in the limit as $\sin\theta_{\tilde{t}} \to \frac{1}{\sqrt{2}}$ we also give the correction for $X_t = 500$ GeV. The corrections grow rather large for small values of M_Q, exceeding the current level of experimental sensitivity of approximately $\Delta\rho \lesssim 2 \times 10^{-3}$ [19][3]. Conversely the corrections become small for large values of the SUSY parameters as SUSY decouples from

[3]The experimental results for $\Delta\rho$ are not given in [19] but bounds on δM_W and $\delta \sin^2\theta_{\text{eff}}$ appear. Bounds on $\Delta\rho$ can be inferred using Eq.2.10.

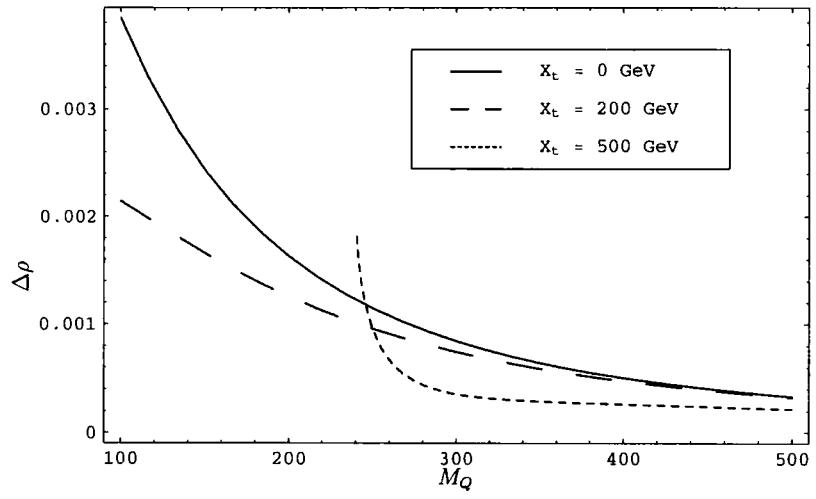

Figure 5.3: $\Delta\rho$ at one-loop against $M_Q = M_{\tilde{t}_L} = M_{\tilde{t}_R} = M_{\tilde{b}_L} = M_{\tilde{b}_R}$, $m_t = 175$ GeV and $\tan\beta = 1.6$. The correction is given for $X_t = 0, 200$ and 500 GeV. $X_b = 0$.

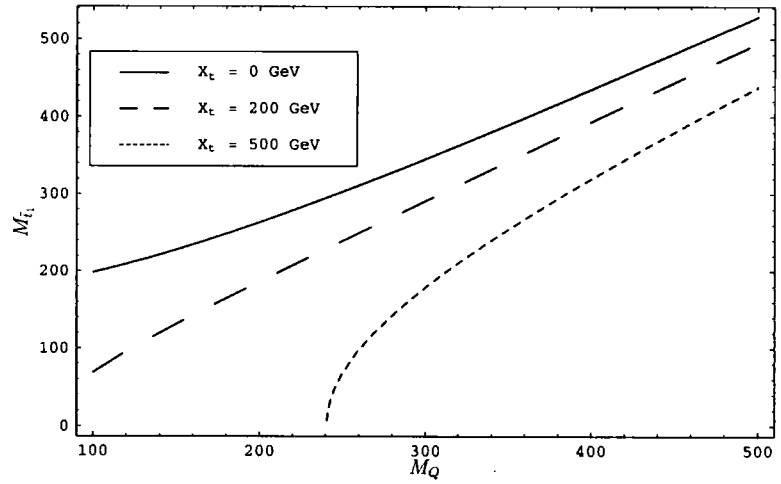

Figure 5.4: $M_{\tilde{t}_1}$ against M_Q in the same scenario as fig 5.3. The correction is given for $X_t = 0, 200$ and 500 GeV

the SM.

The correction for $X_t = 500$ GeV in fig. 5.3 stops abruptly at $M_Q \simeq 250$ GeV. This can be explained by looking at fig. 5.4, which shows the how the $\tilde{t}_1$ mass varies with M_Q in the same scenario. At $M_Q \simeq 250$ GeV for $X_t = 500$ GeV the $\tilde{t}_1$ mass falls to zero (all other squark masses stay above 100 GeV in this

region of the parameter space). Since the experimental lower bound for SUSY particles is $\mathcal{O}(100)$ GeV, the $X_t = 500$ GeV correction has already been excluded for $M_Q < 300$ GeV. In fact the correction for $X_t = 200$ GeV is also excluded for $M_Q \lesssim 150$ GeV. Thus when the simplification $M_Q (= M_{\tilde{t}_L} = M_{\tilde{t}_R} = M_{\tilde{b}_L} = M_{\tilde{b}_R})$ is used as an input variable, care must be taken to avoid regions of the parameter space that produce experimentally excluded physical parameters.

The behaviour of $\Delta\rho$ against $\sin\theta_{\tilde{t}}$, shown in figure 5.5 for three values of $M_Q = 150, 250$ and 500 GeV, is practically flat except in the region $\sin\theta_{\tilde{t}} \sim \frac{-1}{\sqrt{2}}$, where the off-diagonal terms in the stop-mass matrix become large. In this region the behaviour is less clear so the same result is replotted in figure 5.6 against X_t (in this scenario figure 5.6 is merely just a rescaling of the x-axis in the region of $sin\theta_{\tilde{t}} \to \frac{1}{\sqrt{2}}$). The latter plot shows that for $M_Q = 500$ GeV and large off-diagonal elements in the Stop-mass matrix, the corrections to $\Delta\rho$ become very large and again are experimentally excluded. This is in contrast to fig. 5.3 where for large M_Q (but not quite so large X_t) the SUSY contributions decouple. As a final remark we note that for small values of M_Q in figure 5.6 the curve showing the contribution to $\Delta\rho$ again abruptly stop as $M_{\tilde{t}_1} \to 0$ in the corresponding region of X_t.

Both figures 5.3 and 5.5 agree[4] with those published in ref. [30].

We now briefly examine the case when we allow the left and right squark masses to be different. As stated in chapter 3, the SU(2) gauge symmetry enforces the relation $M^2_{\tilde{t}_L} = M^2_{\tilde{b}_L} = M^2_{Q_L}$. For convenience we also use $M^2_{\tilde{t}_R} = M^2_{\tilde{b}_R} = M^2_{Q_R}$. We set $M_{Q_L} = 500$ GeV. Here again $\tan\beta = 1.6$ so sbottom mixing produces negligible effects ($\sin\theta_{\tilde{b}}$ set to zero). The result is plotted in figure 5.7. Note that throughout the parameter space considered here, with the choice of $M_{Q_R} \neq M_{Q_L}$

[4]The small numerical differences with [30] are due to slight differences in the values of M_W, M_Z, and α_s used here.

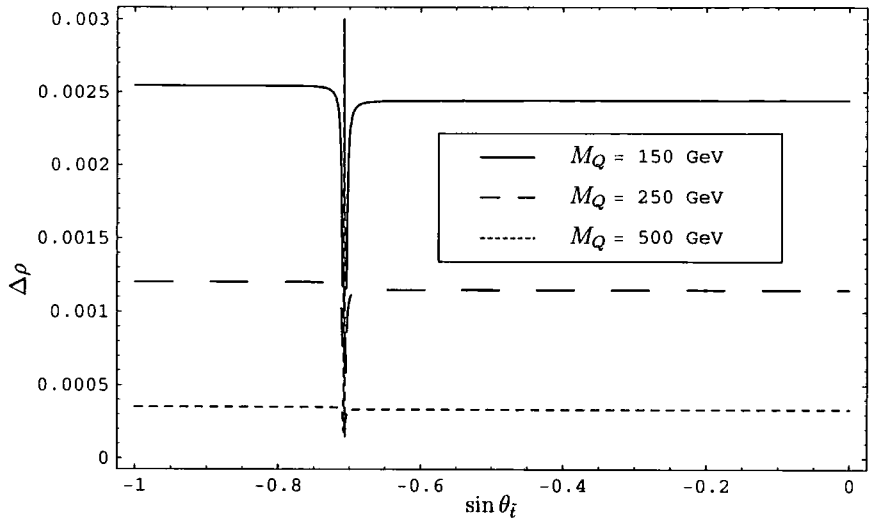

Figure 5.5: $\Delta\rho$ at one-loop against $\sin\theta_{\tilde{t}}$ for $m_t = 175$ GeV and $\tan\beta = 1.6$ The correction is given for $M_Q = 0, 250$ and 500 GeV

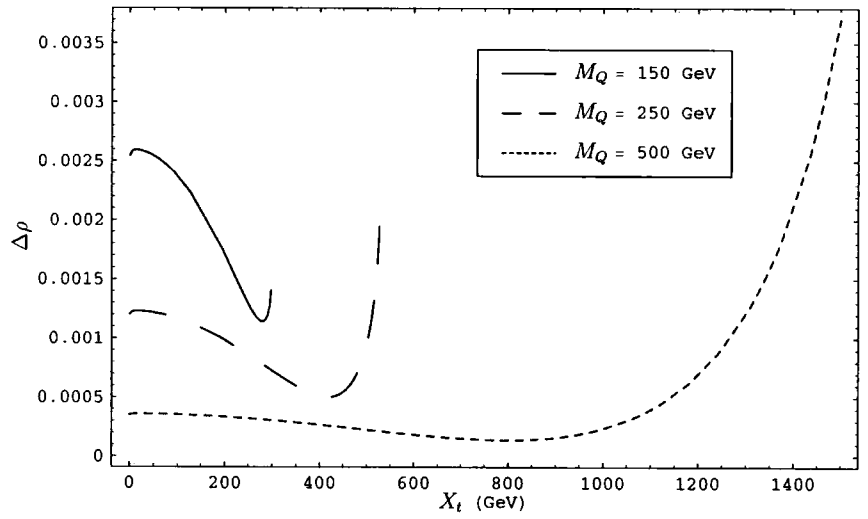

Figure 5.6: $\Delta\rho$ at one-loop against X_t for the same parameters as in fig.5.5 . This is merely a rescaling of fig.5.5, enlarging the region around $\sin\theta_{\tilde{t}} \sim \frac{-1}{\sqrt{2}}$

all physical squark masses are $> \mathcal{O}(100$ GeV) (ie. above the lower experimental bound).

One complication that arises when $M_{Q_R} \neq M_{Q_L}$ is in the definition of the squark rotation matrices (Eq.3.26). The problem is most clearly evident in the limit

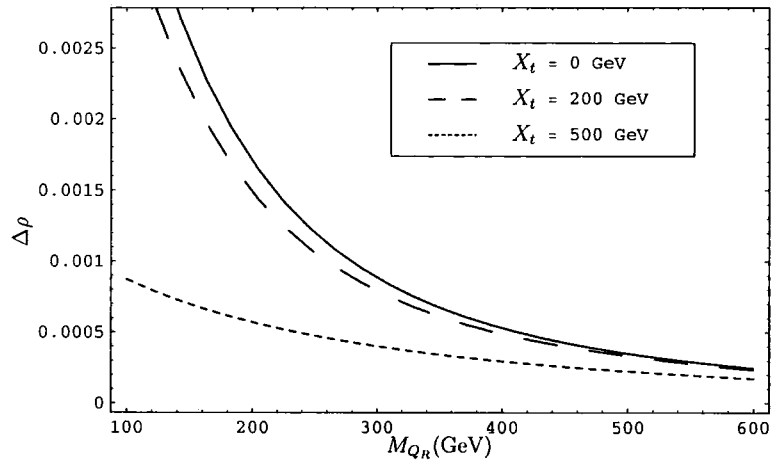

Figure 5.7: $\Delta\rho$ at one-loop against $M_{Q_R} = M_{\tilde{t}_R} = M_{\tilde{b}_R}$ for $M_{\tilde{t}_L} = M_{\tilde{b}_L} = 500\ GeV$ $\tan\beta = 1.6$

$X_{t,b} \to 0$ (referred to as the 'no mixing' case in ref. [30]), where the squark mass-matrices are diagonal. One has a choice as to how to define the rotation matrices, since both

$$\begin{pmatrix} 1 & 0 \\ 0 & 1 \end{pmatrix} \text{ and } \begin{pmatrix} 0 & -1 \\ 1 & 0 \end{pmatrix} \tag{5.4}$$

will diagonalise the squark mass-matrices in the no-mixing limit (the former corresponds to a mixing angle = 0, the latter to $\frac{-\pi}{2}$). The latter matrix has the effect of swapping $\tilde{f}_1$ and $\tilde{f}_2$. One could redefine $\tilde{f}_1(\tilde{f}_2)$ such that $\tilde{f}_1(\tilde{f}_2)$ has the greater (smaller) mass. Given our derivation of equation 5.3 however, it is more convenient to rewrite $\sin\theta_{\tilde{t}}, \sin\theta_{\tilde{b}}$ in terms of $X_{t,b}$ everywhere in the result for $\Delta\rho$. Whilst the freedom to choose $\sin\theta_{\tilde{t}}, \sin\theta_{\tilde{b}}$ etc. as free parameters is lost, the ordering of $\tilde{f}_1$ and $\tilde{f}_2$ is automatically taken care of. The implication for the squark masses is that $M_{\tilde{f}_1} > M_{\tilde{f}_2}$.

Figure 5.7 can be directly compared with 5.3. The results manifestly coincide at

$M_{Q_L} = M_{Q_R} = 500$ GeV. The behaviour is not significantly different except for the case where M_{Q_R} is small and X_t is large (ie. the lowest curve in fig 5.7). In this scenario lowest stop mass, $M_{\tilde{t}_2}$, stays well above zero and curve shows smooth behaviour (unlike the abrupt stop already discussed in fig. 5.3). This is reassuring since without moderate fine-tuning, it is likely that $M_{Q_L} \neq M_{Q_R}$.

5.2 Two-loop calculation

Having reviewed the one-loop result we now discuss the two-loop calculation. The dominant two-loop correction within the SM of $\mathcal{O}(\alpha\alpha_s)$ is given by [33]

$$\Delta\rho^{\mathrm{SM},\alpha\alpha_s}_{\mathrm{2-loop}} = -\Delta\rho^{\mathrm{SM}}_{\mathrm{1-loop}} \frac{2}{3}\frac{\alpha_s}{\pi}\left(1+\pi^2/3\right). \tag{5.5}$$

It screens the one-loop result by approximately 10%.

In the MSSM at the two-loop level there are many thousands of diagrams making a full calculation too laborious and (computer-) time consuming. To overcome this problem we split the calculation into separately renormalisable classes; each class giving a contribution of a given order. We then concentrate on those classes that will give dominant contributions. To begin we calculate the contribution from the squark-gluon loops, of $\mathcal{O}(\alpha\alpha_s)$. A complete and detailed analysis of this contribution can be found in ref. [30].

5.2.1 Renormalisation

The diagrams that contribute are shown in figure 5.8.[5] The counterterm diagrams and insertions required in order to renormalise these two-loop diagrams are shown

[5]Two-loop diagrams containing a squark, a quark and a gluino as internal particles will also give a contribution of $\mathcal{O}(\alpha\alpha_s)$ as shown in ref. [30]. The gluino contribution yields a finite result

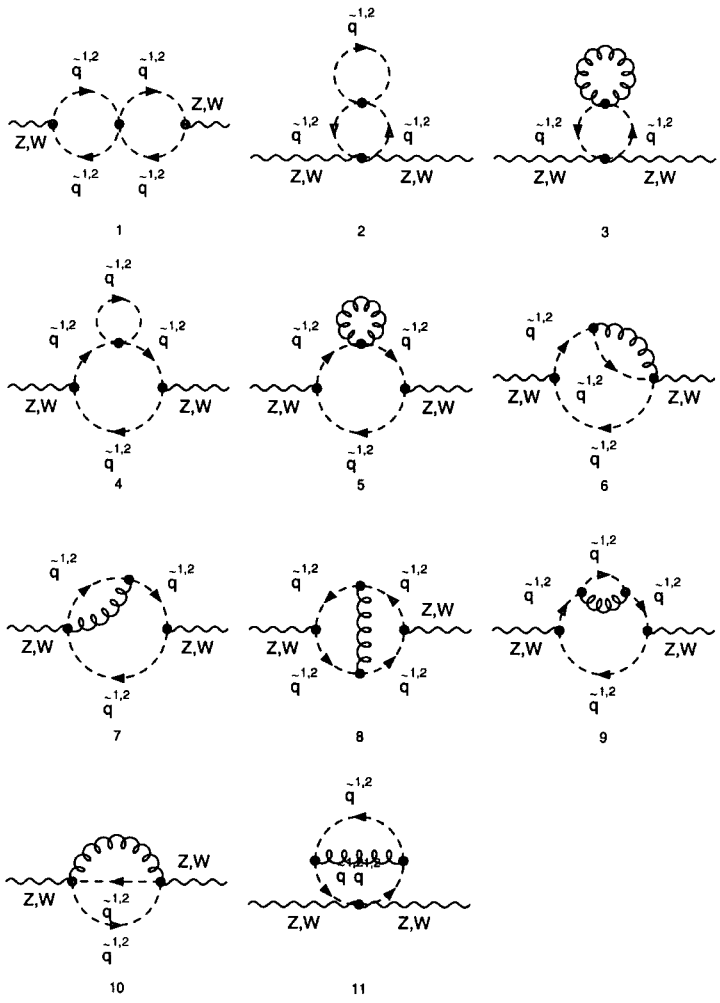

Figure 5.8: Two-loop Z,W self-energy diagrams for the contribution of squark loops to $\Delta\rho$ at $\mathcal{O}(\alpha\alpha_s)$. $\tilde{q}^{1,2} = \tilde{t}_{1,2}/\tilde{b}_{1,2}$ squark.

in figure 5.9. For gluon exchange contributions only squark loops are included here, since gluon exchange in quark loops is just the SM contribution, yielding the result in Eq.5.5. Before calculating these diagrams in full there are a number of simplifications that can be made:

(i) To isolate the contributions of $\mathcal{O}(\alpha\alpha_s)$ the yukawa and electroweak couplings are set to zero in the four squark vertex.

separately and is not reproduced here (although full numerical analysis of the $\mathcal{O}(\alpha\alpha_s)$ result should include the gluino contribution).

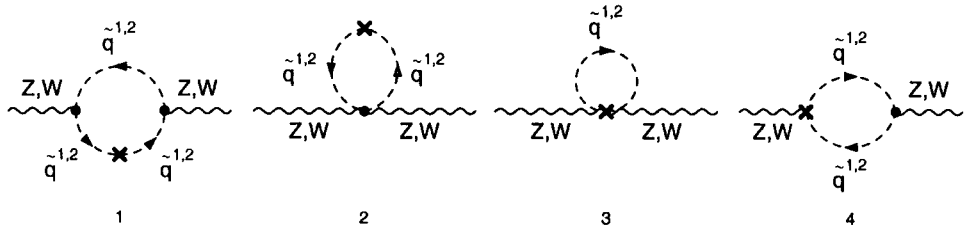

Figure 5.9: Z,W Counterterm diagrams of $\mathcal{O}(\alpha\alpha_s)$ for $\Delta\rho$. $\tilde{q}^{1,2} = \tilde{t}^{1,2}$ or $\tilde{b}^{1,2}$.

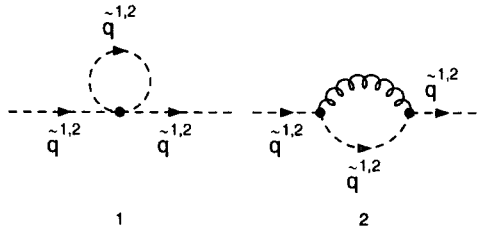

Figure 5.10: Counterterm insertions of $\mathcal{O}(\alpha\alpha_s)$ for $\Delta\rho$. $\tilde{q}^{1,2} = \tilde{t}^{1,2}$ or $\tilde{b}^{1,2}$

(ii) Diagram 1 in figure 5.8 only gives rise to longitudinal modes, which do not contribute to the transverse self-energy.

(iii) Two-loop self-energy diagrams 2 and 4 contain a squark loop sitting on top of another squark loop. Contributions from these two classes of diagram will be cancelled by the counterterm diagrams 1 and 2 (figure 5.9) with squark-loop insertion diagram 1 (figure 5.10). This is because contributions from the 'upper' loop must be independent of the incoming momentum at the four-squark vertex in order to satisfy momentum conservation at this vertex. The counterterm will give rise to exactly the same expression but with the incoming momentum set (eg. in the OnShell scheme) to $p^2 = M_{\tilde{q}}^2$. But having argued that the contribution is independent of the incoming momentum the cancellation is manifest. Since we are, however, performing this calculation in part to verify our method, this result has been explicitly checked.[6]

[6]The squark loop insertion into the vertex counterterms are part of the gluino renormalisation, so do not appear here.

(iv) Diagrams 3 and 5 would not contribute for exactly the same reason as for diagrams 2 and 4 given above were it not for the fact that they both contain a massless gluon loop, giving rise to a scaleless integral. They are manifestly zero and thus we do not include them in the counterterm insertions.

(v) It has been argued that only the second counterterm insertion in figure 5.10 will contribute. Note that there is no $\tilde{q}_1 - \tilde{q}_2 -$ gluon (squark-mixing) vertex giving rise to the counterterm insertion required for renormalising the mixing angle. It is manifest that renormalisation of the squark-mixing angles do not appear in this calculation. A final simplification can then be made by noticing that the vertex counterterms (diagrams 3 and 4 in figure 5.9) only renormalise the squark mixing angles[7] (as opposed to the masses). As there is no renormalisation of the mixing angles, these vertex-counterterm diagrams also do not contribute and need not be calculated.

The results presented here are precisely the same in dimensional regularisation and dimensional reduction, although intermediate unphysical results can (and do) differ. The renormalisation procedure is as follows. We work in the on-shell scheme where the squark masses are defined as the real part of the pole of the corresponding propagators:

$$\delta m^2_{\tilde{f}_i} = \Sigma_{\tilde{f}_i}(m^2_{\tilde{f}_i}) \qquad \text{for } \tilde{f}_i = \tilde{t}_{1,2}, \tilde{b}_{1,2}. \tag{5.6}$$

This definition of the renormalisation constants breaks the SUSY relation Eq.3.25, which requires one of the renormalisation constants to be expressed in terms of the other three (and top and bottom renormalisation constants). The definition above was used initially in ref. [30], however, and will suffice to check our calculation without unnecessary complication of introducing further relations and renormali-

[7] We omit the field renormalisation constants (see later)

sation constants.

In addition, a prescription for the renormalisation of the squark mixing angle is required:

$$\delta\theta_{\tilde{q}}(p^2) = \frac{1}{m^2_{\tilde{q}1} - m^2_{\tilde{q}2}} \Pi_{\tilde{q}1\tilde{q}2}(p^2) \tag{5.7}$$

The renormalisation of the mixing angle is defined to vanish at a given momentum-transfer, p^2. Here we choose $p^2 = M^2_{\tilde{q}_1}$ to allow comparison with ref. [30]. This means that for this value of p^2 the squark masses do not mix but propagate independently. One could choose set p^2 to equal the $\tilde{q}_2$ mass but in practise the numerical result differs only slightly with p^2.

Finally, one ought to include definitions of the field renormalisation constants. However, since none of the internal fields exist in the final state, all these parameters must drop out in the final calculation. This was verified in ref. [30]. Here, to save computing-time, the field renormalisation constants are omitted from the start.

5.2.2 Numerical Analysis

The full result for the gluon contribution has been calculated and is analytically identical to the result given in ref [32]

$$\begin{aligned}\Delta\rho^{gluon}_{2-Loop} = \frac{G_\mu}{4\sqrt{2}\,\pi^2}\frac{\alpha_s}{\pi}\Big[&- \sin^2\theta_{\tilde{t}}\cos^2\theta_{\tilde{t}}F_1(m^2_{\tilde{t}_1}, m^2_{\tilde{t}_2}) - \sin^2\theta_{\tilde{b}}\cos^2\theta_{\tilde{b}}F_1(m^2_{\tilde{b}_1}, m^2_{\tilde{b}_2}) \\ &+ \cos^2\theta_{\tilde{t}}\cos^2\theta_{\tilde{b}}F_1(m^2_{\tilde{t}_1}, m^2_{\tilde{b}_1}) + \cos^2\theta_{\tilde{t}}\sin^2\theta_{\tilde{b}}F_1(m^2_{\tilde{t}_1}, m^2_{\tilde{b}_2}) \\ &+ \sin^2\theta_{\tilde{t}}\cos^2\theta_{\tilde{b}}F_1(m^2_{\tilde{t}_2}, m^2_{\tilde{b}_1}) + \sin^2\theta_{\tilde{t}}\sin^2\theta_{\tilde{b}}F_1(m^2_{\tilde{t}_2}, m^2_{\tilde{b}_2})\Big]\end{aligned} \tag{5.8}$$

with

$$F_1(x,y) = x+y-2\frac{xy}{x-y}log\frac{x}{y}\left[2+\frac{x}{y}ln\frac{x}{y}\right] + \frac{(x+y)x^2}{(x-y)^2}log^2\frac{x}{y} - 2(x-y)Li_2(1-\frac{x}{y}) \quad (5.9)$$

where F_1 has the following properties: $F_1(m_a^2,m_b^2) = F_1(m_b^2,m_a^2)$, $F_1(m^2,m^2) = 0$, $F_1(m^2,0) = m^2(1+\frac{\pi^2}{3})$. Li_2 is defined in appendix A.

Figures 5.11, 5.12 and 5.13 show the two-loop gluon result for $\Delta\rho$.

Figure 5.11 shows the result against the common squark mass M_Q for the same scenario as the one-loop result shown in 5.3. This plot is shown in ref. [30] and is reproduced here again as a check. The behaviour is similar to the one-loop result and the two-loop result increase the one-loop contribution by up to 35% . This is certainly a measurable effect and justifies further analysis at the two-loop level.

Figure 5.12 shows the two-loop result plotted against M_{Q_R} (the right-handed squark mass) with $M_{Q_L} = 500$ GeV, ie. the same scenario as for the one-loop result in figure 5.7. In figure 5.13 we show the behaviour for large $\tan\beta = 40$ where effects from the sbottom-mixing are most noticeable ($X_b = 2000$ GeV). In fact the result barely changes from that shown in figure 5.12, justifying the decision to ignore the sbottom mixing until now.

Figure 5.14 shows the two-loop result against X_t in the same scenario as the one-loop result in figure 5.6 Once again the behaviour is similar to the one-loop result and increases the contribution by around 10%.

Finally, we now go beyond the scenario considered in [30] and examine the behaviour of $\Delta\rho$ against X_b for large $\tan\beta = 40$. The result is shown in figure 5.16 for common squark mass $M_Q = 250$ GeV. The result has been plotted over a much larger range than for X_t (fig. 5.14) in order to show a significant change in $\Delta\rho$.

For small X_t the result for $\Delta\rho$ seems to diverge for large X_b (much larger than required for X_t in fig. 5.14) but falls to zero for $X_t = 500$ GeV, although the curve may diverge for even larger X_b than is plotted here. To examine the behaviour further we rewrite $X_{t,b}$ using equations 3.23 and 3.23 and re-plot the result against $\tan\beta$ for $A_t = A_b = 500$ GeV and for three values of μ (equivalent to varying both X_t and X_b together).

The curves in fig. 5.16 show a marked difference for each value of μ. For larger μ the result diverges. One would expect similar behaviour for $\mu = 200$ GeV in the very large $\tan\beta$ range (going beyond the experimental bounds on $\tan\beta$).

5.3 Chapter summary

In this chapter we have independently verified the dominant gluon contributions to $\Delta\rho$ in the MSSM. The result is the same as that given in ref. [30]. This agreement not only confirms the previous result but serves as a check for our squark counterterm additions to the *FeynArts* code. Contrary to the SM case, these corrections can enter with the same sign as the one-loop result, therefore enhancing the sensitivity to the squark effects. The behaviour of the result is examined for several new scenarios.

In the next two chapters dominant quark and squark Yukawa contributions are presented.

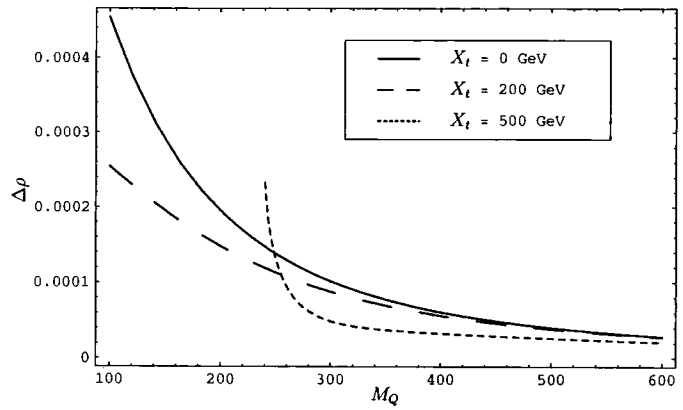

Figure 5.11: $\Delta\rho$ at two-loops against $M_Q = M_{\tilde{t}_L} = M_{\tilde{t}_R} = M_{\tilde{b}_L} = M_{\tilde{b}_R}$, $m_t = 175$ GeV and $\tan\beta = 1.6$. The correction is given for $X_t = 0, 200$ and 500 GeV.

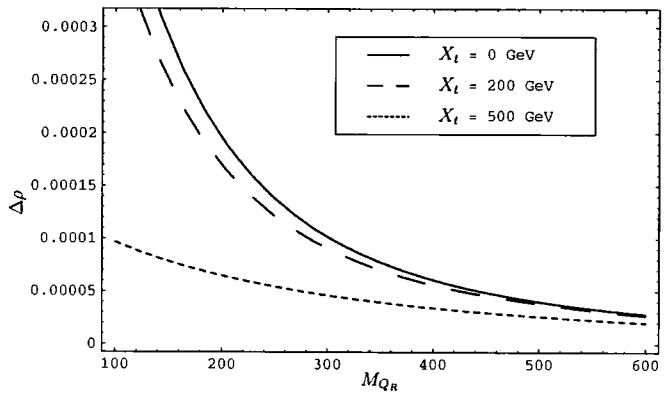

Figure 5.12: $\Delta\rho$ at two-loops against $M_{Q_R} = M_{\tilde{t}_R} = M_{\tilde{b}_R}$ for $M_{\tilde{t}_L} = M_{\tilde{b}_L} = 500$ GeV, $m_t = 175$ GeV and $\tan\beta = 1.6$. The correction is given for $X_t = 0, 200$ and 500 GeV.

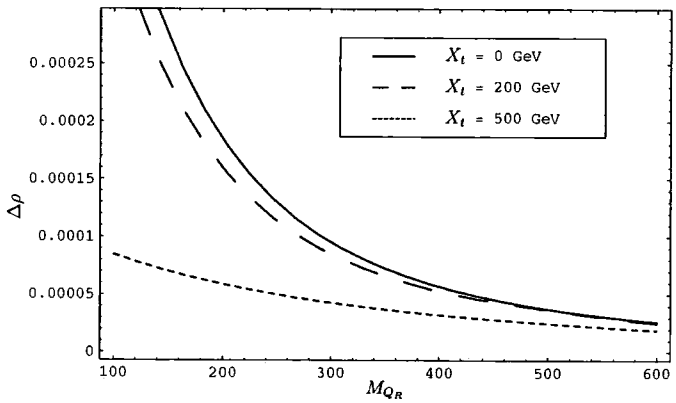

Figure 5.13: $\Delta\rho$ at two-loops against $M_{Q_R} = M_{\tilde{t}_R} = M_{\tilde{b}_R}$ for $M_{\tilde{t}_L} = M_{\tilde{b}_L} = 500$ GeV, $m_t = 175$ GeV and $\tan\beta = 40, X_b = 2000$ GeV. The correction is given for $X_t = 0, 200$ and 500 GeV.

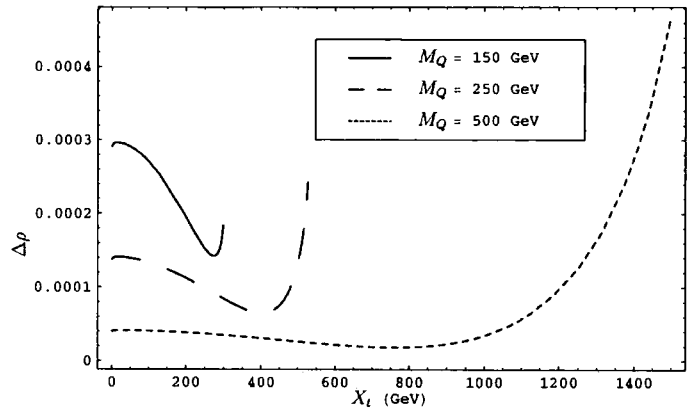

Figure 5.14: $\Delta\rho$ at two-loops against X_t for $M_Q(= M_{\tilde{t}_L} = M_{\tilde{t}_R} = M_{\tilde{b}_L} = M_{\tilde{b}_R}) =$ 150, 250and500 GeV, $m_t = 175$ GeV and $\tan\beta = 1.6$.

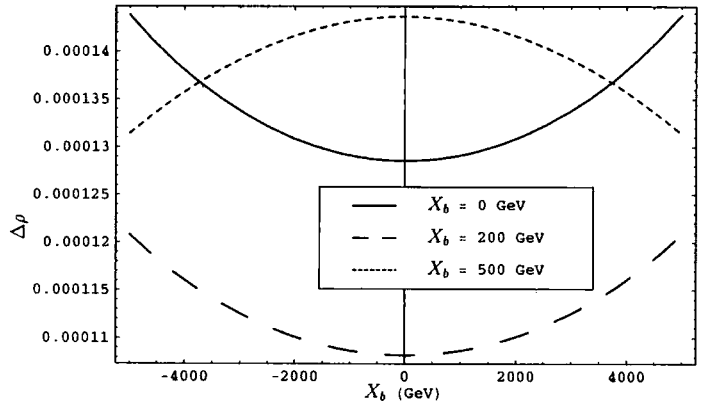

Figure 5.15: $\Delta\rho$ at two-loops against X_b for $M_Q(= M_{\tilde{t}_L} = M_{\tilde{t}_R} = M_{\tilde{b}_L} = M_{\tilde{b}_R}) =$ 250GeV, $m_t = 175$ GeV and $\tan\beta = 40$.

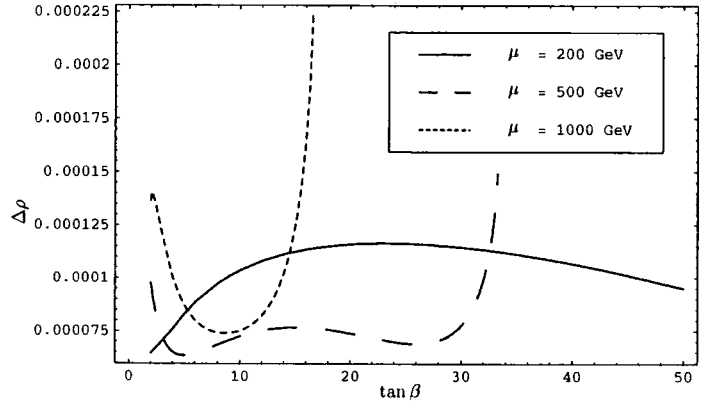

Figure 5.16: $\Delta\rho$ at two-loops against $\tan\beta$ for $M_Q(= M_{\tilde{t}_L} = M_{\tilde{t}_R} = M_{\tilde{b}_L} = M_{\tilde{b}_R}) =$ 250 GeV, $m_t = 175$ GeV. $A_t = A_b = 500$ GeV

Chapter 6

Leading Electroweak corrections to $\Delta\rho$ (part I)

What we call 'Progress' is the exchange of one nuisance for another nuisance

Havelock Ellis (1859 - 1939)

In this and the following chapter we calculate the two-loop MSSM corrections to the EWPO that enter via $\Delta\rho$ at $\mathcal{O}(\alpha_t^2)$, $\mathcal{O}(\alpha_t\alpha_b)$, $\mathcal{O}(\alpha_b^2)$. These are the leading two-loop contributions involving the top and bottom Yukawa couplings and come from three classes of diagrams with quark/squark loop and additional Higgs or Higgsino exchange (sample diagrams for the three classes are shown in Fig. 6.1). These contributions are of particular interest, since they involve corrections proportional to m_t^4 and bottom loop corrections enhanced by $\tan\beta$, the ratio of the vacuum expectation values of the two Higgs doublets of the MSSM.

As a first step, in Ref. [32] the $\mathcal{O}(\alpha_t^2)$, $\mathcal{O}(\alpha_t\alpha_b)$, $\mathcal{O}(\alpha_b^2)$ corrections were calculated in the limit where the scalar quarks are heavy, corresponding to taking into account

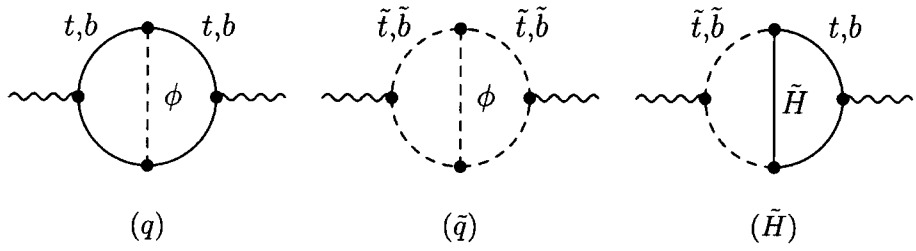

Figure 6.1: Sample diagrams for the three classes of contributions to $\Delta\rho$ considered in this thesis: (q) quark loop with Higgs exchange, $(\tilde{q})$ squark loop with Higgs exchange, $(\tilde{H})$ quark/squark loop with Higgsino exchange. ϕ denotes Higgs and Goldstone boson exchange.

quark/Higgs diagrams (class (q)) only. This result is once again reproduced here for several reasons: To verify the result given in [32]; to check our addition to the *FeynArts* model file of the Higgs-sector counterterms; to give explanation for some of the observations in [32] and prepare the reader for the result presented in the following chapter.

While this class of corrections turned out to be well approximated by the SM contribution (setting the Higgs-boson mass of the SM to the value of the $\mathcal{CP}$-even Higgs-boson mass of the MSSM), a potentially larger effect can be expected from diagrams with squarks and higgsinos, classes $(\tilde{q})$, $(\tilde{H})$ in Fig. 6.1, which do not possess a SM counterpart. This latter result is presented in chapter 7.

6.1 Electroweak two-loop corrections to $\Delta\rho$: the gauge-less limit

The Yukawa contributions of $\mathcal{O}(\alpha_f^2)$ form a set of leading two-loop contributions entering the EWPO only via $\Delta\rho$, where $\alpha_f \equiv y_f^2/(4\pi)$, and y_f is the Yukawa coupling of fermion f. For the top and bottom quarks the Yukawa couplings are

given by

$$y_t = \frac{\sqrt{2}\, m_t}{v \sin\beta}, \quad y_b = \frac{\sqrt{2}\, m_b}{v \cos\beta}, \tag{6.1}$$

where $v \equiv \sqrt{v_1^2 + v_2^2}$. In the SM another subset of leading electroweak two-loop corrections to $\Delta\rho$ is given by the corrections for large Higgs-boson masses of $\mathcal{O}(G_\mu^2 M_H^2 M_W^2)$ [38]. We will focus on the Yukawa corrections in the following.

In order to evaluate the leading Yukawa contributions of $\mathcal{O}(\alpha_f^2)$ the gauge-less limit has to be applied. It consists of neglecting the electroweak gauge couplings $g_{1,2} \to 0$ and thus also $M_W^2 = g_2^2 v^2/2 \to 0$ and $M_Z^2 = (g_1^2 + g_2^2)v^2/2 \to 0$, while keeping the ratio $c_w = M_W/M_Z$ and the vacuum expectation value v fixed. Accordingly, $\Sigma_{Z,W}$ in eq. (2.5) need to be evaluated at $\mathcal{O}(g_{1,2}^2)$ in order to obtain a finite contribution of $\mathcal{O}(g_{1,2}^0)$ to $\Delta\rho$ in the gauge-less limit. In this limit only diagrams with fermions and scalars contribute to $\Delta\rho$, while no gauge bosons appear in the loop diagrams.

At the one-loop level the only non-vanishing contributions to $\Delta\rho$ in the gauge-less limit of the MSSM are the fermion-loop and sfermion-loop contributions as given in eqs. (2.15), (5.1). While the Higgs sector of a general two-Higgs-doublet model yields a contribution to $\Delta\rho$ in the gauge-less limit, the contribution vanishes once the symmetry relations of the MSSM are imposed (see the discussion in Sect. 7.2.1 below).

At the two-loop level the gauge-less limit results in the desired Yukawa contributions of $\mathcal{O}(\alpha_f^2)$. For the quarks and squarks of the third generation this yields in particular terms of $\mathcal{O}(m_t^4/v^4)$ and $\mathcal{O}(m_b^4 \tan^2\beta/v^4)$. It is easy to see that no other contribution to M_W and $\sin^2\theta_{\rm eff}$ besides the gauge-less limit of $\Delta\rho$ yields terms of this order.

In order to extract the contributions of $\mathcal{O}(\alpha_t^2), \mathcal{O}(\alpha_t\alpha_b), \mathcal{O}(\alpha_b^2)$ from the diagrams involving quark and Higgs bosons, the coefficients of $y_t^2, y_t y_b, y_b^2$ have been ex-

tracted. The coefficients of these terms were then evaluated in the gauge-less limit, ie. for $M_W, M_Z \to 0$, keeping $c_W = M_W/M_Z$ fixed. For the Higgs masses appearing in the two-loop diagrams we use the same gauge-less limit relations as those adopted in ref. [32].

$$\begin{aligned} m^2_{H^\pm} &= M^2_{A^0} \\ m^2_{G^0} &= 0 \\ m^2_{G^\pm} &= 0 \end{aligned} \tag{6.2}$$

Applying the gauge-less limit in the neutral $\mathcal{CP}$-even Higgs sector also gives

$$M_{h^0} = 0 \tag{6.3}$$

as well as

$$\begin{aligned} m^2_{H^0} &= M^2_{A^0} \\ \sin\alpha &= -\cos\beta \\ \cos\alpha &= \sin\beta. \end{aligned} \tag{6.4}$$

In the SM the two-loop result for $\Delta\rho$ in the gauge-less limit was first obtained for the special case $M_{H^{\rm SM}} = 0$ [39],

$$\Delta\rho^{{\rm SM},\alpha_t^2}_{\text{2-loop}|M_H=0} = 3\,\frac{G_\mu^2}{128\pi^4}\,m_t^4\,\left(19 - 2\pi^2\right)\,. \tag{6.5}$$

This result was then extended to the case of arbitrary values of $M_{H^{\rm SM}}$ [40]. The

corresponding result is given by

$$\begin{aligned}
\Delta\rho^{\mathrm{SM},\alpha_t^2}_{\text{2-loop}}(M_{H^{\mathrm{SM}}}) \;=\; & 3\,\frac{G_\mu^2}{128\pi^4}\,m_t^4\left\{-3\frac{x^2(10-6x^2+x^4)}{x^2-4}w\log^2\left(\frac{1-w}{2}\right)\right. \\
& +\frac{x^2(x^2-4)}{2}w\log\left(\frac{1-w}{1+w}\right) \\
& -\left(6+6x^2-\frac{x^4}{2}\right)\log\left(x^2\right)+3\frac{x^2(10-6x^2+x^4)}{2(x^2-4)}w\log^2\left(x^2\right) \\
& +25-4x^2+\pi^2\frac{+8-6x^2+x^4-10wx^4+6wx^6-wx^8}{2x^2(x^2-4)} \\
& +6wx^2\frac{10-6x^2+x^4}{x^2-4}\mathrm{Li}_2\left(\frac{1-w}{2}\right) \\
& \left.-\frac{3(x^2-1)^2(x^2-2)}{x^2}\mathrm{Li}_2\left(1-x^2\right)\right\},
\end{aligned} \tag{6.6}$$

where $x = M_{H^{\mathrm{SM}}}/m_t$, and $w = \sqrt{1-4/x^2}$. The effect of going beyond the approximation $M_{H^{\mathrm{SM}}} = 0$ turned out to be numerically very significant. While the numerical value of the result in eq. (6.5) is rather small due to the accidental cancellation of the two terms in the last factor of eq. (6.5), the result is about an order of magnitude larger for values of $M_{H^{\mathrm{SM}}}$ in the experimentally preferred region. As a consequence, the result for the $\mathcal{O}(\alpha_t^2)$ corrections to $\Delta\rho$ with arbitrary Higgs-boson mass as given in eq. (6.6) provides a much better approximation of the full electroweak two-loop corrections to the EWPO [34–37] than the limiting case where $M_{H^{\mathrm{SM}}} = 0$, eq. (6.5). As an example, for $M_{H^{\mathrm{SM}}} = 120$ GeV the resulting shifts in M_W and $\sin^2\theta_{\mathrm{eff}}$ are -10 MeV and $+5 \times 10^{-5}$, respectively.

Within the MSSM also the contributions involving the bottom Yukawa coupling can be relevant at large $\tan\beta$. The corresponding contributions of $\mathcal{O}(\alpha_t^2)$, $\mathcal{O}(\alpha_t\alpha_b)$, and $\mathcal{O}(\alpha_b^2)$ to $\Delta\rho$ have been obtained in Ref. [32] in the limit of heavy scalar quarks. In this limit only the top and bottom quarks and the Higgs bosons (and Goldstone bosons) of the MSSM appear in the loops. The results turned out to be numerically relevant, leading to shifts in M_W and $\sin^2\theta_{\mathrm{eff}}$ of up to 12 MeV and

6×10^{-5}, respectively. Since in the gauge-less limit the couplings of the light $\mathcal{CP}$-even Higgs boson of the MSSM to fermions become SM-like, the $\mathcal{O}(\alpha_t^2)$ correction in the MSSM can be well approximated by the corresponding correction in the SM, as given in eq. (6.6). Potentially larger effects compared to the SM case can be expected from the contribution of supersymmetric particles (with not too heavy masses), since these corrections do not have a SM counterpart.

Because in the SM case the limit $M_H^{SM} \to 0$ turns out to be a poor approximation to the result for arbitrary M_H^{SM} [40], it is desirable to keep M_{h^0} nonzero in the calculation here (formally a higher order effect). Keeping α arbitrary is also necessary to retain non SM-like couplings of the lightest $\mathcal{CP}$-even Higgs boson to the fermions and gauge bosons. It is not possible, however, to keep all parameters in the Higgs sector completely arbitrary as the underlying symmetry of the MSSM Lagrangian must be exploited in order to achieve UV-finiteness of the two-loop corrections to $\Delta\rho$.

It was observed in ref. [32] that in the limit $y_b = 0$, where only the $\mathcal{O}(\alpha_t^2)$ contribution was considered, only the relations in Eq. 6.2 are required for UV-divergences to cancel. For the full $\mathcal{O}(\alpha_t^2), \mathcal{O}(\alpha_t\alpha_b), \mathcal{O}(\alpha_b^2)$ contributions however, the relations in both 6.2 and 6.4 are required but M_{h^0} can be kept arbitrary (an explanation for this observation is given in the following chapter).

Here we have reproduced the full $\mathcal{O}(\alpha_t^2), \mathcal{O}(\alpha_t\alpha_b), \mathcal{O}(\alpha_b^2)$ calculation in the quark sector, applying the full gauge-less limit relations 6.2 and 6.4. M_{h^0} is kept a free parameter but the coupling of the lightest $\mathcal{CP}$-even Higgs boson to gauge bosons and fermions become SM-like.

In order to calculate the $\mathcal{O}(\alpha_t^2), \mathcal{O}(\alpha_t\alpha_b), \mathcal{O}(\alpha_b^2)$, corrections to $\Delta\rho$, the generic Feynman diagrams shown in figure 6.2 have to be evaluated. All possible diagrams involving the t/b doublet and the full MSSM Higgs sector have been included here

in direct analogy with ref. [32] and corresponding to the limit where all SUSY masses are heavy. Absent are the diagrams from the $\tilde{t}/\tilde{b}$ doublet and Higgsino sector (which are presented in next chapter).

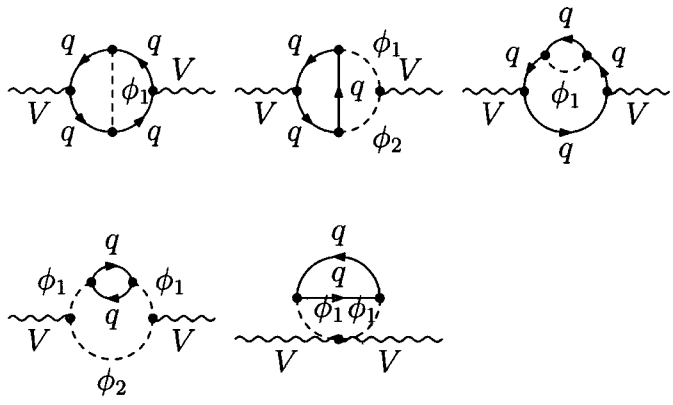

Figure 6.2: Two-loop vector boson self-energies contain t/b quark plus the full MSSM Higgs sector. V = W,Z boson, $\phi_{1,2}$ = physical Higgs or Goldstone boson, q = t,b quark

The two-loop diagrams in figure 6.2 are supplemented with their corresponding one-loop counterterms and insertions. The Counterterms are shown in figure 6.3. The counterterms from the quark sector enter via the top/bottom mass counterterms $\delta m_t, \delta m_b$. Recall from chapter 3 the Higgs sector of the MSSM is pa-

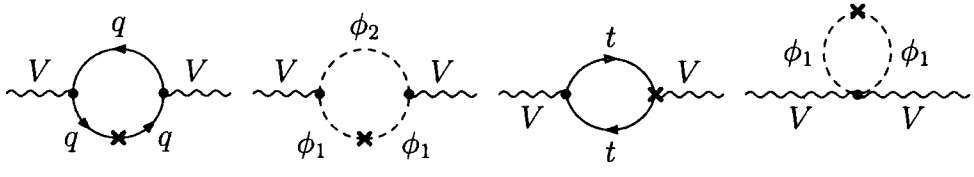

Figure 6.3: Vector boson counterterms to supplement the self-energies shown in fig. 6.2. V = W,Z boson, $\phi_{1,2}$ = Higgs or Goldstone boson, q = t,b quark

rameterised in terms of two variables: M_{A^0} and $\tan\beta$. Thus the Higgs sector renormalisation enters via the the counterterms $\delta M^2_{A_0}$, $\delta\tan\beta$ and the tadpoles δT_h and δT_H. Wave-function renormalisation entering via the diagrams in fig. 6.3 once again must drop out so are omitted from the start (A check of wave-function renormalisation was done in ref. [32]).

6.1.1 Renormalisation

A renormalisation prescription for the Higgs sector is not required since it was observed that all renormalisation parameters drop out when all the second and fourth diagrams in fig. 6.3 are summed (an explanation for this observation is given in the following chapter).

In order to define the renormalisation constants one has to choose a renormalisation scheme. For the SM fermion masses $m_{t,b}$ we always choose the on-shell scheme. This yields for the top mass counterterm

$$\delta m_t = \frac{1}{2} m_t \left[\mathrm{Re}\,\Sigma_{t_L}(m_t^2) + \mathrm{Re}\,\Sigma_{t_R}(m_t^2) + 2\mathrm{Re}\,\Sigma_{t_S}(m_t^2)\right] , \tag{6.7}$$

with the scalar coefficients of the unrenormalized top-quark self-energy, $\Sigma_t(p)$, in the Lorentz decomposition

$$\Sigma_t(p) = \not{p}\omega_-\Sigma_{t_L}(p^2) + \not{p}\omega_+\Sigma_{t_R}(p^2) + m_t\Sigma_{t_S}(p^2) , \tag{6.8}$$

and analogously for the bottom mass counterterm.

The result calculated is analytical identical to the rather lengthy expression given in ref. [32][1] for the full $\mathcal{O}(\alpha_t^2), \mathcal{O}(\alpha_t\alpha_b), \mathcal{O}(\alpha_b^2)$ quark result.

[1]The result was actually compared with an expression obtained from the authors of [32]. A

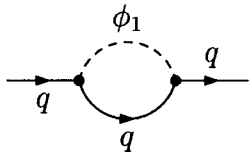

Figure 6.4: Quark self-energy insertion. q = t/b quark, ϕ_1 = Higgs or Goldstone boson.

6.1.2 Numerical analysis $\mathcal{O}(\alpha_t^2), \mathcal{O}(\alpha_t\alpha_b), \mathcal{O}(\alpha_b^2)$ quark result

Since a full numerical analysis is presented in ref. [32], here we briefly show the behaviour of the result calculated above. Our numerical routine differs from that used in [32]. We use the program *FeynHiggs* [41–44] to calculate the mass of the lightest $\mathcal{CP}$-even Higgs boson, M_{h^0} in terms of M_{A^0}, which allows the inclusion of (large) higher order effects in the Higgs sector. In order for *FeynHiggs* to do this we need to specify the parameters in the Higgs sector: $A_t = A_b = 2000$ GeV, $M_{SUSY} = 1000$ GeV, $\mu = 200$ GeV[2]. In addition, the SM parameters used here are $m_t = 174.3$ GeV, $m_b = 4.25$ GeV, $M_W = 80.45$ GeV and $M_Z = 91.187$ GeV.

The $\mathcal{O}(\alpha_t^2), \mathcal{O}(\alpha_t\alpha_b), \mathcal{O}(\alpha_b^2)$ quark result contains parameters from the SM and the Higgs sector of the MSSM. Since the SM parameters are known, the result is shown against the two free parameters in the MSSM Higgs sector, M_{A^0} (which is reparameterised in terms of M_{h^0} and $\tan\beta$.

Figure 6.5 shows the result against M_{h^0} for small and large $\tan\beta$. Since M_{h^0} is a dependent parameter we have varied M_{A^0} from 80 GeV to around 600 GeV. In the large M_{A^0} region, large changes to M_{A^0} cause only small changes in M_{h^0}, thus M_{h^0} does not extend much beyond 130 GeV. Both results converge to a (different) point as M_{A^0} is increased.

direct comparison with the result in [32] has not been performed.

[2]This represents a marginally different scenario to that examined in ref. [32]

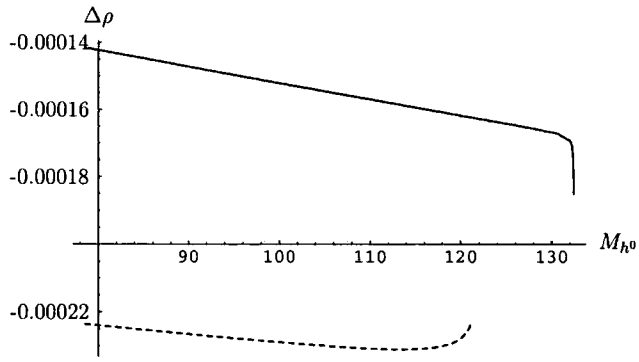

Figure 6.5: $\Delta\rho$ against M_{h^0} for $\tan\beta = 3$ (dashed line) and $\tan\beta = 40$ (solid line).

Figure 6.6 shows the result plotted against $\tan\beta$ for $M_{A^0} = 300$ and 500 GeV.

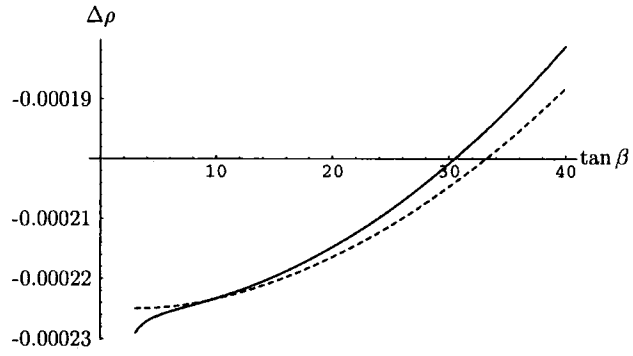

Figure 6.6: $\Delta\rho$ against $\tan\beta$ for $M_{A^0} = 300$ GeV (solid line) and $M_{A^0} = 500$ GeV (dashed line).

The behaviour shown in both figure 6.5 and 6.6 qualitatively agrees with that shown in ref. [32]. The absolute value of the result varies by ~10% because higher order corrections have been included within the Higgs sector (from using *FeynHiggs* to calculate MSSM parameters).

6.2 Chapter summary

The dominant quark-Yukawa contributions to $\Delta\rho$ in the MSSM have been calculated and the result is analytically the same as that given in ref. [32]. We confirm the observations made in [32] that the result is finite for arbitrary M_{h_0} and the Higgs sector renormalisation parameters all drop out. In the following chapter we present the dominant squark-Yukawa contributions to $\Delta\rho$ and give an explanation for the observations made here.

Chapter 7

Leading Electroweak corrections to $\Delta\rho$ (part II)

'There comes a time in every man's life and I've had many of them.'

Casey Stengel (1890 - 1975)

In this chapter new results at $\mathcal{O}(\alpha_t^2)$, $\mathcal{O}(\alpha_t\alpha_b)$, $\mathcal{O}(\alpha_b^2)$ are presented in the light squark limit[1]. In particular, diagrams of the class $\tilde{q}$ and $\tilde{H}$ in figure 6.1 have been calculated. In this chapter we complete the discussion of the $\mathcal{O}(\alpha_t^2)$, $\mathcal{O}(\alpha_t\alpha_b)$,$\mathcal{O}(\alpha_b^2)$ results that began in chapter 6.

For the two-loop Yukawa corrections in the SM it turned out that the dependence on the Higgs-boson mass is numerically important. While the Higgs-boson mass is a free parameter in the SM, the masses of the $\mathcal{CP}$-even Higgs bosons of the MSSM are given in terms of the other parameters of the model. In the gauge-less limit that has to be applied in order to extract the leading two-loop Yukawa corrections,

[1]The material presented in this chapter is original work produced by the author in collaboration with the authors of [45], where some results have also been published.

the mass of the lighter $\mathcal{CP}$-even Higgs boson, M_h, formally has to be put to zero. In the previous chapter it was observed for the calculation of the diagrams of class (q) of fig. 6.1 that M_h can be set to its true value instead of zero in a consistent way. In this chapter we provide a detailed discussion of the gauge-less limit, yielding an explanation of this observation. We will analyse the Higgs-mass dependence also for the other classes of diagrams in Fig. 6.1.

We analyse the numerical effects of the new corrections for various scenarios in the unconstrained MSSM and for SPS benchmark scenarios [52]. We study two different renormalisation schemes and investigate the possible effects of unknown higher-order corrections for M_W and $\sin^2\theta_{\rm eff}$.

7.1 The $\mathcal{O}(\alpha_t^2)$, $\mathcal{O}(\alpha_t\alpha_b)$, $\mathcal{O}(\alpha_b^2)$ contributions to $\Delta\rho$

The purpose of this chapter is to perform a complete calculation of the $\mathcal{O}(\alpha_t^2)$, $\mathcal{O}(\alpha_t\alpha_b)$, and $\mathcal{O}(\alpha_b^2)$ contributions to $\Delta\rho$ in the MSSM, including the contributions of supersymmetric particles. This means that all diagrams have to be evaluated (applying the gauge-less limit) that contain top and bottom quarks (as given in chapter 6), their scalar superpartners stop and sbottom, and Higgs bosons or higgsinos.

The contributions to $\Delta\rho$ at $\mathcal{O}(\alpha_t^2)$, $\mathcal{O}(\alpha_t\alpha_b)$, $\mathcal{O}(\alpha_b^2)$ can be grouped into three classes (see Fig. 6.1):

- (q) diagrams involving t/b quarks and Higgs bosons (see also Ref. [32]),
- $(\tilde{q})$ diagrams with $\tilde{t}/\tilde{b}$ squarks and Higgs bosons (see Fig. 7.1 for generic diagrams),

($\tilde{H}$) diagrams with higgsinos (containing also quarks and squarks) (see Fig. 7.2 for generic diagrams).

The generic diagrams shown in Figs. 7.1, 7.2 have to be evaluated for the Z boson and the W boson self-energy.

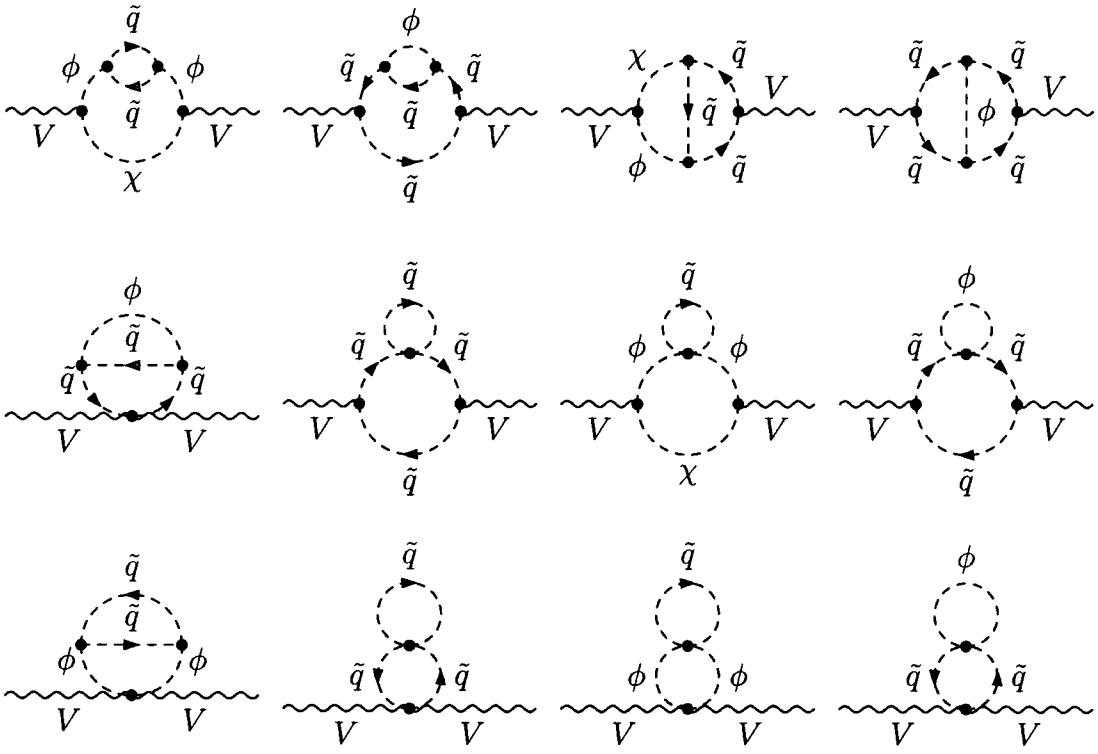

Figure 7.1: Generic Feynman diagrams of class ($\tilde{q}$). V denotes either W or Z, $\tilde{q}$ is either a $\tilde{t}$ or a $\tilde{b}$, and ϕ, χ denote Higgs and Goldstone bosons.

In the following sections we describe the necessary ingredients for the evaluation of these contributions, starting with the relevant sectors of the MSSM.

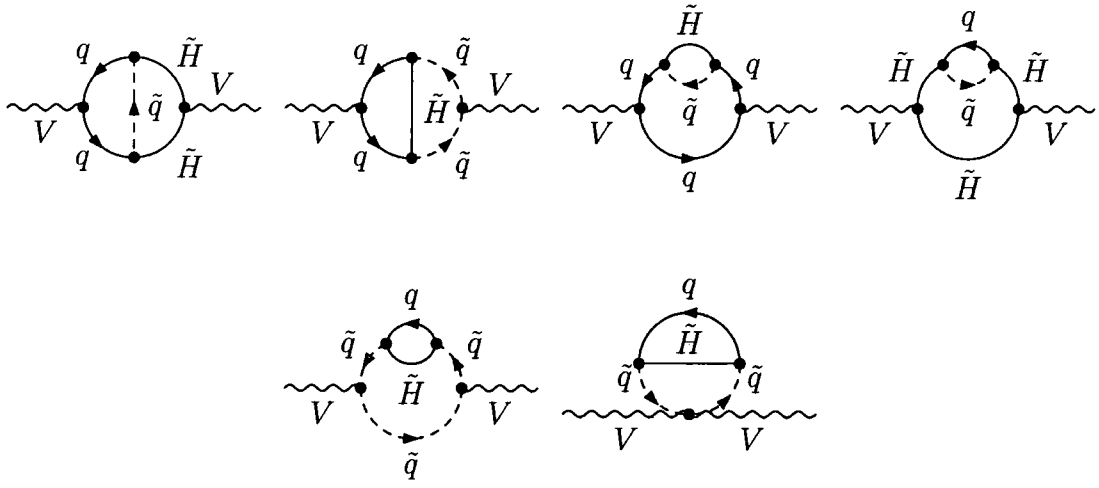

Figure 7.2: Generic Feynman diagrams of class ($\tilde{H}$). V denotes either W or Z, $\tilde{q}$ is either a $\tilde{t}$ or a $\tilde{b}$, while q is a t or a b, and $\tilde{H}$ denotes a higgsino (neutral or charged).

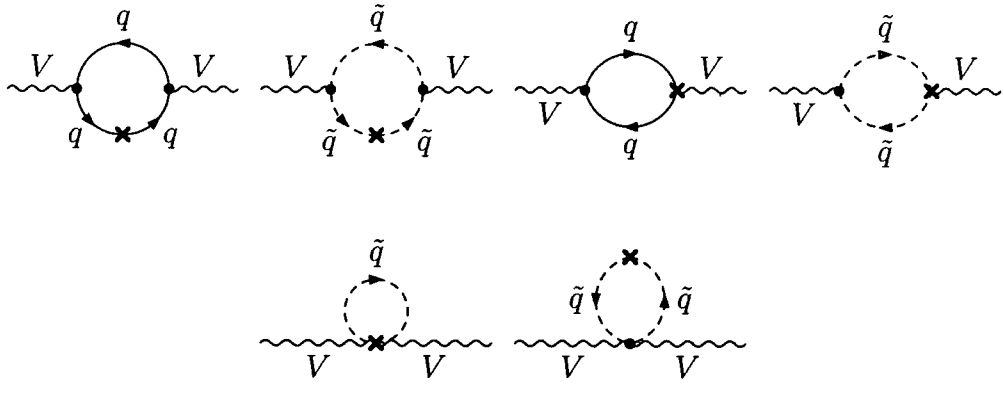

Figure 7.3: Generic Feynman diagrams for the vector boson self-energies with counter-term insertion. V denotes either W or Z, $\tilde{q}$ is either a $\tilde{t}$ or a $\tilde{b}$, while q is a t or a b

7.1.1 The relevant MSSM sectors

Here we specify the MSSM contributions that are relevant for the $\mathcal{O}(\alpha_t^2)$, $\mathcal{O}(\alpha_t\alpha_b)$, $\mathcal{O}(\alpha_b^2)$ corrections. As explained above, the calculation involves the gauge-less

limit where $M_W, M_Z \to 0$ (keeping $c_w = M_W/M_Z$ fixed). Accordingly, we discuss the implications of the gauge-less limit for the different sectors of the MSSM.

The scalar top and bottom sector

The squark mass-matrices were defined in chapter 3. Recall, as a consequence of Eq. 3.25, there are only five independent parameters in the $\tilde{t}/\tilde{b}$ sector. The masses and mixing angles are connected via the relation

$$\sum_{i=1,2} |U^{\tilde{b}}_{i1}|^2 m^2_{\tilde{b}_i} = \sum_{i=1,2} |U^{\tilde{t}}_{i1}|^2 m^2_{\tilde{t}_i} + m_b^2 - m_t^2 - M_Z^2 c_w^2 \cos 2\beta \,. \tag{7.1}$$

In the gauge-less limit the terms proportional to M_Z^2 in the diagonal entries of the mass matrices and in eq. (7.1) vanish.

Except where stated otherwise, we will assume universality of all three soft supersymmetry-breaking parameters in the diagonal entries of the stop/sbottom mass matrices,

$$M_{\text{SUSY}} \equiv M_{\tilde{t}_L} = M_{\tilde{t}_R} = M_{\tilde{b}_R} \,. \tag{7.2}$$

The common squark mass scale is denoted as M_{SUSY}.

The Higgs sector

In the gauge-less limit the Higgs sector parameters satisfy the relations 6.2 and 6.4, as well as Eq 6.3: $M_{h^0} = 0$. These are restated (re-ordered) here for later

convenience:

$$M_{H^\pm}^2 = M_H^2 = M_A^2 \,, \tag{7.3a}$$

$$\sin\alpha = -\cos\beta \,, \quad \cos\alpha = \sin\beta \,, \tag{7.3b}$$

$$M_G^2 = M_{G^\pm}^2 = 0 \,. \tag{7.3c}$$

Because of the accidental cancellation in the SM result for $M_{H^{\rm SM}} = 0$, see eq. (6.5), it is desirable to retain the dependence on M_h as much as possible in the MSSM result. In this way the numerical impact of the M_h-dependence can be studied, which within the MSSM is formally a higher-order effect. This is particularly interesting in view of the fact that higher-order corrections to the masses and mixing angles in the MSSM Higgs sector are sizable, see e.g. Ref. [46] for recent reviews.

We will therefore discuss the implementation of the gauge-less limit in some detail. In particular, we will investigate in how far a consistent result for $\Delta\rho$ can be obtained without imposing eq. (6.3). We will also briefly discuss the case where eq. (7.3b) is relaxed, see Sect. 7.2 below. For higher-order corrections in the Higgs sector we use the results as implemented into the code *FeynHiggs* [41–44].

Higgsinos

In the gauge-less limit the contributions from the chargino and neutralino sector reduce to those of the higgsinos. The Diagonalisation matrices for the chargino

and neutralino sectors (defined in chapter 3) in this limit are given by

$$\mathbf{U} = \mathbf{V} = \begin{pmatrix} 0 & 0 \\ 0 & 1 \end{pmatrix}, \quad \mathbf{N} = \frac{1}{\sqrt{2}} \begin{pmatrix} 0 & 0 & 0 & 0 \\ 0 & 0 & 0 & 0 \\ 0 & 0 & 1 & -1 \\ 0 & 0 & 1 & 1 \end{pmatrix}, \tag{7.4}$$

where $\mathbf{N}$ is the diagonalising matrix for the neutralinos and $\mathbf{U}^*.\mathbf{X}.\mathbf{V}^\dagger$ forms the diagonal matrix for the charginos [25, 47].

The corresponding elements of the diagonalised mass matrices are

$$m_{\tilde{\chi}_i^\pm} = (0, +\mu), \quad m_{\tilde{\chi}_i^0} = (0, 0, +\mu, -\mu). \tag{7.5}$$

All entries corresponding to gauginos are zero since the gaugino couplings vanish in the gauge-less limit. Note that the negative sign in $m_{\tilde{\chi}_4^0}$ has to be taken into account; the physical masses of the charged and neutral higgsinos are all equal to $+|\mu|$ in the gauge-less limit.

7.1.2 Evaluation of the Feynman diagrams

In addition to the two-loop diagrams, one-loop counterterms corresponding to the renormalisation of divergent one-loop sub-diagrams have to be taken into account. The whole calculation can be performed both in dimensional regularisation [11] as well as in dimensional reduction [13]. The Yukawa extraction is performed using the method illustrated in chapter 6. Since no gauge bosons appear in the loops, both regularisation schemes preserve gauge invariance and supersymmetry for the present calculation. Therefore the necessary counterterms correspond to multiplicative renormalisation of the parameters in the MSSM Lagrangian.

7.1.3 Counterterms

The renormalisation constants that are relevant in the gauge-less limit are

$$\delta m_t,\ \delta m_b,\ \delta m^2_{\tilde{t}_1},\ \delta m^2_{\tilde{t}_2},\ \delta\theta_{\tilde{t}},\ \delta m^2_{\tilde{b}_1},\ \delta m^2_{\tilde{b}_2},\ \delta\theta_{\tilde{b}},$$
$$\delta M_A^2,\ \delta\tan\beta,\ \delta t_{h,H},\ \delta\mu, \tag{7.6}$$

corresponding to the renormalisation of the fermion masses, the parameters of the $\tilde{t}/\tilde{b}$ sector, the Higgs sector parameters and tadpoles, and the μ-parameter. It is not necessary to introduce wave function renormalisation constants for the fermions and scalar fields since they drop out in the sum over all diagrams.

There are two possible ways to obtain the counterterm contributions:

1. Generate and evaluate one-loop diagrams with insertions of counterterm vertices, as depicted generically in Fig. 7.3. In order to generate these diagrams, the required counterterm Feynman rules had to be added to the *FeynArts* MSSM model file. In the explicit evaluation of the counterterm diagrams it turned out that the renormalisation constants δM_A^2, $\delta\tan\beta$, $\delta t_{h,H}$, $\delta\mu$, corresponding to the Higgs/higgsino sector, drop out. Only the quark and squark mass and mixing renormalisation constants contribute.

2. The renormalisation transformation $i \to i+\delta i$ for each parameter i appearing in eq. (7.6) is performed directly in the one-loop result $\Delta\rho^{\rm SM+SUSY}_{\rm 1-loop}(i)$. The counterterm contribution for the two-loop calculation is then obtained by expanding $\Delta\rho^{\rm SM+SUSY}_{\rm 1-loop}(i+\delta i)$ to first order in the δi, where the contributions to $\Delta\rho^{\rm SM+SUSY}_{\rm 1-loop}$ have been given in eqs. (2.15), (5.1). In this setup it is obvious that the renormalisation constants δM_A^2, $\delta\tan\beta$, $\delta t_{h,H}$, $\delta\mu$ do not contribute, since the one-loop result in the gauge-less limit consists only of the quark and

squark loop contributions and therefore does not depend on the Higgs-sector parameters. Accordingly, the counterterm contributions for the two-loop calculation, $\Delta\rho_{\rm ct}$, can be written as

$$\Delta\rho_{\rm ct} = \sum_{f=t,b} \left(\delta m_f \partial_{m_f} + \sum_{i=1,2} \delta m^2_{\tilde{f}_i} \partial_{m^2_{\tilde{f}_i}} + \sum_{i,j=1,2} \delta U^{\tilde{f}}_{ij} \partial_{U^{\tilde{f}}_{ij}} \right) \Delta\rho^{\rm SM+SUSY}_{\rm 1-loop} . \quad (7.7)$$

In order to have a non-trivial check of the counterterm contributions, we implemented them using both approaches and found agreement in the final result.

Due to supersymmetry and SU(2) gauge invariance, see eq. (3.25), there are only five independent parameters in the $\tilde{t}/\tilde{b}$ sector, leading to eq. (7.1). As a consequence, not all the parameters appearing in eq. (7.1) can be renormalised independently. Choosing $m^2_{\tilde{b}_1}$ as the dependent parameter, its counterterm $\delta m^2_{\tilde{b}_1}$ can be expressed in terms of the other counterterms. In the gauge-less limit the relation reads

$$\begin{aligned} \delta m^2_{\tilde{b}_1} = \frac{1}{|U^{\tilde{b}}_{11}|^2} \Big(& \sum_{i=1,2} |U^{\tilde{t}}_{i1}|^2 \delta m^2_{\tilde{t}_i} - |U^{\tilde{b}}_{21}|^2 \delta m^2_{\tilde{b}_2} + 2\, U^{\tilde{t}}_{11} U^{\tilde{t}}_{21} (m^2_{\tilde{t}_1} - m^2_{\tilde{t}_2}) \delta U^{\tilde{t}}_{12} \\ & - 2\, U^{\tilde{b}}_{11} U^{\tilde{b}}_{21} (m^2_{\tilde{b}_1} - m^2_{\tilde{b}_2}) \delta U^{\tilde{b}}_{12} - 2 m_t\, \delta m_t + 2 m_b\, \delta m_b \Big) , \end{aligned} \quad (7.8)$$

where the renormalisation transformation of the mixing matrix is defined in chapter 4. Note that the above relation was not used in our analysis of the QCD contributions in chapter 5, since the earlier calculation was performed using the same relations as enforced in [30] in order to provide a full analytical check.

In order to define the renormalisation constants one has to choose a renormalisation scheme. For the SM fermion masses $m_{t,b}$ we always choose the on-shell scheme, as

in the previous chapter. This yields for the top mass counterterm

$$\delta m_t = \frac{1}{2} m_t \left[\mathrm{Re}\, \Sigma_{t_L}(m_t^2) + \mathrm{Re}\, \Sigma_{t_R}(m_t^2) + 2\mathrm{Re}\, \Sigma_{t_S}(m_t^2) \right] . \tag{7.9}$$

and analogously for the bottom mass counterterm (in order to take higher-order QCD corrections into account, we use an effective bottom quark mass value of $m_b = 3$ GeV). For the five independent $\tilde{t}/\tilde{b}$ sector parameters we choose either the on-shell [48, 49] or the $\overline{\mathrm{DR}}$ scheme. The precise definitions will be given in the following section.

7.2 Renormalisation prescriptions and result for $\Delta\rho$

As explained above, the strict implementation of the gauge-less limit in the evaluation of the $\mathcal{O}(\alpha_t^2)$, $\mathcal{O}(\alpha_t\alpha_b)$, $\mathcal{O}(\alpha_b^2)$ contributions to $\Delta\rho$ would imply that the mass of the lightest $\mathcal{CP}$-even Higgs boson has to be set to zero, see eq. (6.3). In the SM case, where $M_{H^{\rm SM}}$ is a free parameter, it turned out that the two-loop Yukawa contribution to $\Delta\rho$ yields a much better approximation of the full electroweak two-loop corrections to the EWPO for (realistic) non-zero values of $M_{H^{\rm SM}}$ than in the limit $M_{H^{\rm SM}} = 0$. It is therefore of interest to investigate the impact of non-zero values of M_h also for the MSSM, where M_h is a dependent quantity that is determined by the other supersymmetric parameters.

It has been observed already in Ref. [32] that the pure fermion contributions of class (q) (see Fig. 6.1) may consistently be obtained even if eq. (6.3) is not employed. In this section we discuss this issue in detail and explain the physical origin of this behaviour. Based on this result we show how the calculation of all

three classes of contributions to $\Delta\rho$, i.e. (q), $(\tilde{q})$, and $(\tilde{H})$, can be organised in such a way that M_h can be set to its true MSSM value essentially everywhere. We will use the resulting expression in order to study the numerical effect of non-zero M_h values for the new corrections calculated in this chapter, namely the squark contribution $(\tilde{q})$ and the higgsino contribution $(\tilde{H})$.

7.2.1 Higgs sector

In order to discuss the implementation of the gauge-less limit it is useful to compare the MSSM case with the one of a general two-Higgs-doublet model (2HDM). In the following "2HDM" is to be understood as a two-Higgs-doublet model including squarks and higgsinos, but without any supersymmetric relations imposed on them. The MSSM can be regarded as a special case of a 2HDM, with supersymmetric relations for couplings and masses. In the 2HDM without these coupling relations, $\Delta\rho$ is also well-defined and can be calculated at $\mathcal{O}(\alpha_t^2)$, $\mathcal{O}(\alpha_t\alpha_b)$, $\mathcal{O}(\alpha_b^2)$ in the gauge-less limit. The corresponding two-loop diagrams are identical to the diagrams of the classes (q), $(\tilde{q})$, $(\tilde{H})$ in the MSSM. However, in contrast to the MSSM, the Higgs-boson masses in the 2HDM are independent parameters and do not have to obey Eqs. 6.2, 6.4, (and 6.3) in the gauge-less limit.

The essential difference between the MSSM and the 2HDM case concerns the renormalisation and counterterm contributions. Restricting ourselves in a first step to class (q), these contributions can be decomposed in the MSSM and the 2HDM as

$$\Delta\rho^{(q)}_{\rm MSSM} = \Delta\rho^{(q)}_{\rm 2-loop} + \Delta\rho^{(q)}_{tb-{\rm ct}} \tag{7.10}$$

$$\Delta\rho^{(q)}_{\rm 2HDM} = \Delta\rho^{(q)}_{\rm 2-loop} + \Delta\rho^{(q)}_{tb-{\rm ct}} + \Delta\rho^{(q)}_{H-{\rm ct}}\,, \tag{7.11}$$

respectively. Here the two-loop contribution $\Delta\rho^{(q)}_{2-\text{loop}}$ and the counterterm contributions from the t/b doublet $\Delta\rho^{(q)}_{tb-\text{ct}}$ are identical in the two models, while the Higgs sector counterterm contribution $\Delta\rho^{(q)}_{H-\text{ct}}$ appears only in the 2HDM result.

As mentioned above, in the MSSM there are no one-loop contributions from the Higgs sector and correspondingly no Higgs sector counterterm contributions at $\mathcal{O}(\alpha_t^2)$, $\mathcal{O}(\alpha_t\alpha_b)$, $\mathcal{O}(\alpha_b^2)$. In the 2HDM, the Higgs sector one-loop contribution to $\Delta\rho$ reads

$$\begin{aligned}\Delta\rho^{\text{2HDM}}_{1-\text{loop}} = \frac{g^2}{128\pi^2 M_W^2}\Big[&F_0(M_{H^\pm}^2, M_A^2) \\ &+ \sin^2(\beta-\alpha)\left(F_0(M_{H^\pm}^2, M_H^2) - F_0(M_A^2, M_H^2)\right) \\ &+ \cos^2(\beta-\alpha)\left(F_0(M_{H^\pm}^2, M_h^2) - F_0(M_A^2, M_h^2)\right)\Big] \end{aligned} \tag{7.12}$$

in the gauge-less limit. Note that this contribution indeed vanishes if the MSSM gauge-less limit relations (6.2, 6.4) hold. The counterterm contribution from the Higgs sector at the two-loop level can be obtained from this expression as

$$\Delta\rho^{(q)}_{H-\text{ct}} \equiv \left(\sum_{\phi=h,H,A^0,H^\pm} \delta M_\phi^2\, \partial_{M_\phi^2} + \delta\tan\beta\,\partial_{\tan\beta} + \delta\sin\alpha\,\partial_{\sin\alpha}\right)\Delta\rho^{\text{2HDM}}_{1-\text{loop}}. \tag{7.13}$$

Since $F_0(x,y)$ and $\partial_x F_0(x,y)$ vanish in the limit $x = y$, we find that $\Delta\rho^{(q)}_{H-\text{ct}}$ vanishes if

$$M_H = M_{H^\pm} = M_A, \quad \cos(\beta-\alpha) = 0, \quad M_h = \text{arbitrary} \tag{7.14}$$

or

$$M_{H^\pm} = M_A, \quad \delta M_{H^\pm}^2 = \delta M_A^2, \quad M_h, M_H, \alpha = \text{arbitrary}. \tag{7.15}$$

The relations in eq. (7.14) are the same as the constraints imposed by the gaugeless limit in the MSSM except for the fact that $M_h = 0$ is not necessary. The observation made in Ref. [32] that the class (q) contributions to $\Delta\rho$ can be evaluated in the MSSM in a meaningful way for non-zero values of M_h can be understood from eq. (7.14). For class (q) the two-loop diagrams and the fermion sector counterterms are identical in the MSSM and the 2HDM. If the relations in eq. (7.14) hold, $\Delta\rho^{(q)}_{H-\mathrm{ct}} = 0$ in eq. (7.11), so that eq. (7.10) and eq. (7.11) become identical. Thus, the calculations in the MSSM and the 2HDM are the same in this case. This means that the result of class (q) derived in the MSSM for non-zero M_h is well-defined and consistent, as it corresponds to a certain special case of the general 2HDM result.

7.2.2 Inclusion of the $\tilde{t}/\tilde{b}$ sector in the on-shell scheme

For the full set of contributions to $\Delta\rho$, also the sfermion diagrams of class $(\tilde{q})$ and the higgsino diagrams of class $(\tilde{H})$ have to be taken into account. In the following, as explained above, we consider a 2HDM including also stops, sbottoms and higgsinos (although without any supersymmetric relations). The analogy of the calculation in the MSSM and the 2HDM does no longer hold, since the sfermion sector renormalisation differs in the two models.

As discussed above, supersymmetry and SU(2) gauge invariance imply that not all parameters in the squark sector can be renormalised independently in the MSSM. Choosing $m_{\tilde{b}_1}$ as the dependent mass in the MSSM, its renormalisation constant $\delta m^2_{\tilde{b}_1}$ is given by eq. (7.8), and no independent renormalisation condition can be imposed on it. We will refer to the expression for $\delta m^2_{\tilde{b}_1}$ in terms of the other counterterms of the fermion and sfermion sector as given in eq. (7.8) as the "symmetric" renormalisation, $\delta m^2_{\tilde{b}_1}\big|_{\mathrm{symm}}$.

In the on-shell scheme [48], the three other squark masses $m_{\tilde{t}_{1,2},\tilde{b}_2}$ are defined as pole masses, and the mixing angle counterterms can be defined via on-shell mixing self-energies:

$$\delta m^2_{\tilde{f}_i} = \mathrm{Re}\,\Sigma_{\tilde{f}_i}(m^2_{\tilde{f}_i}) \qquad \text{for } \tilde{f}_i = \tilde{t}_{1,2}, \tilde{b}_2; \tag{7.16}$$

$$\delta U^{\tilde{f}}_{12} = \frac{\mathrm{Re}\,\Sigma_{\tilde{f}_1\tilde{f}_2}(m^2_{\tilde{f}_1}) + \mathrm{Re}\,\Sigma_{\tilde{f}_1\tilde{f}_2}(m^2_{\tilde{f}_2})}{2(m^2_{\tilde{f}_1} - m^2_{\tilde{f}_2})} \qquad \text{for } \tilde{f} = \tilde{t}, \tilde{b}. \tag{7.17}$$

In a 2HDM with squarks, on the other hand, an on-shell renormalisation can be applied for all four squark masses. In this case $\delta m^2_{\tilde{b}_1}$ is given by

$$\delta m^2_{\tilde{b}_1}\big|_{\mathrm{OS}} = \mathrm{Re}\,\Sigma_{\tilde{b}_1}(m^2_{\tilde{b}_1}), \tag{7.18}$$

where $\Sigma_{\tilde{b}_1}$ is the $\tilde{b}_1$ self-energy. Hence there is a mass shift

$$\Delta m^2_{\tilde{b}_1} = \delta m^2_{\tilde{b}_1}\big|_{\mathrm{symm}} - \delta m^2_{\tilde{b}_1}\big|_{\mathrm{OS}} \tag{7.19}$$

at the one-loop level between the mass parameter $m^2_{\tilde{b}_1}$ as given by the "symmetric" renormalisation and the physical pole mass.

For the class $(\tilde{q}, \tilde{H})$ the decomposition of $\Delta\rho$ in the two models is given by

$$\Delta\rho^{(\tilde{q},\tilde{H})}_{\mathrm{MSSM}} = \Delta\rho^{(\tilde{q},\tilde{H})}_{\mathrm{2-loop}} + \Delta\rho^{(\tilde{q},\tilde{H})}_{tb\mathrm{-ct}} + \Delta\rho^{(\tilde{q},\tilde{H})}_{\tilde{t}\tilde{b}\mathrm{-ct,\,symm}} \tag{7.20}$$

$$\Delta\rho^{(\tilde{q},\tilde{H})}_{\mathrm{2HDM}} = \Delta\rho^{(\tilde{q},\tilde{H})}_{\mathrm{2-loop}} + \Delta\rho^{(\tilde{q},\tilde{H})}_{tb\mathrm{-ct}} + \Delta\rho^{(\tilde{q},\tilde{H})}_{\tilde{t}\tilde{b}\mathrm{-ct,\,full\,OS}} + \Delta\rho^{(\tilde{q},\tilde{H})}_{H\mathrm{-ct}}\,. \tag{7.21}$$

Here $\Delta\rho^{(\tilde{q},\tilde{H})}_{\tilde{t}\tilde{b}\mathrm{-ct,\,symm}}$ corresponds to the "symmetric" renormalisation of the squark sector in the MSSM described above. $\Delta\rho^{(\tilde{q},\tilde{H})}_{\tilde{t}\tilde{b}\mathrm{-ct,\,full\,OS}}$ denotes the contribution from the full on-shell renormalisation of all squarks. As one can see from eqs. (7.20) and (7.21) the MSSM result differs from the 2HDM result even for the case where

$\Delta\rho^{(q)}_{H-\mathrm{ct}} = 0$. The MSSM result therefore does not correspond to a special case of the 2HDM expression.

7.2.3 Result for $\Delta\rho$ in the on-shell scheme

The total result for $\Delta\rho$ at $\mathcal{O}(\alpha_t^2, \alpha_t\alpha_b, \alpha_b^2)$ in the MSSM is given by the sum of eqs. (7.10) and (7.20),

$$\Delta\rho^{(q,\tilde{q},\tilde{H})} = \Delta\rho^{(q)}_{\mathrm{MSSM}} + \Delta\rho^{(\tilde{q},\tilde{H})}_{\mathrm{MSSM}} \,. \tag{7.22}$$

As discussed above, in $\Delta\rho^{(\tilde{q},\tilde{H})}_{\mathrm{MSSM}}$ the "symmetric" renormalisation in the sfermion sector has to be applied, leading to the relations (7.1), (7.8) for $m^2_{\tilde{b}_1}$ and $\delta m^2_{\tilde{b}_1}$. The contribution of class $(\tilde{q}, \tilde{H})$ can be rewritten by using the mass shift as defined in eq. (7.19) (see also Ref. [30]), leading to the expression

$$\Delta\rho^{(q,\tilde{q},\tilde{H})} = \Delta\rho^{(q)}_{\mathrm{MSSM}} + \Delta\rho^{(\tilde{q},\tilde{H})}_{\mathrm{MSSM,\,full\,OS}} + \Delta m^2_{\tilde{b}_1}\, \partial_{m^2_{\tilde{b}_1}} \Delta\rho^{\mathrm{SUSY}}_{1-\mathrm{loop}} \,, \tag{7.23}$$

where $\Delta\rho^{(\tilde{q},\tilde{H})}_{\mathrm{MSSM,\,full\,OS}}$ is given by

$$\Delta\rho^{(\tilde{q},\tilde{H})}_{\mathrm{MSSM,\,full\,OS}} = \Delta\rho^{(\tilde{q},\tilde{H})}_{2-\mathrm{loop}} + \Delta\rho^{(\tilde{q},\tilde{H})}_{tb-\mathrm{ct}} + \Delta\rho^{(\tilde{q},\tilde{H})}_{\tilde{t}\tilde{b}-\mathrm{ct,\,full\,OS}} \,. \tag{7.24}$$

$\Delta\rho^{(q)}_{\mathrm{MSSM}}$ is the result for the fermion-loop contributions as obtained in Ref. [32] (employing an on-shell renormalisation of the fermion masses and inserting non-zero values for M_h). $\Delta\rho^{(\tilde{q},\tilde{H})}_{\mathrm{MSSM,\,full\,OS}}$ is the contribution of the squark and higgsino diagrams obtained by normalising *all* sfermion masses, i.e. including $m^2_{\tilde{b}_1}$, on-shell, while the last term in eq. (7.23) is a symmetry-restoring contribution involving $\Delta m^2_{\tilde{b}_1}$. The one-loop sfermion contribution $\Delta\rho^{\mathrm{SUSY}}_{1-\mathrm{loop}}$ has been defined in eq. (5.1).

Comparing eqs. (7.24) and (7.21) shows that the "full OS" contribution in eq. (7.24)

is UV-finite already for the partial gauge-less limit of eq. (7.14), according to the discussion of the previous two subsections.

Consistency requires that the mass shift in eq. (7.19) has to be UV-finite as well. One can easily check that this requires taking into account both squark/Higgs and quark/higgsino loops. Correspondingly, because of the necessity of this shift only the sum of the $(\tilde{q})$ and $(\tilde{H})$ contributions to $\Delta\rho$ is physically meaningful in the MSSM.

Moreover, the mass shift $\Delta m^2_{\tilde{b}_1}$ is only finite in the gauge-less limit, i.e. it can only consistently be evaluated if all the gauge-less limit relations (7.3a)–(7.3c) *and* $M_h = 0$, eq. (6.3), are used. The last term in eq. (7.23) can therefore only be obtained in the approximation where $M_h = 0$.

The expression in eq. (7.23) represents the main result of this Thesis. For the first term on the right-hand side of eq. (7.23), $\Delta\rho^{(q)}_{\text{MSSM}}$, we keep the full dependence on M_h. As explained above, this is possible because this term is not affected by the renormalisation in the sfermion sector. For the second term, $\Delta\rho^{(\tilde{q},\tilde{H})}_{\text{MSSM, full OS}}$, we will keep the M_h-dependence as well and compare to the strict gauge-less limit case where $M_h = 0$. The mass shift $\Delta m^2_{\tilde{b}_1}$ entering the last term in eq. (7.23) is evaluated for $M_h = 0$.

The last term in eq. (7.23) can be expressed using eqs. (7.20) and (7.21) as

$$\Delta m^2_{\tilde{b}_1}\, \partial_{m^2_{\tilde{b}_1}} \Delta\rho^{\text{SUSY}}_{\text{1-loop}} = \Delta\rho^{(\tilde{q},\tilde{H})}_{\tilde{t}\tilde{b}\text{-ct, symm}}\big|_{M_h=0} - \Delta\rho^{(\tilde{q},\tilde{H})}_{\tilde{t}\tilde{b}\text{-ct, full OS}}\big|_{M_h=0} \,. \tag{7.25}$$

Correspondingly the full result can be rewritten as

$$\begin{aligned} \Delta\rho^{(q,\tilde{q},\tilde{H})} \;=\; & \Delta\rho^{(q)}_{\text{MSSM}} + \Delta\rho^{(\tilde{q},\tilde{H})}_{\text{2-loop}} + \Delta\rho^{(\tilde{q},\tilde{H})}_{\tilde{t}\tilde{b}\text{-ct}} + \Delta\rho^{(\tilde{q},\tilde{H})}_{\tilde{t}\tilde{b}\text{-ct, full OS}} \\ & + \left[\Delta\rho^{(\tilde{q},\tilde{H})}_{\tilde{t}\tilde{b}\text{-ct, symm}}\big|_{M_h=0} - \Delta\rho^{(\tilde{q},\tilde{H})}_{\tilde{t}\tilde{b}\text{-ct, full OS}}\big|_{M_h=0}\right] . \end{aligned} \tag{7.26}$$

All contributions in the first line of eq. (7.26) can be evaluated by keeping the full M_h dependence. For the other parameters of the Higgs sector we impose the gauge-less limit as specified in (7.3a)–(7.3c).

As a result of eq. (7.15), the gauge-less limit can be relaxed in another way. If the sum of all contributions $(q, \tilde{q}, \tilde{H})$ is considered, the relation $\delta M^2_{H^\pm} = \delta M^2_A$ in eq. (7.15) is valid. As a consequence, in the evaluation of the first line of eq. (7.26) it is not even necessary to use the gauge-less limit for $\sin\alpha$ and M_H. Instead, $\sin\alpha$ and M_H can be set to their true MSSM values. We will discuss the case where the gauge-less limit is relaxed also for these two parameters below.

7.2.4 Renormalisation in the $\overline{\text{DR}}$ scheme

As an alternative to the on-shell scheme in the squark sector, we also consider the $\overline{\text{DR}}$ scheme. In this scheme the counterterms of the soft supersymmetry-breaking parameters are defined to be pure divergences. The squark mass and mixing angle counterterms receive finite contributions corresponding to $m_{t,b}$ in the squark mass matrices (3.21), (3.22):

$$\delta m^2_{\tilde{f}_i}|_{\text{fin}} = \left(U^{\tilde{f}} \delta \mathcal{M}^2_{\tilde{f}} U^{\tilde{f}\dagger}\right)_{ii} \text{ for } \tilde{f}_i = \tilde{t}_{1,2}, \tilde{b}_{1,2}; \tag{7.27}$$

$$\delta u^{\tilde{f}}_{12}|_{\text{fin}} = \frac{\left(U^{\tilde{f}} \delta \mathcal{M}^2_{\tilde{f}} U^{\tilde{f}\dagger}\right)_{12}}{m^2_{\tilde{f}_1} - m^2_{\tilde{f}_2}}, \tag{7.28}$$

$$\delta \mathcal{M}^2_{\tilde{f}}|_{\text{fin}} = \delta m_f|_{\text{fin}} \begin{pmatrix} 2m_f & X_f \\ X_f & 2m_f \end{pmatrix}. \tag{7.29}$$

The result for $\Delta\rho^{(q,\tilde{q},\tilde{H})}$ in the $\overline{\text{DR}}$ scheme follows from eq. (7.26) by replacing $\Delta\rho^{(\tilde{q},\tilde{H})}_{\tilde{t}\tilde{b}-\text{ct, full OS}}$ by the corresponding counterterm resulting from eqs. (7.27)–(7.29). As a consequence, the terms in the second line of eq. (7.26) vanish. The results in

the $\overline{\text{DR}}$ scheme depend on the renormalisation scale $\mu^{\overline{\text{DR}}}$.

7.3 Numerical analysis

In this section the numerical effect of the electroweak two-loop correction eq. (7.23), or equivalently eq. (7.26), is analysed, using the formulae in eq. (2.10) to obtain the corresponding shift in M_W and $\sin^2\theta_{\text{eff}}$. In addition to the full MSSM correction resulting from $\Delta\rho^{(q,\tilde{q},\tilde{H})}$, we also present the effective change compared to the SM result (where the SM Higgs boson mass has been set to M_h). This effective change can be decomposed into the contribution from class (q) and from classes $(\tilde{q},\tilde{H})$. The contribution from class (q), which was studied in Ref. [32], reads

$$\Delta\rho^{(q)}(\text{MSSM}-\text{SM}) = \Delta\rho^{(q)}_{\text{MSSM}} - \Delta\rho^{\text{SM},\alpha_t^2}_{\text{2-loop}}(M_{H^{\text{SM}}} = M_h), \tag{7.30}$$

where $\Delta\rho^{\text{SM},\alpha_t^2}_{\text{2-loop}}$ has been given in eq. (6.6). The contribution from classes $(\tilde{q},\tilde{H})$ is given by

$$\Delta\rho^{(\tilde{q},\tilde{H})} = \Delta\rho^{(\tilde{q},\tilde{H})}_{\text{MSSM, full OS}} + \Delta m^2_{\tilde{b}_1}\,\partial_{m^2_{\tilde{b}_1}}\Delta\rho^{\text{SUSY}}_{\text{1-loop}}\,, \tag{7.31}$$

where $M_h = 0$ is used in the second term. Here and in the following we drop the subscript "MSSM" for simplicity.

As SM input parameters we use the values $m_t = 178.0$ GeV, $m_b = 3$ GeV. The bottom quark mass is to be understood as an effective bottom quark mass, taking into account higher-order QCD corrections.

7.3.1 Impact of relaxing the gauge-less limit for M_h and $\sin\alpha$

In the first step we study the impact of evaluating $\Delta\rho^{(\tilde{q},\tilde{H})}_{\text{MSSM, full OS}}$ (see eq. (7.31)) for the true value of the lightest MSSM Higgs-boson mass M_h rather than for $M_h = 0$. Accordingly, we compare the effect on the EWPO resulting from $\Delta\rho^{(q)}(M_h) + \Delta\rho^{(\tilde{q},\tilde{H})}(M_h)$ and $\Delta\rho^{(q)}(M_h) + \Delta\rho^{(\tilde{q},\tilde{H})}(0)$.

We have investigated the numerical effect of keeping the dependence on M_h in the squark and higgsino contributions for various MSSM scenarios. Fig. 7.4 shows an example where the numerical impact on the prediction of M_W and $\sin^2\theta_{\text{eff}}$ is quite sizable. The EWPO are given as a function of M_A with $M_{\text{SUSY}} = -A_{t,b} = 400$ GeV, $\mu = 800$ GeV and $\tan\beta = 50$. The effect of keeping a non-vanishing value of M_h in the squark and higgsino contributions amounts to about +5 MeV in M_W and -3×10^{-5} to $\sin^2\theta_{\text{eff}}$ for all considered M_A values. The effects for other MSSM scenarios are typically smaller than for the example shown in Fig. 7.4. Unless otherwise stated, we will always keep the full M_h dependence in the results shown below. The difference between the result with and without the M_h dependence can be employed for estimating the residual theoretical uncertainties from unknown higher-order corrections, see the discussion in Sect. 7.3.4 below.

Fig. 7.5 illustrates the numerical effect of relaxing the gauge-less limit on $\sin\alpha$. As discussed at the end of Sect. 7.2.3, the sum of the contributions of classes $(q, \tilde{q}, \tilde{H})$ can be evaluated in a meaningful way even if $\sin\alpha$ and M_H are set to their true values in the MSSM instead of their values in the gauge-less limit. Since the corresponding shift in M_H is usually quite small [41] we do not analyse the effects arising from different choices for M_H and use its gauge-less value throughout the paper. The situation is different for the Higgs mixing angle α. Here the full tree-

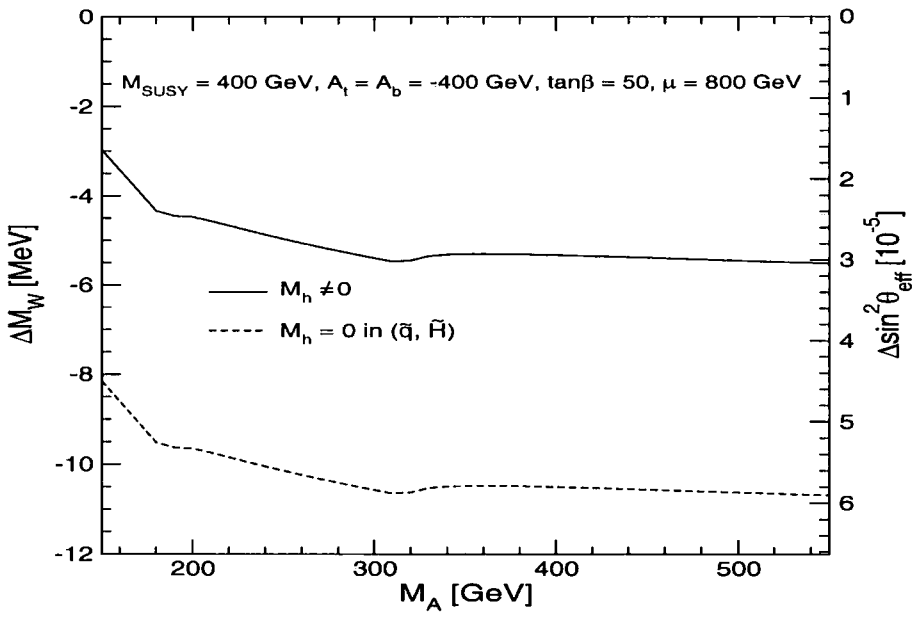

Figure 7.4: ΔM_W and $\Delta \sin^2\theta_{\rm eff}$ are shown as a function for M_A for the case where the full dependence on the mass of the light $\mathcal{CP}$-even Higgs boson is kept, $\Delta\rho^{(q)}(M_h) + \Delta\rho^{(\tilde{q},\tilde{H})}(M_h)$, and for the case where the strict gauge-less limit for M_h has been applied in the squark and higgsino contributions, $\Delta\rho^{(q)}(M_h) + \Delta\rho^{(\tilde{q},\tilde{H})}(0)$.

level value $\sin\alpha^{\rm full}$ as given in eq. (3.9) can significantly deviate from its gauge-less value, $\sin\alpha^{\rm gl} = -\cos\beta$. Fig. 7.5 shows the results for ΔM_W and $\Delta \sin^2\theta_{\rm eff}$ based on $\sin\alpha^{\rm full}$ and $\sin\alpha^{\rm gl}$. The parameters are chosen in such a way as to maximise the influence of $\sin\alpha^{\rm full}$ vs. $\sin\alpha^{\rm gl}$. The value $\tan\beta = 6$ is rather small, and e.g. together with $M_A = 150$ GeV it leads to $\sin\alpha^{\rm full} = -0.31$ and $\sin\alpha^{\rm gl} = -0.16$. For $M_{\rm SUSY} = \mu = 400$ GeV and $A_{t,b} = -800$ this parameter set is in agreement with all experimental constraints from Higgs boson searches [50, 51] and b-physics [4]. Fig. 7.5 shows that even in this scenario the numerical effect of relaxing the gauge-less limit on $\sin\alpha$ is negligible. We have checked that this holds in general. In particular for larger $\tan\beta$ and/or M_A the effect is even smaller. Therefore we will always set $\sin\alpha$ to $\sin\alpha^{\rm gl}$ in the following.

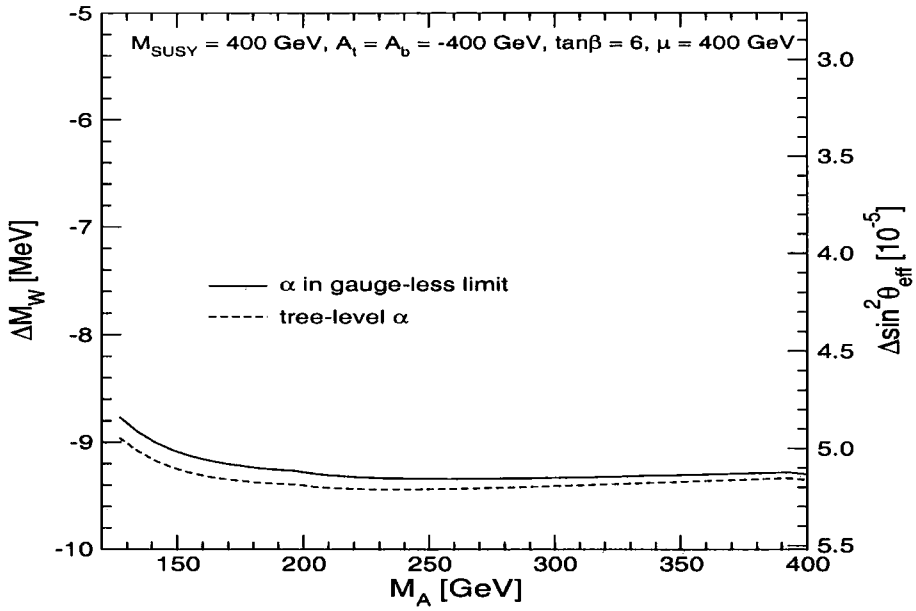

Figure 7.5: ΔM_W and $\Delta \sin^2\theta_{\rm eff}$ are shown for the case where the Higgs mixing angle α obeys either the full tree-level relation, eq. (3.9), or is fixed by the gauge-less limit, eq. (7.3b).

7.3.2 Dependence on supersymmetric parameters

In Figs. 7.6, 7.7 and 7.9 we explore the numerical impact of $\Delta\rho^{(q,\tilde{q},\tilde{H})}$ on M_W and $\sin^2\theta_{\rm eff}$ for various MSSM parameter choices. The values are chosen such that experimental constraints are fulfilled for most parts of the parameter space. Fig. 7.6 shows a scenario with large $\tan\beta$, $\tan\beta = 50$, and $M_{\rm SUSY} = M_A = 300$ GeV and $\mu = 500$ GeV. The results are plotted as functions of the stop-mixing parameter $X_t = \tilde{A} - \mu/\tan\beta$ (see eq. (3.21)), and we chose $A_b = \tilde{A}$. The two-loop contributions ΔM_W and $\Delta \sin^2\theta_{\rm eff}$ are decomposed into the SM result, $\Delta\rho^{\rm SM,\alpha_t^2}_{\rm 2-loop}(M_{H^{\rm SM}} = M_h)$, as given in eq. (6.6) (shown with reversed sign for better visibility), $\Delta\rho^{(q)}(\text{MSSM} - \text{SM})$ as given in eq. (7.30), and $\Delta\rho^{(\tilde{q},\tilde{H})}$ as given in eq. (7.31). For the latter contribution both the result with the correct MSSM value for M_h and with $M_h = 0$ is shown. We find that $\Delta\rho^{(\tilde{q},\tilde{H})}$ induces shifts in M_W and $\sin^2\theta_{\rm eff}$ of up to $+8$ MeV in M_W and -4×10^{-5} in $\sin^2\theta_{\rm eff}$. The

corrections are significantly larger than the effective change compared to the SM arising from class (q), $\Delta\rho^{(q)}(\text{MSSM} - \text{SM})$. The impact of relaxing the gauge-less limit on M_h in $\Delta\rho^{(\tilde{q},\tilde{H})}$ is clearly visible, although not as pronounced as in Fig. 7.4. It should be noted that small mixing in the stop sector (in this scenario values of $|X_t| \lesssim 350$ GeV) is disfavoured by the LEP Higgs searches [50, 51], i.e. the dependence on M_h is largest where its value is already experimentally excluded. For small values of $|X_t|$ the supersymmetric contribution $\Delta\rho^{(q)}(\text{MSSM} - \text{SM}) + \Delta\rho^{(\tilde{q},\tilde{H})}$ is almost as large as the SM result, $\Delta\rho^{\text{SM},\alpha_t^2}_{\text{2-loop}}(M_{H^{\text{SM}}} = M_h)$, and largely compensates it. For large values of $|X_t|$ the supersymmetric contribution reduces the SM result by about 40%.

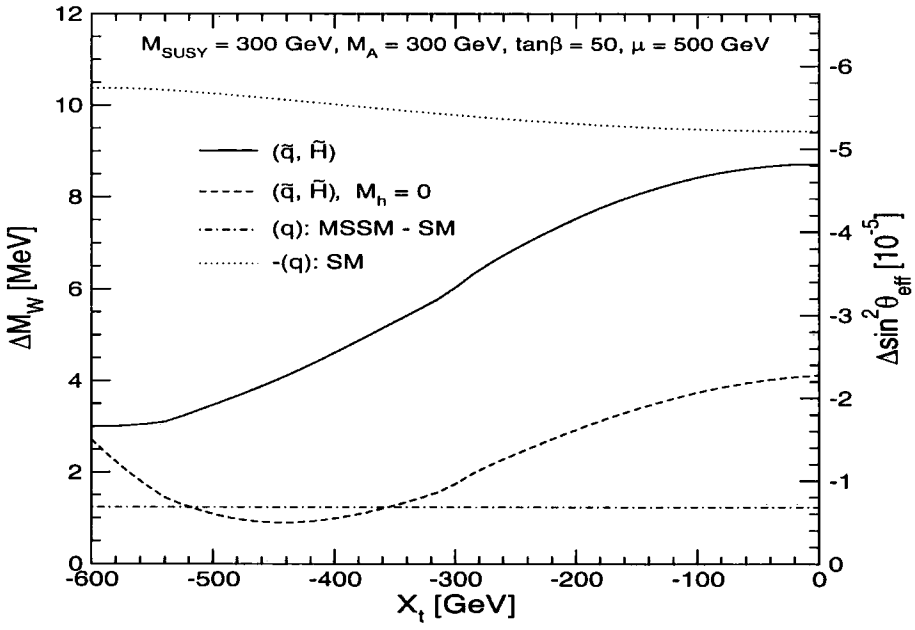

Figure 7.6: ΔM_W and $\Delta \sin^2\theta_{\text{eff}}$ are shown as a function of X_t in a scenario with large $\tan\beta$. The two-loop contribution involving squarks and higgsinos, $\Delta\rho^{(\tilde{q},\tilde{H})}$, is shown for the correct MSSM value of M_h and for $M_h = 0$. For the class (q) the effective change from the SM to the MSSM is shown and compared with the pure SM contribution (with the sign reversed for better visibility).

In Fig. 7.7 we show a similar plot for a parameter scenario with small Higgsino mass, $\mu = 200$ GeV, and $\tan\beta = 6$, $M_{\text{SUSY}} = 400$ GeV, $M_A = 300$ GeV. The

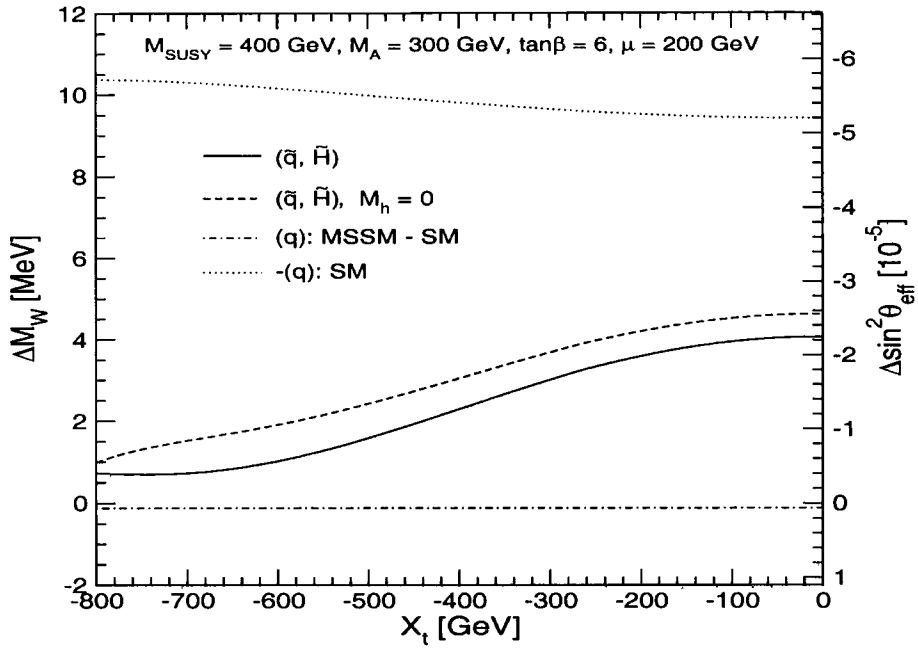

Figure 7.7: ΔM_W and $\Delta \sin^2\theta_{\rm eff}$ are shown as a function of X_t in a scenario with small μ and $\tan\beta$. The two-loop contribution involving squarks and higgsinos, $\Delta\rho^{(\tilde{q},\tilde{H})}$, is shown for the correct MSSM value of M_h and for $M_h = 0$. For the class (q) the effective change from the SM to the MSSM is shown and compared with the pure SM contribution (with the sign reversed for better visibility).

contribution of $\Delta\rho^{(\tilde{q},\tilde{H})}$ amounts to about 1–2 MeV in M_W and -1×10^{-5} in $\sin^2\theta_{\rm eff}$ in this case. The fermion loop contribution $\Delta\rho^{(q)}(\mathrm{MSSM} - \mathrm{SM})$ is very small here because the small value of $\tan\beta$ does not lead to an enhancement of α_b in the MSSM with respect to the SM.

Fig. 7.8 shows the one-loop results, $\Delta\rho^{\rm SUSY}_{\rm 1-loop}$, corresponding to the scenarios of Figs. 7.6, 7.7. Due to the larger value of $M_{\rm SUSY}$ and the small value of $\tan\beta$ the one-loop contributions for the second scenario are relatively small. The region of small $|X_t|$ is again ruled out by LEP Higgs searches. The largest effects visible in Fig. 7.8 are thus experimentally excluded. Comparing the one-loop with the two-loop results, one can see that the two-loop contributions from $\Delta\rho^{(\tilde{q},\tilde{H})}$ amounts to about 10% of the one-loop supersymmetric contributions.

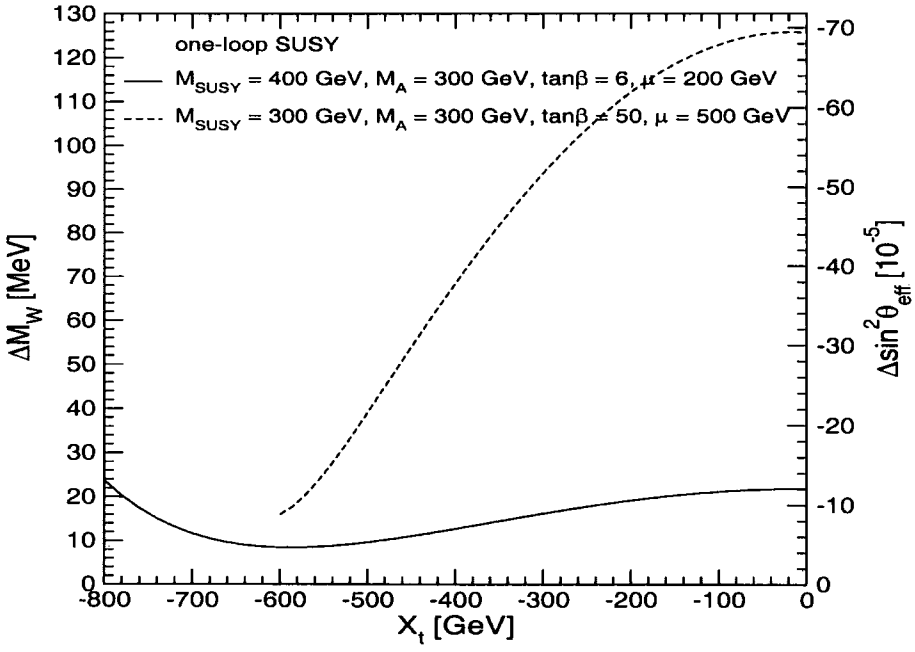

Figure 7.8: One-loop SUSY contributions to ΔM_W and $\Delta \sin^2 \theta_{\rm eff}$ are shown as a function of X_t. The parameters correspond to the two scenarios analysed in Figs. 7.6 and 7.7.

A common feature of the two scenarios, visible in Figs. 7.6, 7.7, 7.8, is that both the one- and two-loop supersymmetric contributions first decrease for increasing $|X_t|$ until a minimum is reached in the vicinity of $X_t \sim -2M_{\rm SUSY}$. For even larger mixing one stop mass becomes very small and the supersymmetric contributions increase again.

7.3.3 Results in SPS scenarios and renormalisation scheme dependence

Fig. 7.9 shows the results for $\Delta\rho^{(\tilde{q},\tilde{H})}$ in the SPS 1a benchmark scenario [52] for a moderate value of $\tan\beta = 10$ and four different combinations for μ and M_A,

$$(\mu/\text{GeV}, M_A/\text{GeV}) = (200, 200), (200, 1000), (500, 500), (500, 1000). \qquad (7.32)$$

In order to display the dependence on the scale of supersymmetry, we start from the nominal values of the MSSM parameters corresponding to the SPS 1a point [52] (besides μ and M_A that are chosen as specified in eq. (7.32)) and vary the parameters $M_{\rm SUSY}$ and $A_{t,b}$ using a common scale factor; the results are then shown as functions of $M_{\rm SUSY}$.[2] The range of $M_{\rm SUSY}$ values shown in Fig. 7.9 has been chosen such that compatibility with Higgs-boson mass [51] and b-physics [4] constraints is ensured for most parts of the parameter space. For small values of $M_{\rm SUSY}$ the corrections differ by up to 4 MeV depending on the choice of M_A and μ. Smaller values of M_A and μ result in larger corrections to M_W and $\sin^2\theta_{\rm eff}$. In all cases the result decreases with increasing $M_{\rm SUSY}$ as expected. The corresponding supersymmetric one-loop contributions induced by $\Delta\rho^{\rm SUSY}_{\rm 1-loop}$ are shown in Fig. 7.10 for comparison. The two-loop correction from $\Delta\rho^{(\tilde{q},\tilde{H})}$ amounts up to 25% of the MSSM one-loop result.

We now study the renormalisation scheme dependence of the one-loop and two-loop results for three benchmark SPS scenarios. Besides the "standard" scenario SPS 1a, we also investigate the SPS 1b scenario, which is characterised by a larger $\tan\beta$ value, $\tan\beta = 30$, and SPS 5, which involves a relatively light $\tilde{t}$ [52]. Fig. 7.11 shows the one-loop results for the three scenarios, while Figs. 7.12, 7.13, 7.14 display the two-loop results. As above, the results are shown as functions of $M_{\rm SUSY}$. We have started from the nominal values of the MSSM parameters for the three benchmark points and varied the parameters $M_{\rm SUSY}$, $A_{t,b}$, μ (for the $\overline{\rm DR}$ results also the scale $\mu^{\overline{\rm DR}}$) using a common scale factor. The actual SPS 1a, SPS 1b and SPS 5 benchmark points correspond to $M_{\rm SUSY} = 495.9$, 762.5, 535.2 GeV, respectively [52].

For a meaningful comparison of the results in the on-shell and the $\overline{\rm DR}$ renormal-

[2] More precisely, for the SPS points the soft supersymmetry-breaking parameters $M_{\tilde{t}_L,\tilde{t}_R,\tilde{b}_R}$ for the left- and right-handed $\tilde{t}$, $\tilde{b}$ are all slightly different. $M_{\rm SUSY}$ is identified with $M_{\tilde{t}_L}$.

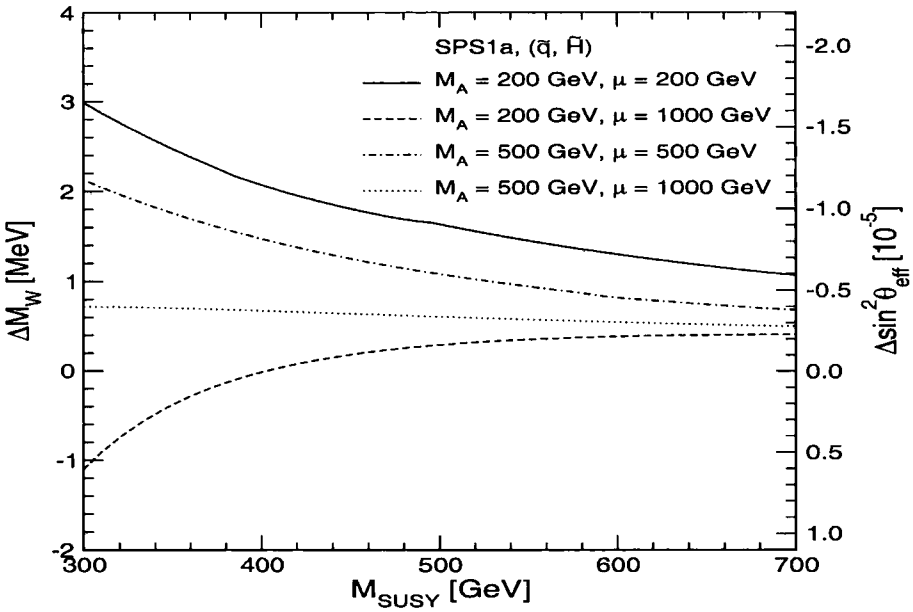

Figure 7.9: The shifts ΔM_W and $\Delta \sin^2\theta_{\text{eff}}$ induced by $\Delta\rho^{(\tilde{q},\tilde{H})}$ are shown as a function of M_{SUSY} in the SPS 1a scenario for four combinations of and $M_A = 200, 500$ GeV and $\mu = 200, 500, 1000$ GeV.

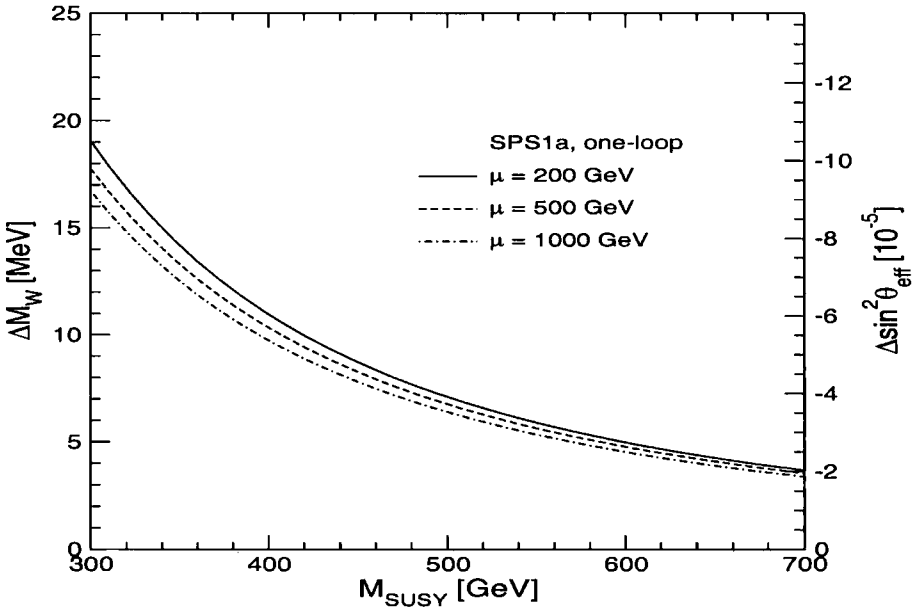

Figure 7.10: The shifts ΔM_W and $\Delta \sin^2\theta_{\text{eff}}$ induced by the supersymmetric one-loop contributions are shown as a function of M_{SUSY} in the SPS 1a scenario for $\mu = 200, 500, 1000$ GeV and $\tan\beta = 10$.

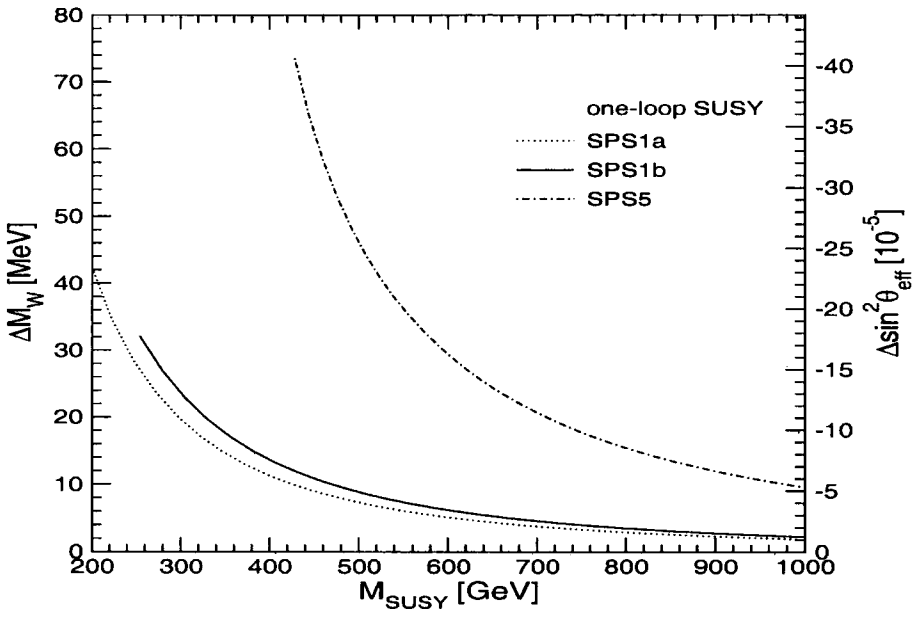

Figure 7.11: The shifts ΔM_W and $\Delta \sin^2\theta_{\rm eff}$ induced by the supersymmetric one-loop contribution $\Delta\rho^{\rm SUSY}_{\rm 1-loop}$ are shown for the three benchmark scenarios SPS 1a, SPS 1b and SPS 5 as a function of $M_{\rm SUSY}$. The parameters of the squark sector correspond to the on-shell scheme.

isation schemes, the input parameters in the two schemes have to be physically equivalent, which implies that they are numerically different. Since the parameters in the SPS scenarios are defined as $\overline{\rm DR}$ parameters, they can directly be used as input parameters in the $\overline{\rm DR}$ scheme. The corresponding input parameters for the calculation in the on-shell scheme are obtained by requiring

$$(m^2_{\tilde{f}_i} + \delta m^2_{\tilde{f}_i})^{\rm OS} = (m^2_{\tilde{f}_i} + \delta m^2_{\tilde{f}_i})^{\overline{\rm DR}} \tag{7.33}$$

for the squark masses and similarly for the mixing angles.

In the one-loop results $\Delta\rho^{\rm SUSY}_{\rm 1-loop}$ for the three SPS scenarios shown in Fig. 7.11 the squark sector parameters correspond to the on-shell scheme. The shift in the precision observables induced by $\Delta\rho^{\rm SUSY}_{\rm 1-loop}$ is found to be particularly large for the SPS 5 scenario, as a consequence of the large splitting between the squark masses

in this scenario.

In Figs. 7.12–7.14 we show the one-loop result parametrised in terms of on-shell parameters (dotted line) and the two-loop $(\tilde{q}, \tilde{H})$ results obtained in the $\overline{\text{DR}}$ (full line) and the OS scheme (dot-dashed line), in all cases relative to the one-loop result parametrised in terms of the $\overline{\text{DR}}$ parameters. Accordingly, the three lines in each plot correspond to

$$\left\{ \begin{array}{l} \Delta\rho_{\text{1-loop}}^{\text{SUSY,OS}} \\ \Delta\rho_{\text{1-loop}}^{\text{SUSY},\overline{\text{DR}}} + \Delta\rho^{(\tilde{q},\tilde{H}),\overline{\text{DR}}} \\ \Delta\rho_{\text{1-loop}}^{\text{SUSY,OS}} + \Delta\rho^{(\tilde{q},\tilde{H}),\text{OS}} \end{array} \right\} - \Delta\rho_{\text{1-loop}}^{\text{SUSY},\overline{\text{DR}}}. \tag{7.34}$$

The pure two-loop correction in the $\overline{\text{DR}}$ scheme is given by the full line, while the two-loop correction in the on-shell scheme corresponds to the difference between the dot-dashed and the dashed line.

The numerical impact of the two-loop correction $\Delta\rho^{(\tilde{q},\tilde{H})}$ in the scenarios SPS 1a, 1b amounts to about 5–6 MeV in M_W and -3×10^{-5} in $\sin^2\theta_{\text{eff}}$ for small M_{SUSY} and decreases to about 1 MeV in M_W (-0.5×10^{-5} in $\sin^2\theta_{\text{eff}}$) for larger values of M_{SUSY}. For SPS 5 the corrections are slightly smaller. While in the scenarios SPS 1a, 1b the two-loop results in the two schemes are very close to each other, a larger deviation is visible in the SPS 5 scenario. In the latter scenario the two-loop corrections in the on-shell scheme are less than 1 MeV, while in the $\overline{\text{DR}}$ scheme they are more than twice as large. Comparison with the one-loop results given in Fig. 7.11 shows that the two-loop corrections amount to about 10% one-loop MSSM contribution.

The comparison of the renormalisation schemes shows that the scheme dependence is strongly reduced by going from the one-loop to the two-loop level. At the

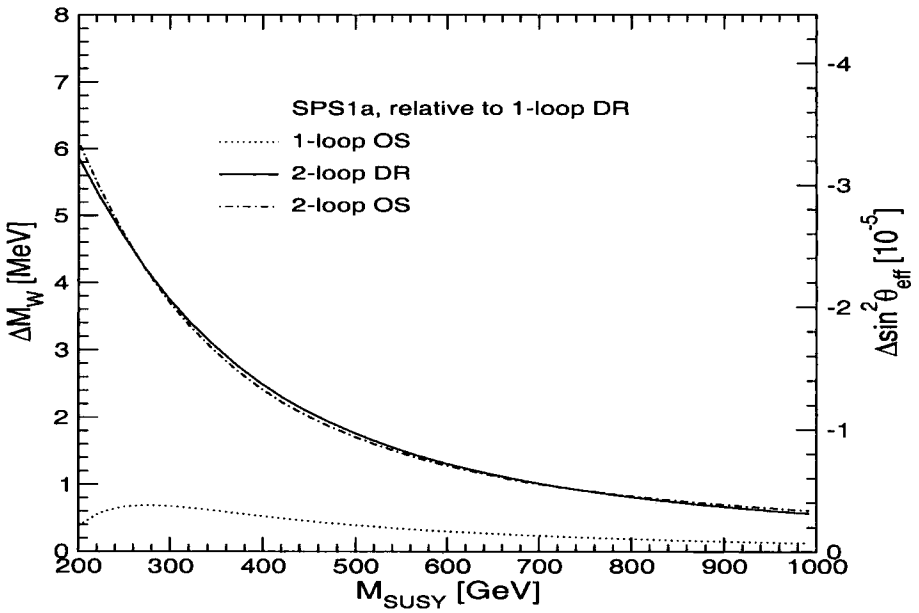

Figure 7.12: ΔM_W and $\Delta \sin^2\theta_{\rm eff}$ are shown in the SPS 1a scenario as a function of $M_{\rm SUSY}$. The results for the one-loop contribution expressed in terms of on-shell parameters and for the two-loop result $\Delta\rho^{\rm SUSY}_{\rm 1-loop} + \Delta\rho^{(\tilde{q},\tilde{H})}$ in the on-shell and the $\overline{\rm DR}$ scheme are given relative to the one-loop result expressed in terms of $\overline{\rm DR}$ parameters, see eq. (7.34).

one-loop level, where the scheme difference is entirely due to the different input parameters for the squark masses and mixing angles, the difference between the on-shell and the $\overline{\rm DR}$ scheme is of $\mathcal{O}(1\ {\rm MeV})$ in M_W. Taking into account the two-loop corrections reduces the difference below 0.1 MeV for SPS 1a,b and about 0.2 MeV for SPS 5.

The size of the two-loop corrections for SPS 1a,b is found to be much larger than the difference between the two schemes at the one-loop level, which is only about 1 MeV for these scenarios. This indicates that the difference between the results in two renormalisation schemes, if taken as the only measure for estimating the theoretical uncertainties from unknown higher-order corrections, may result in a significant underestimate of the actual theoretical uncertainty. The SPS 5 scenario, on the other hand, is an example where the two-loop corrections turn out to be

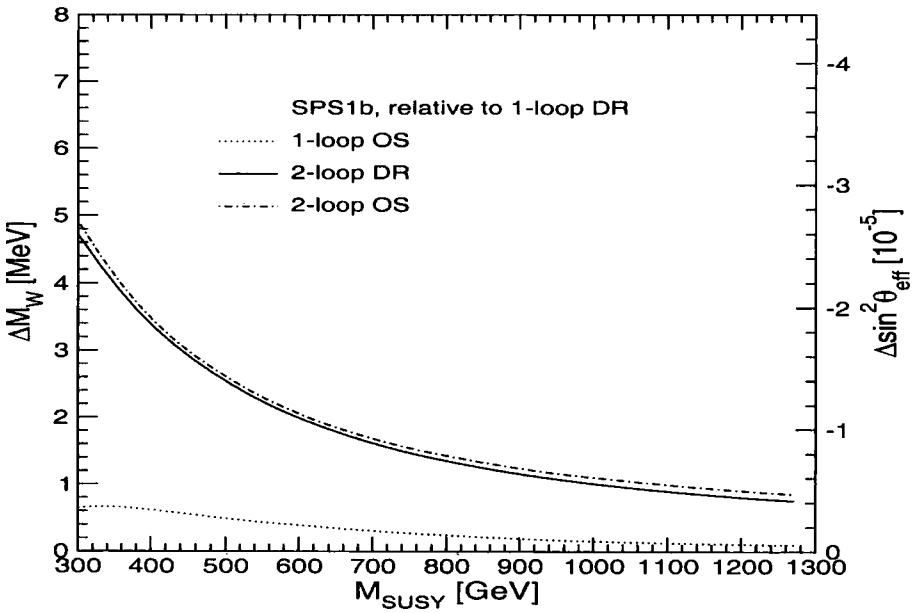

Figure 7.13: ΔM_W and $\Delta \sin^2\theta_{\rm eff}$ are shown in the SPS 1b scenario as a function of $M_{\rm SUSY}$. The results for the one-loop contribution expressed in terms of on-shell parameters and for the two-loop result $\Delta\rho^{\rm SUSY}_{\rm 1-loop} + \Delta\rho^{(\tilde{q},\tilde{H})}$ in the on-shell and the $\overline{\rm DR}$ scheme are given relative to the one-loop result expressed in terms of $\overline{\rm DR}$ parameters, see eq. (7.34).

smaller than the scheme difference at one-loop order.

Finally we compare the two-loop results for the $(\tilde{q},\tilde{H})$ contributions obtained in this paper with the two-loop QCD corrections of $\mathcal{O}(\alpha\alpha_s)$ as obtained in Ref. [30]. In Fig. 7.15 we show the results in the on-shell scheme for the three SPS scenarios as a function of $M_{\rm SUSY}$ (as explained above). For SPS 1a and 1b both corrections are roughly of the same size and compensate each other to a large extent. Only for the case of SPS 5 the QCD corrections are significantly larger than the two-loop Yukawa corrections. Both the QCD and the Yukawa corrections are non-negligible in view of the anticipated future experimental accuracies and are larger than the current theoretical uncertainties in the SM.

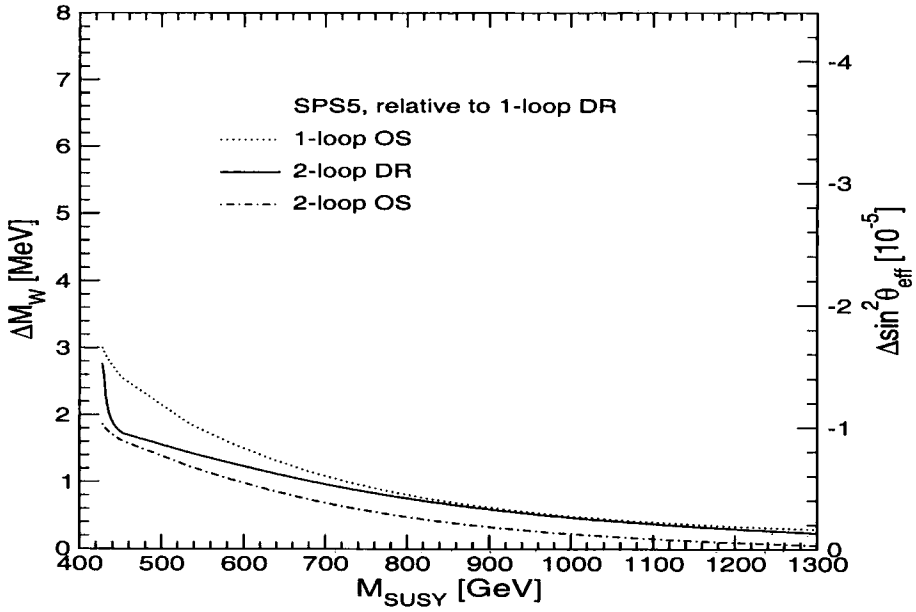

Figure 7.14: ΔM_W and $\Delta \sin^2\theta_{\rm eff}$ are shown in the SPS 5 scenario as a function of $M_{\rm SUSY}$. The results for the one-loop contribution expressed in terms of on-shell parameters and for the two-loop result $\Delta\rho^{\rm SUSY}_{\rm 1-loop} + \Delta\rho^{(\tilde{q},\tilde{H})}$ in the on-shell and the $\overline{\rm DR}$ scheme are given relative to the one-loop result expressed in terms of $\overline{\rm DR}$ parameters, see eq. (7.34).

7.3.4 Estimate of unknown higher-order corrections

As discussed above, the theoretical evaluation of the EWPO in the SM is significantly more advanced than in the MSSM. In order to obtain an accurate prediction for the EWPO within the MSSM it is therefore useful to take all known SM corrections into account. This can be done by writing the MSSM prediction for the observable O ($O = M_W, \sin^2\theta_{\rm eff}, \ldots$) as

$$O_{\rm MSSM} = O_{\rm SM} + O_{\rm MSSM-SM} \,, \tag{7.35}$$

where $O_{\rm SM}$ is the prediction in the SM including all known corrections, and $O_{\rm MSSM-SM}$ is the difference between the MSSM and the SM predictions, evalu-

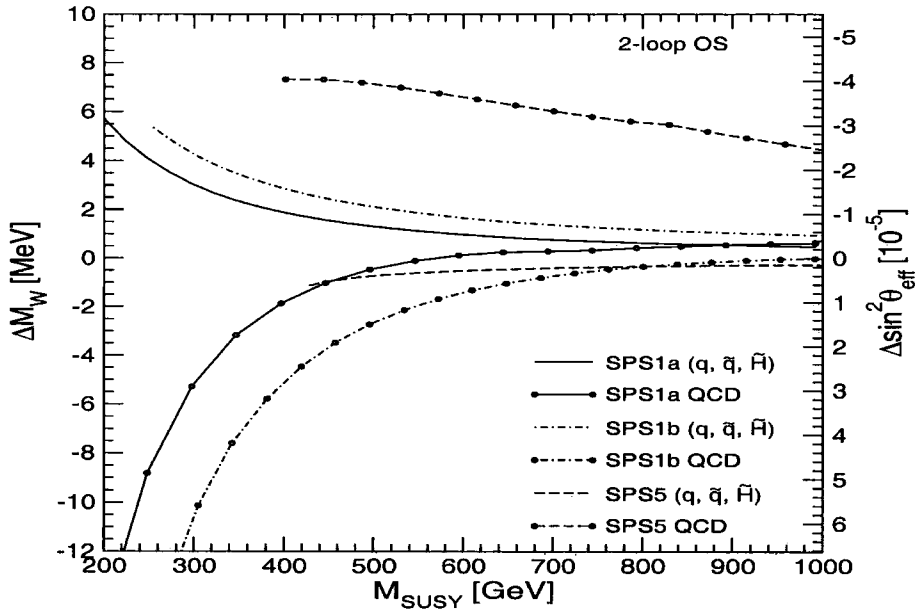

Figure 7.15: The effect of the two-loop Yukawa corrections from squark and higgsino loops is compared with the squark-loop corrections of $\mathcal{O}(\alpha\alpha_s)$. ΔM_W and $\Delta \sin^2\theta_{\text{eff}}$ are shown in the three SPS scenarios as a function of M_{SUSY} in the on-shell scheme.

ated at the level of precision of the known MSSM corrections. The expression given in eq. (7.35) contains higher-order contributions that are only known for SM particles in the loop but not for their superpartners (e.g. two-loop electroweak corrections beyond the leading Yukawa contributions calculated in this thesis and three-loop corrections of $\mathcal{O}(\alpha\alpha_s^2)$). In the decoupling limit where all superpartners are heavy and the Higgs sector becomes SM-like, the result of eq. (7.35) obviously yields a more precise prediction than a result based on only those corrections which are known in the full MSSM. In this case the second term in eq. (7.35) goes to zero, so that the MSSM result approaches the SM result with $M_{H^{\text{SM}}} = M_h$. For lower values of the scale of supersymmetry the contribution from supersymmetric particles in the the loop may be of comparable size as the known SM corrections. In view of the experimental bounds on the masses of the supersymmetric particles (and the fact that supersymmetry has to be broken), however, a complete can-

cellation between the SM and supersymmetric contributions is not expected. It therefore seems appropriate to apply eq. (7.35) also in this case.

Expressing the predictions for the EWPO as in eq. (7.35) implies that the theoretical uncertainties from unknown higher-order corrections reduce to those in the SM in the decoupling limit. In the SM, based on all higher-order contributions that are currently known, the remaining uncertainties in M_W [35] and $\sin^2\theta_{\rm eff}$ [36] have been estimated to be

$$\delta M_W^{\rm SM} = 4 \text{ MeV}, \quad \delta \sin^2\theta_{\rm eff}^{\rm SM} = 5 \times 10^{-5} . \tag{7.36}$$

Below the decoupling limit an additional theoretical uncertainty arises from higher-order corrections involving supersymmetric particles in the loops. In the following we will estimate this additional theoretical uncertainty in the prediction of M_W and $\sin^2\theta_{\rm eff}$ depending on the supersymmetric parameters. We will provide estimates for the uncertainty for three values of the squark mass scale, $M_{\rm SUSY} = 200$, 500, 1000 GeV. A similar approach of estimating the remaining uncertainties from unknown higher-order corrections with dependence on the supersymmetric parameters has recently been applied to the Higgs sector and implemented in the program *FeynHiggs*2.2, see Ref. [44] for details.

The remaining uncertainties from unknown higher-order corrections involving supersymmetric particles mainly arise from the following sources:

- Electroweak two-loop corrections beyond the leading Yukawa corrections evaluated in this paper:

  We estimate the numerical effect of these corrections by assuming that the ratio of the sub-leading electroweak two-loop corrections to the two-loop Yukawa corrections is the same in the SM as in the MSSM. Inserting the

known SM corrections [34,35] we infer an estimate of the possible size of the missing supersymmetric electroweak two-loop contributions.

- $\mathcal{O}(\alpha\alpha_s)$ corrections beyond the $\Delta\rho$ approximation:

  We estimate the size of these corrections by assuming that the ratio of the contribution entering via $\Delta\rho$ to the full result is the same as for the known SM result [53].

- $\mathcal{O}(\alpha\alpha_s^2)$ corrections:

  We use three different methods for estimating the possible size of these corrections. The unknown ratio of the $\mathcal{O}(\alpha\alpha_s^2)$ supersymmetric contributions to the $\mathcal{O}(\alpha\alpha_s)$ supersymmetric contributions can be estimated by assuming that it is the same as for the corresponding corrections in the SM [54] (estimate (a)) and, using geometric progression from lower orders, by assuming that it is the same as the ratio of the $\mathcal{O}(\alpha\alpha_s)$ supersymmetric contributions and the $\mathcal{O}(\alpha)$ supersymmetric contributions (estimate (b)). As a further indication of the possible size of unknown corrections of $\mathcal{O}(\alpha\alpha_s^2)$ we vary the renormalisation scale of $\alpha_s(\mu^{\overline{\rm DR}})$ entering the $\mathcal{O}(\alpha\alpha_s)$ result according to $m_t/2 \leq \mu^{\overline{\rm DR}} \leq 2m_t$ (estimate (c)). It should be noted that this variation of $\alpha_s(\mu^{\overline{\rm DR}})$ corresponds to only a part of the higher-order corrections, so that estimates (a) and (b) should be regarded as more conservative.

- $\mathcal{O}(\alpha^2\alpha_s)$ corrections:

  Similarly as for the $\mathcal{O}(\alpha\alpha_s^2)$ corrections, we again use three different methods for estimating these corrections. The unknown ratio of the $\mathcal{O}(\alpha^2\alpha_s)$ supersymmetric contributions to the $\mathcal{O}(\alpha^2)$ (leading Yukawa) supersymmetric contributions can be estimated by assuming that it is the same as for the corresponding corrections in the SM [55] (estimate (a)) and by assuming that it is the same as the ratio of the $\mathcal{O}(\alpha\alpha_s)$ supersymmetric contributions and

the $\mathcal{O}(\alpha)$ supersymmetric contributions (estimate (b)). As a further indication of possible corrections of $\mathcal{O}(\alpha^2\alpha_s)$ we change the value of m_t in the result for the two-loop supersymmetric Yukawa corrections from the on-shell value, $m_t^{\rm OS}$, to the running mass $m_t(m_t)$, where $m_t(m_t) = m_t^{\rm OS}/(1+4/(3\pi)\,\alpha_s(m_t))$ (estimate (c)). The latter replacement accounts only for a subset of the unknown $\mathcal{O}(\alpha^2\alpha_s)$ corrections.

- Electroweak three-loop corrections:

  As an indication of the possible size of these corrections we use the renormalisation scheme dependence of our result for the supersymmetric two-loop Yukawa corrections, see Figs. 7.12–7.14.

We have evaluated the above estimates for the three scenarios SPS 1a, SPS 1b, and SPS 5, each for $M_{\rm SUSY} = 1000$ GeV, 500 GeV, and for $M_{\rm SUSY} < 500$ GeV [3] (as above we have varied $M_{\rm SUSY}$, $A_{t,b}$ and μ using a common scale factor). The estimated theoretical uncertainties for M_W arising from the different classes of unknown higher-order corrections are shown in Tab. 7.1. The result given in each entry corresponds to the largest value obtained in the three considered SPS scenarios. The three numbers given for the $\mathcal{O}(\alpha\alpha_s^2)$ and $\mathcal{O}(\alpha^2\alpha_s)$ corrections correspond to the estimates (a), (b) and (c) described above.

As expected, the estimated uncertainties associated with the supersymmetric higher-order contributions decrease for increasing $M_{\rm SUSY}$. For the $\mathcal{O}(\alpha\alpha_s^2)$ and $\mathcal{O}(\alpha^2\alpha_s)$ corrections, method (c) that accounts only for a part of the higher-order corrections yields in both cases the most optimistic estimate. As discussed earlier, by taking into account the true MSSM-value of M_h, certain parts of the electroweak

[3] The lowest values considered for $M_{\rm SUSY}$ are 200, 300, 400 GeV for SPS1a, SPS1b, SPS5, respectively. These are the lowest values shown in Figs. 7.12, 7.13, 7.14. For lower values the parameter points are excluded by Higgs mass constraints.

$M_{\rm SUSY}$	<500 GeV	500 GeV	1000 GeV
$\mathcal{O}(\alpha^2)$ sub-leading	6.0	2.0	0.8
$\mathcal{O}(\alpha\alpha_s)$ sub-leading	1.8	0.9	0.5
$\mathcal{O}(\alpha\alpha_s^2)$	3.0, 5.3, 1.5	1.4, 1.1, 0.7	0.9, 2.2, 0.5
$\mathcal{O}(\alpha^2\alpha_s)$	1.5, 2.2, 1.4	0.6, 0.8, 0.4	0.2, 0.2, 0.2
$\mathcal{O}(\alpha^3)$	0.3	0.3	0.3

Table 7.1: Estimated uncertainties for M_W in MeV for different classes of unknown higher-order corrections involving supersymmetric particles are given for three values of $M_{\rm SUSY}$. The estimates have been obtained using the results for the SPS 1a, SPS 1b, and SPS 5 scenarios. The three entries for the $\mathcal{O}(\alpha\alpha_s^2)$ and $\mathcal{O}(\alpha^2\alpha_s)$ corrections correspond to three different methods for estimating the uncertainties (see text).

corrections, beyond the leading two-loop Yukawa corrections, are included in our result. The difference between $\Delta\rho^{(\tilde{q},\tilde{H})}(M_h)$ and $\Delta\rho^{(\tilde{q},\tilde{H})}(0)$ may be interpreted as an estimate of the size of further, not included higher-order electroweak corrections. The numerical analysis in Sects. 7.3.1 and 7.3.2 shows that this estimate is typically smaller than the estimated total uncertainty in Tab. 7.1.

We now combine the values given in Tab. 7.1 into our total estimate of the remaining theoretical uncertainties from unknown higher-order corrections involving supersymmetric particles. Adopting the largest of the three values for the $\mathcal{O}(\alpha\alpha_s^2)$ and $\mathcal{O}(\alpha^2\alpha_s)$ as a conservative error estimate and adding the different estimates in quadrature we obtain

$$\begin{aligned} \delta M_W &= 8.5 \text{ MeV for } M_{\rm SUSY} < 500 \text{ GeV}, \\ \delta M_W &= 2.7 \text{ MeV for } M_{\rm SUSY} = 500 \text{ GeV}, \\ \delta M_W &= 2.4 \text{ MeV for } M_{\rm SUSY} = 1000 \text{ GeV}. \end{aligned} \tag{7.37}$$

An analogous analysis of the remaining higher-order uncertainties can also be carried out for $\sin^2\theta_{\rm eff}$. Since parts of the missing higher-order corrections to $\sin^2\theta_{\rm eff}$ and M_W are related to each other, we employ eq. (2.10) to infer estimates for $\sin^2\theta_{\rm eff}$ from our results for M_W. This yields

$$\begin{aligned}
\delta\sin^2\theta_{\rm eff} &= 4.7\times10^{-5} \text{ for } M_{\rm SUSY} < 500 \text{ GeV},\\
\delta\sin^2\theta_{\rm eff} &= 1.5\times10^{-5} \text{ for } M_{\rm SUSY} = 500 \text{ GeV},\\
\delta\sin^2\theta_{\rm eff} &= 1.3\times10^{-5} \text{ for } M_{\rm SUSY} = 1000 \text{ GeV}.
\end{aligned} \tag{7.38}$$

The full theory uncertainty in the MSSM can be obtained by adding in quadrature the SM uncertainties from eq. (7.36) and the SUSY uncertainties from eqs. (7.37)–(7.38). This yields $\delta M_W = (4.7 - 9.4)$ MeV and $\delta\sin^2\theta_{\rm eff} = (5.2 - 6.7)\times10^{-5}$ depending on the SUSY mass scale.

The estimated uncertainties are smaller than the estimates in Ref. [19] (where an overall estimate has been given without analysing the dependence on the supersymmetric parameters), reflecting the improvement associated with the new corrections calculated in this paper.

The other source of theoretical uncertainties besides the one from unknown higher-order corrections is the parametric uncertainty induced by the experimental errors of the input parameters. The current experimental error of the top-quark mass [5] induces the following parametric uncertainties in M_W and $\sin^2\theta_{\rm eff}$

$$\delta m_t^{\rm exp} = 2.9 \text{ GeV} \;\Rightarrow\; \delta M_W^{{\rm para},m_t} = 17.5 \text{ MeV},\;\; \delta\sin^2\theta_{\rm eff}^{{\rm para},m_t} = 9.4\times10^{-5}\,. \tag{7.39}$$

This uncertainty will decrease during the next years as a consequence of a further improvement of the accuracy on m_t at the Tevatron and the LHC. Ultimately

it will be reduced by more than an order of magnitude at the ILC [56]. The accuracy of the theoretical predictions for M_W and $\sin^2\theta_{\rm eff}$ will then be limited by the uncertainty from unknown higher-order corrections (for a discussion of the parametric uncertainties induced by the other SM input parameters see Ref. [19]). A further reduction of the uncertainties from higher-order SM-type corrections (see eq. (7.36)) and corrections involving supersymmetric particles (see eqs. (7.37)–(7.38)) therefore seems to be required in order to fully exploit the prospective experimental accuracies on M_W, $\sin^2\theta_{\rm eff}$ and m_t reachable at the next generation of colliders [56, 57].

7.4 Chapter summary

In this chapter we have calculated the two-loop corrections of $\mathcal{O}(\alpha_t^2)$, $\mathcal{O}(\alpha_t\alpha_b)$, $\mathcal{O}(\alpha_b^2)$ to the electroweak precision observables M_W and $\sin^2\theta_{\rm eff}$ in the MSSM. These are the leading, Yukawa-enhanced electroweak two-loop contributions; they enter via $\Delta\rho$ and arise from diagrams involving SM quarks, squarks, Higgs bosons and higgsinos. While previously only the contribution from the diagrams with quarks and Higgs bosons had been known (corresponding to the limiting case where all supersymmetric particles are infinitely heavy), we have evaluated the complete set of Yukawa corrections including the effects of supersymmetric particles.

We have given a detailed account of the theoretical basis of the calculation, focusing on the implications of the parameter relations enforced by supersymmetry. In the gauge-less limit that needs to be employed to extract the Yukawa corrections of $\mathcal{O}(\alpha_t^2)$, $\mathcal{O}(\alpha_t\alpha_b)$, $\mathcal{O}(\alpha_b^2)$ the lightest MSSM Higgs boson mass M_h vanishes. We have studied in how far the true MSSM value for M_h can be taken into account in a consistent way. We have shown that the result can be expressed in such

a way that the M_h-dependence, being formally a sub-leading effect, can be kept essentially everywhere and we have compared this result with the case where the gauge-less limit is strictly imposed.

In our numerical analysis we have put the main emphasis on the new supersymmetric contributions involving squarks and higgsinos. We have analyzed the results of the new contributions as functions of the squark mass scale $M_{\rm SUSY}$, the stop mixing X_t and the higgsino and Higgs boson mass parameters μ and M_A. For squark masses of about 300 GeV we find corrections of typically +4 MeV in M_W and -2×10^{-5} in $\sin^2\theta_{\rm eff}$. In certain parameter regions, in particular slightly smaller values of $M_{\rm SUSY}$ or small mixing in the stop sector, we find shifts up to +8 MeV in M_W and -4×10^{-5} in $\sin^2\theta_{\rm eff}$. For a wide range of parameters, the squark and higgsino two-loop corrections increase the corresponding one-loop contributions by about 10%.

We have derived our result in two renormalization schemes, the on-shell scheme and the $\overline{\rm DR}$ scheme for the squark sector parameters. Comparing the two-loop results with the one-loop result expressed in terms of the parameters of the two schemes shows a significant reduction of the scheme dependence.

Chapter 8

Conclusion

'After all is said and done, a lot more will be said than done.'

Unknown

In the first four chapters we introduced and motivated the calculation of EWPO and in particular $\Delta\rho$. We justify the need to renormalise the calculation and give details of the procedure used. We give a brief introduction to supersymmetry, defining our notation and conventions as required.

We give explicit details of three large two-loop calculations in chapters 5 – 7. These are the dominant $\mathcal{O}(\alpha\alpha_s)$ and $\mathcal{O}(\alpha_t^2)$, $\mathcal{O}(\alpha_t\alpha_b)$, $\mathcal{O}(\alpha_b^2)$ results. In chapters 5 and 6 we verify two previously published results, the $\mathcal{O}(\alpha\alpha_s)$ and the quark $\mathcal{O}(\alpha_t^2)$, $\mathcal{O}(\alpha_t\alpha_b)$, $\mathcal{O}(\alpha_b^2)$ result and find complete analytical agreement. In chapter 7 we complete the discussion of the $\mathcal{O}(\alpha_t^2)$, $\mathcal{O}(\alpha_t\alpha_b)$, $\mathcal{O}(\alpha_b^2)$ by including all dominant squark and higgsino loops.

The class of diagrams with squarks and higgsinos, which has no SM counterpart, gives rise to significant deviations from the SM predictions. This is in contrast

with the contribution of the diagrams involving quarks and Higgs bosons, which can be well approximated by the corresponding SM contribution (setting the SM Higgs-boson mass equal to the mass of the lightest $\mathcal{CP}$-even Higgs boson of the MSSM). We have compared our result for the two-loop Yukawa correction of $\mathcal{O}(\alpha_t^2)$, $\mathcal{O}(\alpha_t\alpha_b)$, $\mathcal{O}(\alpha_b^2)$ to M_W and $\sin^2\theta_{\text{eff}}$ with the $\mathcal{O}(\alpha\alpha_s)$ correction, which is the only other genuine two-loop contribution to M_W and $\sin^2\theta_{\text{eff}}$ known in the full MSSM. We find that the two corrections are of comparable size and can largely compensate each other for small values of M_{SUSY} (depending on the other supersymmetric parameters).

We have shown how the known corrections to the electroweak precision observables in the SM and the MSSM can be combined such that the currently most accurate prediction in the MSSM is obtained. In the decoupling limit, where all supersymmetric particles are heavy, the theoretical uncertainty from unknown higher-order corrections reduces to the uncertainty of the SM contribution. For non-vanishing contributions of the supersymmetric particles an additional theoretical uncertainty arises from unknown higher-order corrections involving supersymmetric particles.

We have estimated the current uncertainty from unknown higher-order corrections involving supersymmetric particles for different values of the squark mass scale M_{SUSY}. This has been done using geometric progression from lower orders, employing known results for corresponding SM corrections, investigating the renormalisation scheme dependence, varying the renormalisation scale, and taking into account formally sub-leading M_h-dependent contributions. For a squark mass scale below 500 GeV we obtain an estimated uncertainty of about 8.5 MeV in M_W and 4.5×10^{-5} in $\sin^2\theta_{\text{eff}}$. These uncertainties reduce to about 2.5 MeV in M_W and 1.5×10^{-5} in $\sin^2\theta_{\text{eff}}$ for $M_{\text{SUSY}} = 1$ TeV. They can be combined quadratically with the theory uncertainty from unknown higher-order SM contributions to ob-

tain the full MSSM theory uncertainties. While currently these uncertainties (for $M_{\rm SUSY} < 500$ GeV) are about a factor of two smaller than the parametric theoretical uncertainties induced by the experimental error of the top-quark mass, their impact will become more pronounced with the expected improvement of the experimental precision of m_t. The new two-loop corrections evaluated in this thesis have been important to reduce the theoretical uncertainties to the present level. Further efforts on higher-order corrections in the MSSM will be necessary in order to reduce the theoretical uncertainties from unknown higher order corrections within the MSSM to the level that has been reached for the SM.

Appendix A

Scalar Integrals

The B_0, A_0 and T_{134} integrals used through-out calculations presented in this thesis are defined here. Each integral is given as an expansion in ε (ε_1 in the case of B_0). The parameters γ_E and $\frac{1}{4\pi}$ have been absorbed into the divergences. The renormalisation scale, μ, must drop out of all the calculations of physical parameters calculated in this thesis, hence μ is set to 1 (ie. $\log \mu = 0$) in all the definitions.

The B_0 integral is given by

$$B_0[p^2, m_1, m_2] = \frac{1}{\varepsilon_1} + B_{0,finite}[p^2, m_1, m_2] + \varepsilon_1 B_{0,\varepsilon_1}[p^2, m_1, m_2] \quad \text{(A.1)}$$

$$
\begin{aligned}
B_{0,finite}[p^2, m_1, m_2] &= 2 + \frac{(m_1^2 - m_2^2)Log[m_2/m_1]}{p^2} - Log[m_1 m_2] \\
&\quad -\frac{1}{p^2} m_1 m_2 \Big(\frac{2\, i m_1 m_2}{\varepsilon_2 + m_1^2 + m_2^2 - p^2 + \lambda} \\
&\quad -\frac{-i\varepsilon_2 + m_1^2 + m_2^2 - p^2 + \lambda}{2 m_1 m_2} \Big). \\
&\quad Log[\frac{-i\varepsilon_2 + m_1^2 + m_2^2 - p^2 + \lambda}{2 m_1 m_2}]
\end{aligned} \tag{A.2}
$$

$$
\begin{aligned}
B_{0,finite}[p^2, 0, m] &= 2 - Log[m^2] - \frac{(m^2 - p^2)Log[m^2]}{p^2} \\
&\quad + \frac{(m^2 - p^2)Log[-i\varepsilon_2 + m^2 - p^2]}{p^2}
\end{aligned} \tag{A.3}
$$

$$
B_{0,finite}[m^2, 0, m] = 2 - Log[m^2] \tag{A.4}
$$

where $\lambda = \sqrt{-4m_1^2 m_2^2 + (i\varepsilon_2 - m_1^2 - m_2^2 + p^2)^2}$. It is not necessary to define the function B_{0,ε_1} since all coefficients of such functions drop out in the results in this thesis.

The A_0 integral is given by

$$
A_0[m] = \frac{1}{\varepsilon} m^2 + A_{0,finite}[m] + \varepsilon A_{0,\varepsilon}[m] \tag{A.5}
$$

$$
A_{0,finite}[m] = m^2(1 - Log[m^2]) \tag{A.6}
$$

$$
A_{0,\varepsilon}[m] = m^2(1 + \frac{1}{2}\zeta(2) + \frac{1}{2}(Log[m^2])^2 - Log[m^2]) \tag{A.7}
$$

and $\zeta(2) = \pi^2/6$.

The T_{134} integral is given by:

$$T_{134}[m_1, m_3, m_4] = T_{div,134}[m_1, m_3, m_4] + T_{finite,134}[m_1, m_3, m_4] \tag{A.8}$$

$$\begin{aligned} T_{div,134}[m_1, m_3, m_4] &= \frac{m_1^2 + m_3^2 + m_4^2}{2\varepsilon^2} \\ &+ \frac{3(m_1^2 + m_3^2 + m_4^2) - 2(m_1^2 L[m_1^2] - m3^2 L[m_3^2] - m4^2 L[m_4^2])}{2\varepsilon} \end{aligned} \tag{A.9}$$

$$\begin{aligned} T_{finite,134}[m_1, m_3, m_4] &= \frac{1}{4}\{\frac{1}{3}(m_1^2 + m_3^2 + m_4^2)(42 + \pi^2) \\ &+ \sum_{i=1,3,4} (4m_i^2(-3 + L[m_i^2])L[m_i^2]) \\ &- (m_1^2 + m_3^2 - m_4^2)L[m_1^2/m_3^2]^2 \\ &- (m_1^2 - m_3^2 + m_4^2)L[m_1^2/m_4^2]^2 \\ &+ (m_1^2 - m_3^2 - m_4^2)L[m_3^2/m_4^2]^2 \\ &+ \frac{1}{3}(2m_4^2\ \Lambda[\frac{m_1^2}{m_4^2}, \frac{m_3^2}{m_4^2}]). \\ &\quad (\pi^2 - 3L[m_1^2/m_4^2]L[m_3^2/m_4^2] \\ &\quad +6L[\frac{m_1^2 - m_3^2 + m_4^2 - m_4^2\ \Lambda[\frac{m_1^2}{m_4^2}, \frac{m_3^2}{m_4^2}]}{2m_4^2}]. \\ &\quad L[\frac{-m_1^2 + m_3^2 + m_4^2 - m_4^2\ \Lambda[\frac{m_1^2}{m_4^2}, \frac{m_3^2}{m_4^2}]}{2m_4^2}] \\ &\quad -6Li_2[\frac{m_1^2 - m_3^2 + m_4^2 - m_4^2\ \Lambda[\frac{m_1^2}{m_4^2}, \frac{m_3^2}{m_4^2}]}{2m_4^2}] \\ &\quad -6Li_2[\frac{-m_1^2 + m_3^2 + m_4^2 - m_4^2\ \Lambda[\frac{m_1^2}{m_4^2}, \frac{m_3^2}{m_4^2}]}{2m_4^2}])\} \end{aligned} \tag{A.10}$$

where $\Lambda[x, y] = \sqrt{1 + x^2 + y^2 - 2x - 2y - 2xy}$, $L[x] = Log[x]$ and

$$Li_n[x] = \sum_{k=1}^{\infty} \frac{x^k}{k^n} \tag{A.11}$$

Bibliography

[1] F.Halzen, A.D.Martin – *Quarks and Leptons: An introductory Course in Modern Particle Physics* – J Wiley & Sons 1984

[2] Manual Drees – *An introduction to Supersymmetry* hep-ph/9611409

[3] D.A.Dicus and V.S.Mathur, Phys.Rev **D7**,3111 (1973); B W Lee, C.Quigg and H.Thacker, Phys Rev **D16**1519 (1977).

[4] LEP Eletroweak Working Group
`http://lepewwg.web.cern.ch/LEPEWWG/Welcome.html`

[5] The CDF Collaboration, the D0 Collaboration, the Tevatron Electroweak Working Group *Combination of CDF and D0 Results on the Top-Quark Mass*, hep-ex/0507091

[6] R.E.Behrends, R.J.Finkelnstein, A.Sirlin *Phys. Rev.* **101** (1956) 866.
T.Kinoshita, A.Sirlin, *Phys. Rev.* **113** (1956) 1652.
T. Van Ritbergen and R.G Stuart, *Phys. Rev. Lett.***82**(1999) 488, hep-ph/9808283
T. Van Ritbergen and R.G Stuart, *Nucl.Phys. B***564**(2000) 343, hep-ph/9904240

[7] M. Veltman, *Nucl. Phys.* **B 123** (1977) 89.

[8] R.K.Ellis *Standard model phenomenology* from summer school lectures on *Large Hadron Collider Phenomenology* – I.o.P. 2004

[9] See, for example, L.Ryder – *Quantum Field Theory* – Cambridge University Press

[10] G.'t Hooft, M.Veltman, *Nucl. Phys* **B 153** (1979) 365;

[11] G. 't Hooft and M. Veltman, *Nucl. Phys.* **B 44** (1972) 189;
C. Bollini and J. Giambiagi, *Nuovo Cimento* **B 12** (1972) 20;
J. Ashmore, *Nuovo Cimento Lett.* **4** (1972) 289. P.Breitenlohner and D.Maison, Commun. Math. Phys. **52** (1977) 11.

[12] D. Stöckinger, *JHEP* **0503** (2005) 076, hep-ph/0503129.

[13] W. Siegel, *Phys. Lett.* **B 84** (1979) 193;
D. Capper, D. Jones and P. van Nieuwenhuizen, *Nucl. Phys.* **B 167** (1980) 479;
W. Siegel, *Phys. Lett.* **B 94** (1980) 37;
L. Avdeev, *Phys. Lett.* **B 117** (1982) 317;
L. Avdeev and A. Vladimirov, *Nucl. Phys.* **B 219** (1983) 262;
I. Jack and D. Jones, hep-ph/9707278, in *Perspectives on Supersymmetry*, ed. G. Kane (World Scientific, Singapore), p. 149;

[14] J.Küblbeck, M Böhm and A.Denner, *Comp. Phys. Comm.* **60** (1990) 165;
T.Hahn and M. Perez-Victoria, *Comput. Phys. Commum.* **118** (1999) 153, hep-ph/9807565;
T.Hahn *Nucl. Phys Proc. Suppl.* **89** (2000) 231, hep-ph/0005029; *Comput.*

Phys.Commum. **140** (2001) 418, hep-ph/0012260

The program is available at `www.feynarts.de`

[15] T. Hahn and C. Schappacher, *Comput. Phys. Commun.* **143** (2002) 54, hep-ph/0105349.

[16] G. Weiglein, R. Scharf and M. Böhm, *Nucl. Phys.* **B 416** (1994) 606, hep-ph/9310358;

G. Weiglein, R. Mertig, R. Scharf and M. Böhm, in *New Computing Techniques in Physics Research 2*, ed. D. Perret-Gallix (World Scientific, Singapore, 1992), p. 617.

[17] G. Passarino and M. Veltman, *Nucl. Phys.* **B 160** (1979) 151.

[18] A. Davydychev und J. B. Tausk, *Nucl. Phys.* **B 397** (1993) 123;

F. Berends und J. B. Tausk, *Nucl. Phys.* **B 421** (1994) 456.

[19] S. Heinemeyer, W. Hollik and G.Weiglein, *Electroweak Precision Observables in the Minimal Supersymmetric Standard Model*, hep-ph/0412214

[20] J.Wess and B.Zumino *Nucl. Phys* **B 70** 39 (1974)

J.Wess and B.Zumino *Nucl. Lett* **49B** 52 (1974)

[21] J. Gunion, H. Haber, G. Kane and S. Dawson, *The Higgs Hunter's Guide*, Addison-Wesley, 1990.

[22] S.Heinemeyer, *The Higgs Boson Sector of the Complex MSSM in the Feynman-diagrammatic approach*, hep-ph/0108059

[23] S.Eidelman et al. [Particle Data Group], *Phys. Lett* **B 592** (2004) 1.

[24] Y. Okada, M. Yamaguchi and T. Yanagida, *Prog. Theor. Phys.* **85**, 1 (1991), and *Phys. Lett.* **B262**, 54 (1991);

R. Barbieri, M. Frigeni and F. Caravaglio, *Phys. Lett.* **B258**, 167 (1991);
H.E. Haber and R. Hempfling, *Phys. Rev. Lett.***66**, 1815 (1991);
J. Ellis, G. Ridolfi and F. Zwirner, *Phys. Lett.***B257**, 83 (1991), and **B262**, 477 (1991).

[25] T.Fritzsche and W. Hollik, *Complete one-loop corrections to the mass spectrum of charginos and neutralinos in the MSSM*, hep-ph/0203159

[26] H.P. Nilles, *Phys. Rep.* **110** (1984) 1;
H.E. Haber and G.L. Kane, *Phys. Rep.* **117**, (1985) 75;
R. Barbieri, *Riv. Nuovo Cim.* **11**, (1988) 1.

[27] R. Barbieri and L. Maiani, *Nucl. Phys.* **B 224** (1983) 32;
C. S. Lim, T. Inami and N. Sakai, *Phys. Rev.* **D 29** (1984) 1488;
E. Eliasson, *Phys. Lett.* **B 147** (1984) 65;
Z. Hioki, *Prog. Theo. Phys.* **73** (1985) 1283;
J. A. Grifols and J. Sola, *Nucl. Phys.* **B 253** (1985) 47;
B. Lynn, M. Peskin and R. Stuart, CERN Report 86-02, p. 90;
R. Barbieri, M. Frigeni, F. Giuliani and H.E. Haber, *Nucl. Phys.* **B 341** (1990) 309;
M. Drees and K. Hagiwara, *Phys. Rev.* **D 42** (1990) 1709.

[28] M. Drees, K. Hagiwara and A. Yamada, *Phys. Rev.* **D 45** (1992) 1725;
P. Chankowski, A. Dabelstein, W. Hollik, W. Mösle, S. Pokorski and J. Rosiek, *Nucl. Phys.* **B 417** (1994) 101;
D. Garcia and J. Solà, *Mod. Phys. Lett.* **A 9** (1994) 211.

[29] S. Heinemeyer, W. Hollik, F. Merz, S. Peñaranda, to appear in *Eur. Phys. Jour.* **C**, hep-ph/0403228.

[30] A. Djouadi, P. Gambino, S. Heinemeyer, W. Hollik, C. Jünger and G. Weiglein, *Phys. Rev. Lett.* **78** (1997) 3626, hep-ph/9612363; *Phys. Rev.* **D 57** (1998) 4179, hep-ph/9710438.

[31] S. Heinemeyer, PhD thesis, see `www-itp.physik.uni-karlsruhe.de/prep/phd/`; G. Weiglein, hep-ph/9901317.

[32] S. Heinemeyer and G. Weiglein, *JHEP* **0210** (2002) 072, hep-ph/0209305; hep-ph/0301062.

[33] A. Djouadi and C. Verzegnassi, *Phys. Lett.* **B 195** (1987) 265;
A. Djouadi, *Nuovo Cim.* **A 100** (1988) 357.

[34] A. Freitas, W. Hollik, W. Walter and G. Weiglein, *Phys. Lett.* **B 495** (2000) 338 [Erratum-ibid. **B 570** (2003) 260], hep-ph/0007091;
A. Freitas, W. Hollik, W. Walter and G. Weiglein, *Nucl. Phys.* **B 632** (2002) 189 [Erratum-ibid. **B 666** (2003) 305], hep-ph/0202131;
M. Awramik and M. Czakon, *Phys. Lett.* **B 568** (2003) 48, hep-ph/0305248;
M. Awramik and M. Czakon, *Phys. Rev. Lett.* **89** (2002) 241801, hep-ph/0208113;
A. Onishchenko and O. Veretin, *Phys. Lett.* **B 551** (2003) 111, hep-ph/0209010;
M. Awramik, M. Czakon, A. Onishchenko and O. Veretin, *Phys. Rev.* **D 68** (2003) 053004, hep-ph/0209084.

[35] M. Awramik, M. Czakon, A. Freitas and G. Weiglein, *Phys. Rev.* **D 69** (2004) 053006, hep-ph/0311148.

[36] M. Awramik, M. Czakon, A. Freitas and G. Weiglein, *Phys. Rev. Lett.* **93** (2004) 201805, hep-ph/0407317.

[37] W. Hollik, U. Meier and S. Uccirati, hep-ph/0507158.

[38] J. van der Bij and M. Veltman, *Nucl. Phys.* **B 231** (1984) 205.

[39] J. van der Bij and F. Hoogeveen, *Nucl. Phys.* **B 283** (1987) 477.

[40] R. Barbieri, M. Beccaria, P. Ciafaloni, G. Curci and A. Vicere, *Nucl. Phys.* **B 409** (1993) 105;
J. Fleischer, F. Jegerlehner and O.V. Tarasov, *Phys. Lett.* **B 319** (1993) 249.

[41] S. Heinemeyer, W. Hollik and G. Weiglein, *Comp. Phys. Comm.* **124** 2000 76, hep-ph/9812320; *Eur. Phys. J.* **C 9** (1999) 343, hep-ph/9812472. The code is accessible via `www.feynhiggs.de` .

[42] M. Frank, S. Heinemeyer, W. Hollik and G. Weiglein, hep-ph/0202166.

[43] G. Degrassi, S. Heinemeyer, W. Hollik, P. Slavich and G. Weiglein, *Eur. Phys. J.* **C 28** (2003) 133, hep-ph/0212020.

[44] T. Hahn, S. Heinemeyer, W. Hollik and G. Weiglein, hep-ph/0507009;
M. Frank, T. Hahn, S. Heinemeyer, W. Hollik and G. Weiglein, *in preparation.*

[45] J. Haestier, S. Heinemeyer, D. Stöckinger, G. Weiglein *Eletroweak Precision Observables: Two-loop Yukawa Corrections of Supersymmetric Particles* hep-ph/0508139

[46] S. Heinemeyer, hep-ph/0407244;
A. Djouadi, hep-ph/0503173.

[47] S. Heinemeyer, W. Hollik and G. Weiglein, hep-ph/0412214.

[48] W. Hollik, E. Kraus, M. Roth, C. Rupp, K. Sibold and D. Stöckinger, *Nucl. Phys.* **B 639** (2002) 3, hep-ph/0204350;
W. Hollik and H. Rzehak, *Eur. Phys. J.* **C 32** (2003) 127, hep-ph/0305328.

[49] S. Heinemeyer, W. Hollik, H. Rzehak and G. Weiglein, *Eur. Phys. J.* **C 39** (2005) 465 hep-ph/0411114.

[50] G. Abbiendi et al. [ALEPH, DELPHI, L3, OPAL Collaborations and LEP Working Group for Higgs boson searches], hep-ex/0107030, hep-ex/0107031.

[51] G. Abbiendi et al. [ALEPH, DELPHI, L3, OPAL Collaborations and LEP Working Group for Higgs boson searches], *Phys. Lett.* **B 565** (2003) 61, hep-ex/0306033.

[52] B. Allanach et al., *Eur. Phys. J.* **C 25** (2002) 113, hep-ph/0202233;
The definition of the MSSM parameter for the SPS points can be found at `www.ippp.dur.ac.uk/~georg/sps/` .

[53] B. Kniehl, *Nucl. Phys.* **B 347** (1990) 89;
F. Halzen and B. Kniehl, *Nucl. Phys.* **B 353** (1991) 567;
B. Kniehl and A. Sirlin, *Nucl. Phys.* **B 371** (1992) 141; *Phys. Rev.* **D 47** (1993) 883;
A. Djouadi and P. Gambino, *Phys. Rev.* **D 49** (1994) 3499 [Erratum-ibid. **D 53** (1994) 4111], hep-ph/9309298.

[54] L. Avdeev et al., *Phys. Lett.* **B 336** (1994) 560 [Erratum-ibid. **B 349** (1995) 597], hep-ph/9406363;
K. Chetyrkin, J. Kühn and M. Steinhauser, *Phys. Lett.* **B 351** (1995) 331, hep-ph/9502291; *Phys. Rev. Lett.* **75** (1995) 3394, hep-ph/9504413.

[55] M. Faisst, J. Kühn, T. Seidensticker and O. Veretin, *Nucl. Phys.* **B 665** (2003) 649, hep-ph/0302275.

[56] S. Heinemeyer, S. Kraml, W. Porod and G. Weiglein, *JHEP* **0309** (2003) 075, hep-ph/0306181.

[57] S. Heinemeyer, T. Mannel and G. Weiglein, hep-ph/9909538;

J. Erler, S. Heinemeyer, W. Hollik, G. Weiglein and P. Zerwas, *Phys. Lett.* **B 486** (2000) 125, hep-ph/0005024;

J. Erler and S. Heinemeyer, hep-ph/0102083.